

**Best  
Available  
Copy**

AD-770 642

SELECTED MATERIAL FROM SOVIET  
TECHNICAL LITERATURE, SEPTEMBER 1973

Stuart G. Hibben

Informatics, Incorporated

Prepared for:

Air Force Office of Scientific Research  
Advanced Research Projects Agency

6 November 1973

DISTRIBUTED BY:

**NTIS**

National Technical Information Service  
U. S. DEPARTMENT OF COMMERCE  
5285 Port Royal Road, Springfield Va. 22151

AD770 642

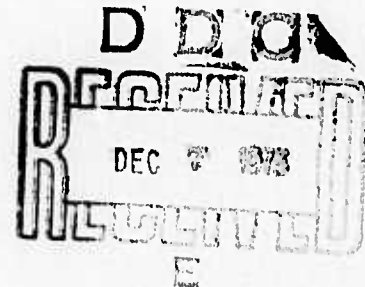
SELECTED MATERIAL  
FROM  
SOVIET TECHNICAL LITERATURE

September, 1973

Sponsored by  
Advanced Research Projects Agency

ARPA Order No. 1622-4

November 6, 1973



ARPA Order No. 1622-4  
Program Code No: 62701E3F10  
Name of Contractor:  
Informatics Inc.  
Effective Date of Contract:  
January 1, 1973  
Contract Expiration Date:  
December 31, 1973  
Amount of Contract: \$343,363

Contract No. F44620-72-C-0053, P00001  
Principal Investigator:  
Stuart G. Hibben  
Tel: (301) 770-3000 or  
(301) 779-2850  
Program Manager:  
Klaus Liebhold  
Tel: (301) 770-3000  
Short Title of Work:  
"Soviet Technical Selections"

This research was supported by the Advanced Research Projects Agency of the Department of Defense and was monitored by the Air Force Office of Scientific Research under Contract No. F44620-72-C-0053. The publication of this report does not constitute approval by any government organization or Informatics Inc. of the inferences, findings, and conclusions contained herein. It is published solely for the exchange and stimulation of ideas.

informatics inc

System and Design Company  
5000 Executive Boulevard  
Rockville, Maryland 20852  
(301) 770-3000 Telex: 89 521

Approved for public release; distribution unlimited.

Reproduced by  
NATIONAL TECHNICAL  
INFORMATION SERVICE  
U S Department of Commerce  
Springfield VA 22151

UNCLASSIFIED

SECURITY CLASSIFICATION OF THIS PAGE (When Data Entered)

REPORT DOCUMENTATION PAGE		READ INSTRUCTIONS BEFORE COMPLETING FORM
1. REPORT NUMBER <b>AEOSR - TR - 73 - 2066</b>	2. GOVT ACCESSION NO.	3. RECIPIENT'S CATALOG NUMBER
4. TITLE (and Subtitle) SELECTED MATERIAL FROM SOVIET TECHNICAL LITERATURE, SEPTEMBER 1973		5. TYPE OF REPORT & PERIOD COVERED Scientific ... Interim
		6. PERFORMING ORG. REPORT NUMBER
7. AUTHOR(s) Stuart G. Hibben		8. CONTRACT OR GRANT NUMBER(s) F44620-72-C-0053, P00001
9. PERFORMING ORGANIZATION NAME AND ADDRESS Informatics Inc. 6000 Executive Boulevard Rockville, Maryland 20852		10. PROGRAM ELEMENT, PROJECT, TASK AREA & WORK UNIT NUMBERS 62701E3F10 AO 1622-4
11. CONTROLLING OFFICE NAME AND ADDRESS Advanced Research Projects Agency/NMR 1400 Wilson Boulevard Arlington, Virginia 22209		12. REPORT DATE November 6, 1973
		13. NUMBER OF PAGES 183
14. MONITORING AGENCY NAME & ADDRESS (if different from Controlling Office) Air Force Office of Scientific Research/NP 1400 Wilson Boulevard Arlington, Virginia 22209		15. SECURITY CLASS. (of this report) UNCLASSIFIED
		15a. DECLASSIFICATION/DOWNGRADING SCHEDULE
16. DISTRIBUTION STATEMENT (of this Report)  Approved for public release; distribution unlimited		
17. DISTRIBUTION STATEMENT (of the abstract entered in Block 20, if different from Report)		
18. SUPPLEMENTARY NOTES		
19. KEY WORDS (Continue on reverse side if necessary and identify by block number) Laser Plasma, Laser Damage, Explosion Effects, Seismology, Dense Electron Beams, High Temperature Effects, High Pressure Effects, Superconductivity, Atmospheric Physics		
20. ABSTRACT (Continue on reverse side if necessary and identify by block number)  This report includes abstracts and bibliographic lists on contractual subjects that were completed in September, 1973. The major topics are: laser technology, effects of strong explosions, geosciences, particle beams, and material sciences. A section on atmospheric physics and one on items of miscellaneous interest are included as optional topics; material on geo-magnetic pulsations is to be abstracted in a separate report. Laser coverage is generally limited to high power effects; all current laser material is routinely entered in the quarterly laser bibliographies.		

DD FORM 1 JAN 73 1473

EDITION OF 1 NOV 65 IS OBSOLETE

UNCLASSIFIED

19 SECURITY CLASSIFICATION OF THIS PAGE (When Data Entered)

## INTRODUCTION

This report includes abstracts and bibliographic lists on contractual subjects that were completed in September, 1973. The major topics are: laser technology, effects of strong explosions, geosciences, particle beams, and material sciences. A section on atmospheric physics and one on items of miscellaneous interest are included as optional topics; material on geomagnetic pulsations is to be abstracted in a separate report.

Laser coverage is generally limited to high power effects; all current laser material is routinely entered in the quarterly laser bibliographies.

An index identifying source abbreviations and a first-author index to the abstracts are appended.

## TABLE OF CONTENTS

1. Laser Technology	
A. Abstracts . . . . .	1
B. Recent Selections . . . . .	18
2. Effects of Strong Explosions	
A. Abstracts . . . . .	21
B. Recent Selections . . . . .	32
3. Geoscience	
A. Abstracts . . . . .	36
4. Particle Beams	
A. Abstracts . . . . .	83
B. Recent Selections . . . . .	88
5. Material Science	
A. Abstracts . . . . .	89
B. Recent Selections . . . . .	115
6. Atmospheric Physics	
A. Abstracts . . . . .	124
B. Recent Selections . . . . .	138
7. Miscellaneous Interest . . . . .	
A. Abstracts . . . . .	158
B. Recent Selections . . . . .	171
8. List of Source Abbreviations. . . . .	173
9. Author Index to Abstracts . . . . .	179

A. Abstracts

Barchukov, A. I., F. V. Bunkin, V. I. Konov, and A. M. Prokhorov. Low-threshold air breakdown near a target under CO<sub>2</sub> laser radiation, and the associated strong recoil pulse. ZhETF, P, v. 17, no. 8, 1973, 413-416.

In experiments with CO<sub>2</sub> laser radiation focussed near the surface of various targets, the air breakdown threshold intensity was lower by more than two orders of magnitude in comparison to the threshold earlier observed in a cited American study (Lencioni et al, Bull. Am. Phys. Soc., v. 16, Ser. II, 1971, 1292). A multimode, transverse-discharge CO<sub>2</sub> laser was used, generating at  $\lambda = 2.36 \mu$  single pulses of 15  $\mu$ sec duration and up to 4 joules energy (E). Air breakdown from single pulses was observed only near a target (Al, Cu, Mg, NaCl, etc.), at  $\approx 0.5$  cm from its surface. The breakdown threshold is mainly a function of the surface roughness and ambient gas pressure. Apparently the breakdown is initiated by strongly absorptive macroscopic surface particles.

Recoil pulses up to a maximum 45 dyne x sec/joule at E = 1 joule were measured from a Mg target. The recoil pulse data obtained from flat and cylindrical targets are interpreted as the effect of a shock wave generated in air by a point explosion in the focal volume. Hence the experiments confirm that air optical breakdown can occur from interaction of CO<sub>2</sub> laser radiation at  $(5-10) \times 10^6$  w/cm<sup>2</sup> power density with a target. The recoil pulse must be symmetrical, as illustrated by experiments with a pendulum.

Uglov, A. A. Material from the seminar on physics and chemistry of material processing by concentrated energy fluxes. (Baykov Institute, Moscow, June 22-23, 1972). FiKhOM, no. 2, 1973, 157-159.

The 36th regular seminar on the title subject was held under chairmanship of Academician N. N. Rykalin in the presence of over 80 representatives from organizations in various Soviet cities. The seminar was devoted to the studies of laser and electron beam interaction with materials. Short summaries are given of the nine papers presented at the Seminar; all but two deal with laser beam effects. In addition to a theoretical study of vacuum vaporization, the results are given and discussed of experimental studies on laser or electron beam interaction with metals (3), film resistors (2), semiconductors (2), and dielectrics (1). The studies on metals deal with laser application to welding (V. P. Babenko and N. V. Grevtsev et al, both from Moscow) and hole drilling in thin films (G. R. Levinson and V. I. Smilga, Moscow). Precision sizing and trimming with a laser beam were the topics of the two papers on film resistors. The effect of giant laser pulses on electrophysical properties of Ge and Si whiskers, and electron-beam heat treatment of Ge and Si single crystals, were discussed in two papers on semiconductors. Destruction of plexiglas by a laser beam was treated in the single paper on dielectrics.

Bergel'son, V. I., and I. V. Nemchinov.  
Plane self-similar motion of a radiation-  
heated gas with strong re-radiation. PMM,  
v. 37, 1973, 236-242.

The interaction of a powerful monochromatic optical beam with a solid surface is analyzed, with allowance for re-emission from a hot layer of vaporized material. Energy flux is emitted from this layer partly in a direction away from the surface, and partly towards it. Heat losses on account of self-radiation are assumed to be purely volumetric, and the beam mean free path to be of the same order of magnitude as the thickness of the heated vapor layer. In this case, the two-dimensional problem of the heated gas motion is formulated by a set of equations of state, motion, continuity, energy, and incident radiation transfer. This set of equations can be reduced to a set of ordinary differential equations in self-similar variables  $P$ ,  $V$ ,  $E$ , and  $U$ , on the assumption of a high intensity self-radiation. Assuming, in addition, that the incident radiation density is an exponential function of time, the authors develop another set of self-similar equations. Both sets of equations are solved by integration for  $P$ ,  $V$ ,  $E$ , and  $U$ . Numerical solutions are shown for a completely ionized gas, and radiation fluxes of both constant and linearly rising density.

Novikov, N. P. Damage mechanism of  
plexiglass-type transparent dielectrics  
from laser radiation. MP, no. 2, 1973,  
232-238.

The mechanism of destructive crack initiation in PMMA-type transparent dielectrics from laser radiation is discussed from the viewpoint

of mechanics of crack development and physics of laser beam interaction with solids. The mechanics of crack formation require formation of a certain gas microvolume during laser pulse action, and hence determine pulse parameters. Gas formation occurs by gasification of the polymer, and the gasification characteristics are determined by the physics of the beam solid interaction.

A gasification mechanism is proposed on the basis of a partial multiphoton degradation of polymer molecules with formation of free radicals, which triggers a radical-chain reaction mechanism of destruction. Gas formation is described by a set of equations, and laser pulse threshold characteristics calculated from these equations agree with the measured characteristics. The assumption that absorption of laser radiation, the primary act in gasification, occurs by discharge in micropores of a dielectric material, is confirmed by experimental data from the literature. A set of equations describing development of large cracks, e.g.,  $r_k = 50-100 \mu$  in PMMA, is established from analysis of the process kinetics. The proposed damage mechanism of transparent dielectrics agrees well with all available experimental

assuming that the law of pressure  $p$  variation is given by solution of a gas dynamic equation without allowance for radiation. True spectral structure and directivity pattern of radiation are accounted for in the equation of radiation transport.

The problem reduces to numerical solution of a set of ordinary differential equations for each spherical layer of the hot gas sphere. The spectral absorption coefficients  $k_{\nu j}$  of air from tabulated data were used in calculations. The calculated plots of temperature  $T$  distribution along the fireball radius and  $T$ ,  $p$ , and density at its center versus time, show that for a 5.3 j total energy of laser explosion, the initially rapid cooling of the fireball slows down and the  $T$  profile exhibits steps. The latter are connected with the O and N ion recombination and a sharp change in  $k_{\nu j}$  at  $T \sim 20,000^\circ \text{K}$ . Spectral and total radiation fluxes from the fireball and  $W$  as a function of time are calculated.

Pustovalov, V. K. Radiation heating of a two-temperature plasma, taking electron thermal conductivity into account. Self-similar solution. DAN BSSR, no. 4, 1973, 313-315.

The problem of heating a two-temperature stationary plasma of constant electron and ion densities by means of monochromatic radiation is analyzed, with allowance made for electron-ion relaxation and electron thermal conductivity  $\chi$ . This problem may arise in plasma diagnostics and plasma heating from laser pulses. A solution to the problem is presented in the form of a set of equations in self-similar variables which account for the finite velocity  $c$  of light. The solution is of the traveling wave type and gives dimensionless electron ( $T_{1e}$ ) and ion ( $T_{1i}$ ) temperatures and radiant flux

density  $q_1$  for a completely ionized plasma. Also, formulas for self-similar coordinate  $\xi_0$  and propagation velocity are derived from the cited solution.

The formula for  $\xi_0$  for the practically important range of radiation fluxes  $q \geq 10^9 \text{ w/cm}^2$  at  $1.06 \mu$  wavelength and  $\approx 10^{10}$  sec pulse duration is simplified here by eliminating  $c$  and  $\chi$ , owing to negligibly small heat transfer by thermal conductivity in relation to that by radiation. At the limit  $c \rightarrow \infty$  the self-similar solution describes a quasistationary propagation of radiation in a two-temperature plasma.

Abrikosova, I. I., and B. V. Anshukov.

Role of laser self-focusing in breakdown  
of liquid He<sup>4</sup>. ZhETF, v. 64, no. 4, 1973,  
1141-1145.

The controversial mechanism of optical breakdown in liquid and gaseous He is examined in the light of experiments with interaction of a multimode ruby laser beam with liquid He. In the cited experiments, 30 nsec. pulses from a laser of 20 Mw maximum power were focused by a lens with  $f = 4.5 \text{ cm}$ . In purified liquid He, a weak diffuse track of the focused beam was recorded near the focus, which is attributed to molecular scattering. Repeated pulses caused a breakdown in the form of a bright white spark in the focal region facing the lens or, in some cases, a bright red glow which duplicated the discrete structure of the breakdown spark.

The breakdown initiation is ascribed tentatively to submicroscopic particles detached from the wall by the first laser pulse and suspended in the liquid He. In the presence of these impurities, a glow structure in the focus can be observed separately from the breakdown. It is suggested that breakdown occurs owing to beam collapse and that breakdown occurrence is determined by conditions promoting self-focusing.

Anisimov, S. I., and B. I. Makshantsev.  
Role of absorptive inhomogeneities in optical  
breakdown of transparent materials. FTT,  
no. 4, 1973, 1091-1095.

The effect of small ( $<10^{-5}$  cm) inhomogeneities in transparent materials on optical breakdown, as from laser radiation of these materials, is discussed to explain the available experimental data on breakdown. The fact that even an intense heating of small inhomogeneities cannot cause noticeable destruction of material led to introduction of a breakdown mechanism different from that proposed earlier for large absorptive inhomogeneities.

It is assumed that an intense heating of small inclusions induces light absorption by the initially transparent material. This in turn leads to increased dimensions of an inclusion and, at an optical intensity above a certain critical value, to generation of an absorption wave which propagates from the inclusion surface into the bulk of the material. Ultimately energy absorption causes the observed destruction. The cited destruction mechanism was used as a basis for calculation of the breakdown threshold as a function of dimensions and optical characteristics of both strongly and weakly absorptive inclusions. In both cases, the resulting calculated critical flux densities, typically  $\cong 10^9$  w/cm<sup>2</sup>, were in agreement with the experimental values for glass and fused quartz. The formation time for an absorption wave (aureole) is evaluated at  $\sim 10^{-8}$  sec. at an intensity slightly above threshold.

Askar'yan, G. A. Particle motion in a laser beam. UFN, v. 110, no. 1, 1973, 115-116.

The author offers a brief summary of the main mathematical relationships governing particle motion in a laser beam. The work is given as an addendum to an accompanying translation of Ashkin's review article on pressure of laser light (Scientific American, 2/72, 63).

The study is first limited to action of e-m radiation on particles smaller than exciting wavelength  $\lambda$ . In this case two forces are present, a field gradient  $F_{\Delta}$  and optical pressure  $P_{\text{opt}}$ , whose ratio  $F_{\Delta} / P_{\text{opt}} = \lambda^2 / \alpha L$ . Here  $\alpha$  is the polarizability index of the particle, and  $L$  = unit change in field intensity.

It then can be shown that particles will undergo either attraction ( $\epsilon_p > \epsilon$ ), or repulsion ( $\epsilon_p < \epsilon$ ), e. g. for atoms whose size is three order less than excitation wavelength. For a small field gradient, a relatively large particle size, or large polarizability, optical pressure will exceed the field force. The factors which then govern the imparted velocity  $u$  are identified. In an example given a field of  $10^6$  CGSE, corresponding to a focused power on the order of hundreds of megawatts, would develop  $u$  on the order of  $10^5$  cm/sec, i. e. lightscattered particle velocities approaching sonic, which could be verified in the spectral response of the scattered light (cf Askar'yan, Sel. Mat. Sov. Tech. Lit., Sept. 1972, p. 1).

The forces connected with optical absorption are next considered. These are convective, associated with heating and motion of the medium; radiometric pressure; and optical recoil pressure owing to vaporization from the particle. Where absorption is appreciable, these factors will far exceed the optical pressure. A typical example thus gives  $P_{\text{react}} / P_{\text{opt}} \sim 10^4$ , which could yield recoil pressures up to  $10^{12}$  atm. This could accelerate macro-particles, including plasma generation at a target surface, as suggested by

Ashkin. In this context Askar'yan mentions the idea of using a powerful c-w gasdynamic laser to alter the trajectory of a satellite.

Papirov, I. I., S. S. Avotin, E. P. Krivchikova,  
and L. A. Korniyenko. Deformation of beryllium  
single crystals by laser irradiation. FiKhOM,  
no. 2, 1973, 147-148.

Single crystals of beryllium with orientations (0001) and (1120), obtained by the method of zone melting, ground and electrically polished to a mirror finish, were irradiated by a GOR-100M pulsed laser operating in a free-running mode. Radiation effects were noted as follows.

On the base and prism planes around a crater 2.2 mm in diameter, an annular zone was formed with traces of strong plastic deformation, mainly by twins. The width of the zone was 0.5 - 1 mm. A feature of the twins forming on the base and prism planes is an uneven, strongly dissected form of the boundaries, as well as the presence of tetrahedrally shaped twins. The observation of tetrahedral twinning, as well as the presence of numerous old and new boundaries of the twins, is a definite indication of the complex character of the plastic deformation of beryllium single crystals during irradiation: following the wave of compressive stresses, which generates numerous twins, there occurs a change of sign in stress, and partial detwinning.

Twins forming in the base plane are, as a rule, crystallographically oriented with respect to one another at angles of 60 and 120°. The twins on a prism plane are situated relatively chaotically, and the large twins frequently have odd shapes that are atypical for the usual kinds of deformation. Dendritic structures, formed by twins of various sizes, are frequently observed in the vicinity of the crater; such structures are previously unknown.

A feature of the large twins near the crater is the rough structure of their surface. Possibly this structure, as well as the odd shape, is a result of fusion of the surface of the twins. Fusion of a surface that does not contain twins, in the vicinity of the crater, also takes place. However, the width of this zone (about 100 microns) is less than the width of the region in which fused twins are observed.

Traces of slip are observed on the prism plane and, to a lesser extent, on the base plane. Cracks are sometimes observed on the prism plane; these are due to cohesion of the crystal along the base plane. Usually, such cracks are associated with sharp peaks of the twins.

The structure of the crater itself is extremely nonuniform. In the crater are observed numerous microcraters and "ripples" of metal crystallized after fusion. Also to be noted is the fact of the formation of craters in a zone that had not been directly subjected to irradiation. The cause of the formation of such craters is not clear.

The results confirm the fact that during the irradiation of solids by laser pulses, large stresses and strains develop in the zone adjacent to the crater, and that the strains differ essentially from the deformation that takes place during static tests.

Zakharov, V. P., and V. I. Zaliva. Change in specific conductivity of germanium chalcogenide amorphous thin films under pulsed heating. FizKhOM, no. 2, 1973, 141-142.

An investigation is made of the phase transition from an amorphous to a polycrystal state in thin films (thickness -- about  $1000\text{\AA}$ ) of germanium telluride and germanium selenide, obtained by deposition in a

vacuum onto cold glass substrates, during the action upon them of powerful light pulses, according to a procedure previously employed by the authors for the investigation of analogous processes in germanium and carbon films. The structural conversions in the films were registered by the change of their specific conductivity, and electron diffraction. Measurements of the specific conductivity were carried out by a contactless method on the basis of change of the level of an shf signal as structural conversions were stimulated by powerful light pulses.

In Fig. 1. is presented a typical oscillogram which shows the change of absorption of shf power in a germanium telluride film during the phase transition from amorphous to polycrystalline. The bottom trace is the photomultiplier signal from the light pulse of a gas-discharge tube. It can be seen on the top oscillogram that the specific conductivity of the GeTe film increases irreversibly during phase transition, as a consequence of which the signal level passing through the film decreases.

In the initial state the films constitute structureless formations and the diffraction maxima from such films have the form of washed-out halos. After exposure of the films to light pulses of a certain energy, crystals are observed to grow in them to sizes of about 2-3 microns. The structure of such crystals resembles the NaCl lattice ( $a = 6.02 \text{ \AA}$ ). The growth of the crystals and the accompanying irreversible change of the specific conductivity of GeTe films takes place over a period of about 50-60 microseconds; thus the crystals grow at a rate of about 5-6 cm/sec.

Similar research was conducted for GeSe films and in principle the same results were obtained, with the exception of their specific conductivity during the phase transition. In this case, at a specific film

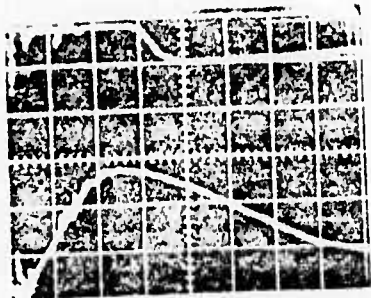


Fig. 1. Change of shf power passing through a GeTe film during its irradiation by a powerful light pulse, and the signal from the photomultiplier. Scale = 100 microseconds/div.

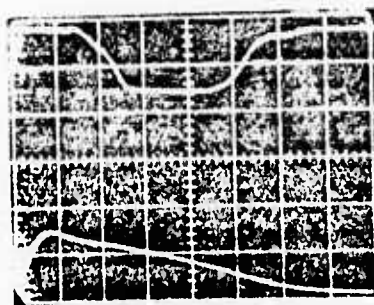


Fig. 2. Same as in Fig. 1, but for a GeSe film. Scale = 200 microseconds/div.

temperature an increase in the specific conductivity of the film is observed, the existence of the attained level during a rather long period of time (400-500 microseconds), and its drop to values only 2-3 times greater than those of the initial conductivity of the film (Fig. 2).

Veyko, V. P., G. A. Kotov, and M. N. Libenson. Thermal action of laser radiation on various polymers. FizKhOM, no. 2, 1973, 16-18.

The article deals with features of the influence of pulsed laser radiation upon polyvinyl cinnamates (PVC) and naphthoquinone diazides (NQD) in the visible and near infrared region of the spectrum, where fundamental absorption of such materials is negligibly small. Preliminary investigation showed that under laser radiation, polymerization of PVC and destruction of NQD occurred only in photoresistor layers applied on an opaque substrate; this unequivocally indicates the reaction to be thermal rather than photochemical at flux densities of  $q = 10^4 \text{ -- } 10^5 \text{ watts/cm}^2$ .

Under pulsed heat the characteristic temperature of the process at which perceptible ejecta from of the substance is observed, is higher than with the application of steady heat. This is a general rule, and is applicable to all processes, the kinetics of which are described by an activation formula.

The experimentally determined average mean values of the damage-threshold laser radiation on photoresistors were found to be  $400^{\circ}\text{C}$  for PVC polymerization and  $140^{\circ}\text{C}$  and NQD destruction. Hence, such a temperature threshold in the case of laser radiation is perceptibly higher for PVC than for NQD, just as in the case of steady heating.

The possibility of heat localization by means of a laser beam permits the use of a new class of substances, in photoengraving, including thermoreactive resins and certain coloring materials, with the concurrent elimination of a number of purely technological difficulties pertaining to the protection of complex light-sensitive polymers against exposure; the protection of complex light-sensitive polymers against exposure, the possibility of prolonged preservation, etc.

Batanov, V. A., V. A. Bogatyrev, N. K.

Sukhodrev, V. B. Fedorov. Spectral diagnostics of a plasma flare, generated by vapor products from laser-irradiated metals. ZhETF, v. 64, no. 3, 1973, 825-832.

Spectral diagnostics are described of a low-temperature plasma flare, produced by interaction of intense millisecond optical radiation with Bi and Al targets. The radiation source used was a 10 kjoule Nd glass laser with pulse duration  $\tau = 0.8$  msec. Temperature distribution was measured

along the flare over the intensity range  $I = (0.3-3) \times 10^7 \text{ w/cm}^2$  at pressures of (0.1-5) atm. It was seen that for the Al target the temperature variation profile along the flare at pressure  $p \leq 1 \text{ atm}$  corresponded to a gas dynamic vapor flow. For Bi, the characteristic temperature variation along the flare was observed in a gas dynamic regime with stationary shock wave and in a regime of strong metal shielding by the plasma, when the flare detached from the target. Maximum temperatures of  $T \approx 1.5-2 \text{ ev}$  were observed at a distance from the metal surface corresponding to the stationary shock wave relative to the target.

The vapor temperature near the target, i.e. at a distance of about the size of the irradiated spot, was found to be several times greater than the critical temperature for the target metal under test. This is direct proof that laser radiation of intensity  $I \approx 10^7 \text{ w/cm}^2$  primarily heats the dense vapor near the target. Electron density  $N_e$  was also measured in the plasma flare and it was noted that  $N_e$  at the shock wave front for pressures  $p \leq 1$  was  $2 \times 10^{17} / \text{cm}^3$  for Bi and  $8 \times 10^{16} / \text{cm}^3$  for Al. At a distance from the target of the order of irradiated spot diameter, the electron density  $N_e$  was found to be 2-4 times more than the above values. The article includes four graphs and four plasma flare spectrograms.

Gernitts, E., V. Ye. Mitsuk, and V. A. Chernikov. Study of laser radiation absorption in a laser spark in air. ZhTF, no. 3, 1973, 563-569.

The mechanism of laser radiation absorption in a laser spark was experimentally investigated. The time dependence of absorption during optical breakdown in air at atmospheric pressure was studied in two mutually perpendicular directions: along the axis of the excitation beam and perpendicular to it. The experiment was conducted with a ruby laser (peak

power = 30 Mw, pulse duration = 45 nsec, beam divergence  $\sim 8'$ ), according to the scheme shown in Fig. 1. An optical spark was formed during laser

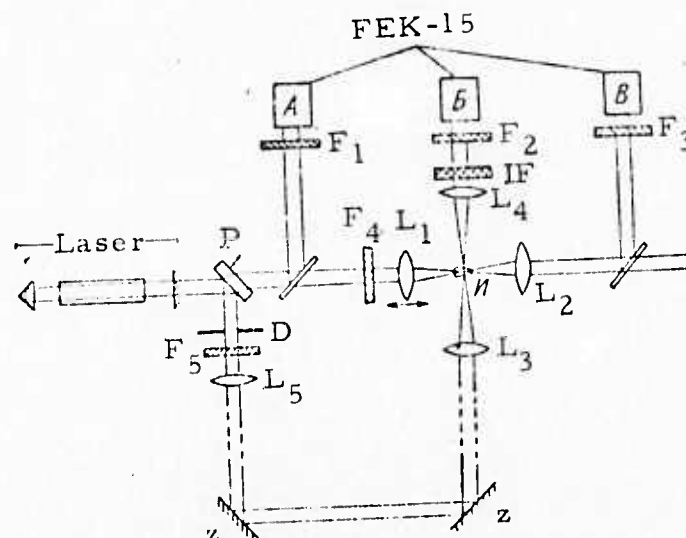


Fig. 1. Experimental diagram.

$L_1$ - $L_5$  - lens;  $F_1$ - $F_5$  - filter; IF - interference filter; z - mirror; D - diaphragm; P - plane-parallel plate.

radiation by focusing lens  $L_1$  ( $f = 24$  mm). Oscillograms were recorded of laser pulses incident on the spark and passing through it, as shown in Fig. 2. A sharp drop was noted in transient power after the breakdown, which

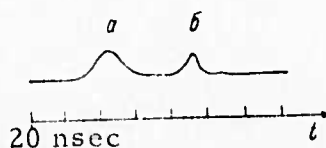


Fig. 2. Oscillograms of laser pulses:

(a) - incident; (b) - transmitted

took place during  $\sim 15$ -20 nsec; the fraction of energy absorbed by plasma in this case was  $\sim 50\%$ . Figures 3 and 4 show the time characteristics of the optical thickness  $\tau$  corresponding to the amplitudes of incident and

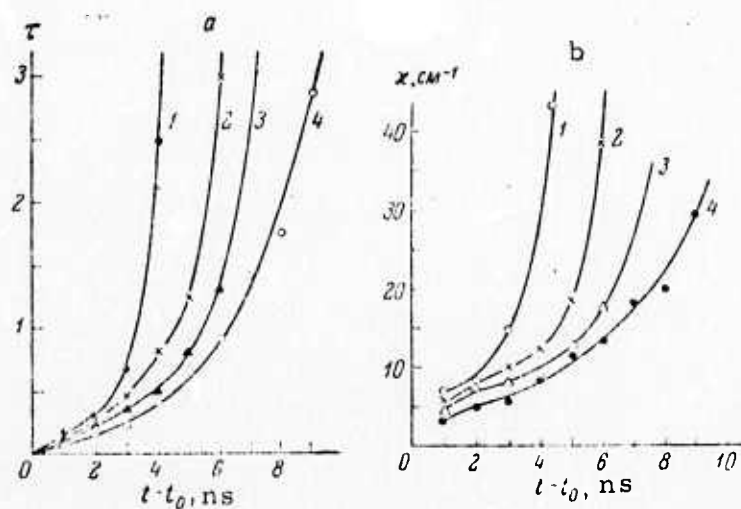


Fig. 3. Optical thickness (a) and absorption coefficient (b) of laser spark as a function of time  $t_0$  after breakdown.

1.  $I/I_p = 2$ ; 2.  $I/I_p = 1.6$ ; 3.  $I/I_p = 1.4$ ;  
4.  $I/I_p = 1.02$  where  $I$  = intensity of incident radiation,  $I_p$  = threshold radiation.

transmitted pulse, and absorption coefficient  $\chi$  of the plasma in axial and transverse directions, respectively. The absorption of laser radiation was found to take place in a comparatively narrow plasma layer  $\approx 0.4$ -0.5 mm, which propagates towards the laser beam with an average velocity of  $10^7$  cm/sec. The plasma velocity was determined by a DFS-2 diffraction spectrograph with a lattice of 1200 lines/mm and linear dispersion of  $4.2 \text{ \AA/mm}$ . Similar values of velocity were also obtained from experimental measurements of Doppler shift of laser radiation lines, scattered in the plasma. Experimental

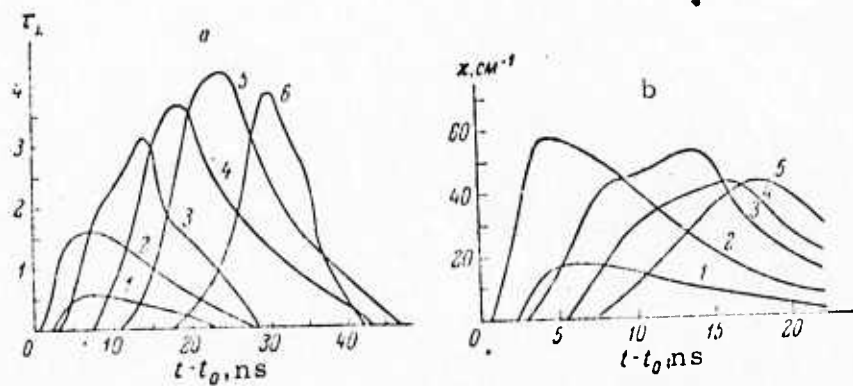


Fig. 4. Optical thickness (a) and absorption coefficient (b) of laser spark as a function of time after breakdown at different locations of arc channel along the axis:

1.  $x = -0.25$ ; 2.  $x = 0.1$ ; 3.  $x = 0.45$ ; 4.  $x = 0.8$ ;
5.  $x = 1.15$ ; 6.  $x = 1.5$  mm.

results are compared with theoretical calculations, based on the detonation mechanism of laser radiation absorption in an optical spark.

## B. Recent Selections

### i. Beam-Target Effects

Aleksandrov, V. I., A. G. Solov'yev, and P. I. Ulyakov. Space-time distribution of laser radiation with generation duration of the order of 1 msec, and its effect on interaction with a substance. FiKhOM, no. 4, 1973, 30-33.

Balatskiy, A. A., and M. S. Baranov. Effect of thermophysical properties on the behavior of fusing various metals by laser radiation. FiKhOM, no. 4, 1973, 8-13.

Bondarenko, B. V., V. A. Kuznetsov, and A. A. Shchuka. Field-emission microscopy of the interaction of laser radiation with a tungsten single crystal. ZhTF, no. 9, 1973, 1993-1995.

Bondarenko, G. G., L. I. Ivanov, and V. A. Yanushkevich. Interaction of giant laser pulses with the microstructure of aluminum. FiKhOM, no. 4, 1973, 19-21.

Gurevich, G. L., and V. A. Murav'yev. Effect of the temperature dependence of reflection coefficient on thin-film heating by laser radiation. FiKhOM, no. 4, 1973, 26-29.

Kask, N. Ye., L. S. Korniyenko, and G. M. Fedorov. Thermal destruction mechanism of optical glass by laser radiation. DAN SSSR, v. 211, no. 6, 1973, 1317-1319.

Marin, O. Ye., N. F. Pilipetskiy, and V. A. Upadyshev. Self-oscillating propagation of laser cracks. MP, no. 3, 1973, 475-481.

Popova, M. N., B. V. Rusetskiy, and S. I. Sviridov. Low-inertia energy transfer in KCl-In crystals, irradiated by laser light. AN LatSSR, Seriya fiziko-tekhnicheskikh nauk, no. 4, 1973, p. 121.

Popova, M. N., and I. Pelant. Band structure of silver halide crystals. Polarization relationship of two-photon absorption in AgCl. IN: *ibid.*, p. 16.

Uglov, A. A., A. N. Kokora, and M. A. Krishtal. Distribution of various elements in interaction zones of a laser beam during treatment of alloys. FiKhOM, no. 4, 1973, 3-7.

Uglov, A. A. Seminar on physics and chemistry of material processing by concentrated energy flux. FiKhOM, no. 4, 1973. 157-159.

Urazaliyev, U. S., Yu. M. Ukrainskiy, L. M. Goman'kov, and B. D. Galkin. Crystal structure and chemical composition of thin permalloy films, formed by laser radiation pulses in a free-running regime. FiKhOM, no. 4, 1973, 151-152.

Volod'kina, V. I., and V. L. Komolov. Thermal breakdown of semiconductors by light. ZhTF, no. 8, 1973, 1766-1769.

ii. Beam-Plasma Interaction

Bonch-Bruyevich, A. M., L. N. Kaporskiy, and A. A. Romanenkov. Effect of dielectric surface on optical breakdown of a gas. ZhTF, no. 8, 1973, 1746-1747

Gusev, V. K., G. M. Malyshev, G. T. Razdobarin, and L. V. Sokolova. Determining plasma parameters on the Tuman-2 during ohmic heating and compression by scattering. ZhTF, no. 8, 1973, 1748-1749.

Kiselevskiy, L. I. Spectroscopic and laser methods of plasma diagnosis. IN: Nauch. tr. In-t. mekh. Mosk. Un-ta., no. 20, 1973, 93-104. (RZhMekh, 8/73, no. 8B79)

Orayevskiy, V. N. Propagation and stability of waves of finite amplitude in plasma. IN: Sb. Probl. teorii plazmy. Kiyev, 1972, 219-230. (RZhMekh, 8/73, no. 8B124)

Zhuravlev, V. A., G. D. Petrov, and E. F. Yurchuk. Laser radiation scattering by a low-temperature plasma. TVT, no. 4, 1973, 874-875.

## 2. Effects of Strong Explosions

### A. Abstracts

Semiletenko, B. G., B. N. Sobkolov, and V. N. Uskov. Diagram of shock wave processes from unsteady interaction of a jet with a barrier. IAN SO SSSR. Ser. tekhn. nauk, v. 13, no. 3, 1972, 39-41.

When a supersonic underexpanded jet flows onto a flat barrier, the size of which considerably exceeds the maximum diameter of the jet, a stable regime and an unstable regime of interaction are observed. The stable regime is characterized by high-frequency oscillations at the barrier. The amplitude of these oscillations is small, and the shock waves in the jet before the barrier are practically stationary.

In a highly unstable regime the frequency of the pressure oscillations at some distance from the nozzle to the barrier decreases sharply, and the amplitude increases. The structure of the shock waves is very blurred with the central shock wave oscillating at high amplitude and frequency, corresponding to the frequency of the pressure oscillation.

The main feature of the interaction of a jet with a limitless flat barrier consists in the fact that the instability of the tangential discontinuity (see Fig. 1) causes a fluctuation of the size of the annular gap through which spreads the stream which has passed through the central shock wave of the jet. As a result, already during stable flow of the jet onto the barrier, when the pressure at the center of the barrier is maximal, the perturbations brought about by the oscillations of the annular gap propagate upstream along the subsonic stream of the central region, reaching the central shock wave. High-frequency pressure oscillations then take place at the barrier. During strong instability, when the pressure at the center of the barrier is smaller than at the periphery, closure of the central region as a result of adhesion of the tangential discontinuity to the surface of the barrier may be observed. The site of adhesion is located on the barrier at a distance from the jet axes, approximately equal to the radius of the jet.

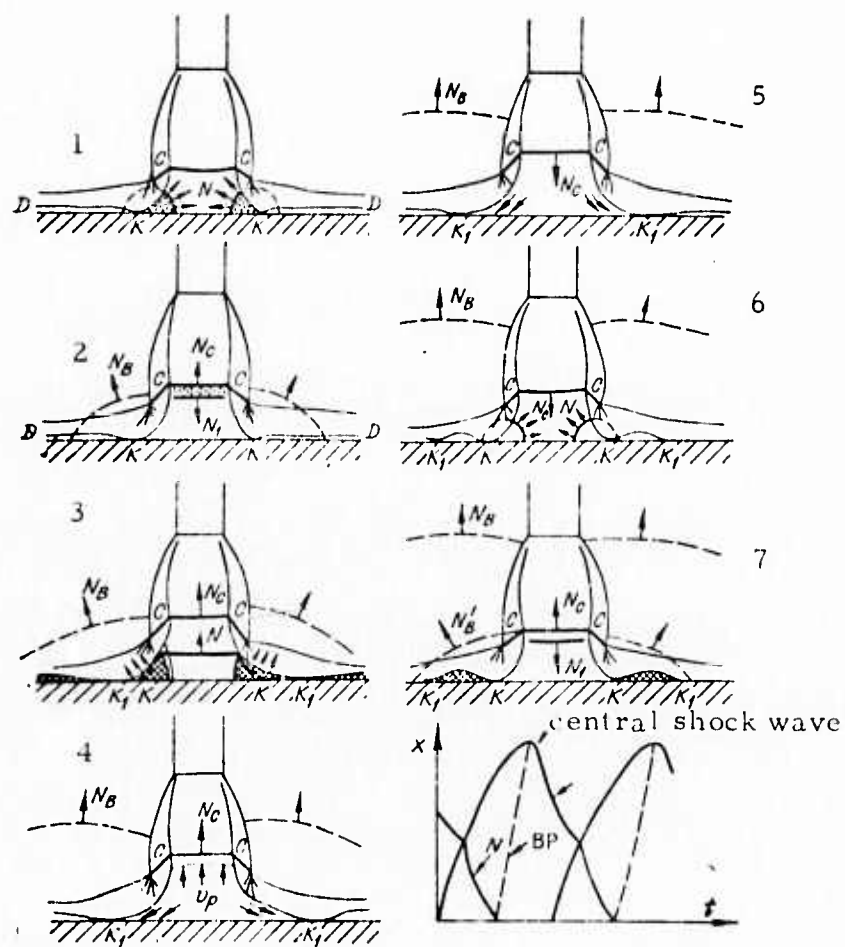


Fig. 1. Diagram of the shock-wave processes in a jet before a barrier in a regime of strong instability.

$N_c$  -- central shock wave    BP -- rarefaction wave

Figure 1 shows a diagram of the shock-wave process during such a collapse of the tangential discontinuity. Shock wave N originates at the moment of adhesion of the tangential discontinuity to the barrier in the vicinity of the point of adhesion K; part of it propagates from point K into the subsonic region towards the central shock wave. At the same time the annular supersonic stream displaces the gas which had previously been passing beneath the tangential gap, and shifts it along the barrier.

The process repeats itself, and may be considered to be self-oscillating. The change of position of the waves in front of the barrier with respect to time is shown schematically in the diagram, in accordance with the described shock-wave process. An explanation of the pattern of sound generation in the surrounding medium can be given, which is consistent with the adopted hypothesis of the course of the above process during the unstable interaction of a jet with a barrier.

Gershbeyn, E. A., N. N. Pilyugin, V. M.  
Ovsyannikov, O. N. Suslov, and G. A. Tirskey.  
Hypersonic flow around axisymmetric blunt  
bodies under intensive effects of convective and  
radiative heating. IN: Sbornik XIII Mezhdunarodnyy  
kongress po teoreticheskoy i prikladnoy mekhanike,  
1972. Sbornik annotatsiy, Moskva, Izd-vo Nauka,  
1972, 48-49. (RZhMekh, 1/73, no. 1B233)  
(Translation)

Navier-Stokes equations for laminar, multicomponent,  
partially-ionized gas mixtures, with radiation taken into account, are transformed  
into independent variables of the boundary-layer type. Boundary conditions

are formulated for a shock wave and for the disintegrating surface of a solid. The solution of the system of differential equations is found by the iteration method. The solution of a parabolic system of equations of a thin shock layer is used as the zero-order approximation. In the succeeding approximations, the discarded terms are taken into account. The effect of separation of the chemical elements in ionized, chemically balanced flows was found to influence convective currents and mass removal. The position of a "hanging" boundary layer was obtained; the distribution laws of radiative and convective heat fluxes were established, as well as those of the rate of mass removal along the generatrix of a body of revolution.

Kozlov, V. Effect of an underwater explosion on fish, and determination of the danger zone radius. Rybnoye khozyaystvo, no. 2, 1973, 18.

The effect of an underwater explosion on fish is described, and a procedure for determining the danger zone radius is presented. The well-known behavior of the hydraulic shock wave generated by the detonation wave of an exploding trotyl charge is summarized. A brief description is given of the pulsation of the gas bubble formed by the explosion products as a result of interaction with the shock wave; the number of pulsations may attain 10 cycles.

The value of the frontal pressure of a trotyl charge in water is calculated according to the following formula:

$$p = 532 \left( \frac{\sqrt[3]{G}}{R} \right)^{1.13},$$

where  $p$  is the maximum pressure within the shock wave front,  $\text{kg/cm}^2$ ; 532 is the trotyl coefficient which takes into account the properties of the

explosive; G is the mass of the explosive, kg; and R is the distance from the charge to the point under consideration, m.

The most unfavorable factor of those acting upon the fish is the hydrodynamic pressure within the shock-wave front. The internal organs and tissues near the swimming bladder are, by virtue of this pressure, displaced most strongly of all, within a fraction of a second, toward the center of the air volume of the bubble. As a consequence thereof excess pressures originate within the fish tissues, which cause their rupture. The more air the fish has in the swimming bladder, the greater is the damage incurred by it. A pressure of 40-50 kg force/cm<sup>2</sup> is assumed to endanger the life of a fish. A stunned fish, possessing a small reserve of air, ceases to be displaced and sinks.

The danger zone for fish is defined by means of the Cole formula and with knowledge of the value of the dangerous dynamic pressure (40 kg/cm<sup>2</sup>), namely

$$R^{1.13} = \frac{532 (\sqrt[3]{G})^{1.13}}{40}$$

In order to avoid even the slightest stunning of fish, the calculation formula must be increased by a factor of 5; this must be adopted as the safety radius. The remaining factors act within a much smaller radius than the cited danger radius and in this case their influence may be disregarded.

Bakhrakh, S. M., V. N. Zubarev, and  
A. A. Shanin. Shock waves in media with  
phase transitions. IN: Sb. Goreniye i  
vrryv, Moskva, Izd-vo Nauka, 1972, 554-  
560.

Shock wave propagation in a medium with phase transitions, i.e., a mixture of different phases, is described by a physicomathematical model. The physical model is a homogeneous continuum in a state of thermal and dynamic equilibrium. The mathematical description of medium motion is based on a set of gas dynamic equations, to which equations for pressure  $p$  as a function of density  $\rho$ , specific internal energy, and mass concentrations  $\alpha_i$  of each phase are added. The conversion kinetics equation completes the mathematical model. The equations of state of each phase are given.

The algorithm of solution to the formulated model is developed by the Newton iteration method or, more readily, by the method of component  $p$  equalization. Numerical calculation of  $\rho$ ,  $p$ ,  $\alpha_i$  is made for a graphite-diamond system. Using the parameter values from the equations of state, the authors calculate shock waves which are generated in graphite by the impact of an aluminum plate. The calculated velocities of a graphite-free surface behind a shock wave for different graphite thicknesses coincide with the experimental values.

Pashkov, P. O. Phase transitions in solids during treatment by strong shock waves. IN: Trudy volgogradskogo politekhnicheskogo instituta, no. 4, 1972, 129-140. (RZhMetallurgiya, 5/73, no. 51279)(Translation)

During strong dynamic compression, such as hydrostatic, phase transitions take place similar to those which follow during the decrease of shock volume, e.g.  $\alpha \rightleftharpoons \gamma$  transformations in Fe alloys. The temperature of martensite transition during application of pressure was lowered for achieving a nearly complete retransition back to the original in Fe-Ni alloys. by means of shock loading. Since the phase transition temperature increases with pressure increase, it is possible to obtain a transition by increasing the level of heat content, either by using a 'hot' scheme of shock loading, e.g. shear loading together with a plane shock wave, or by preliminary preheating of the specimen. It was noted that separation of the carbide phase from the monophase martensite of a series of carbon and alloyed steel is possible, if the plane wave pressure is sufficiently great ( $>400$  kbar). It is shown that Fe and Ti recrystallize as a result of  $\alpha-\gamma-\alpha$ -transitions (for Ti,  $\alpha \rightarrow \beta$  transition), if the plane wave pressure  $> 800$  and  $380$  kbar respectively. In case of Fe recrystallized by a shock from  $\alpha-\gamma-\alpha$ -transitions, the tendency towards cold brittleness was found to sharply decrease, while relationships of its plasticity and strength varied favorably at room and low temperature testings. The most difficult phase transition to achieve by shock compression was the one that takes place at below room temperature, followed by a volume increase.

Dolmatov, K. I. Plasmoids generated by electric wire explosion in air. IAN Uzb, no. 2, 1973, 57-59.

The article presents a detailed study of the plasma discharge generated by electric wire explosion in a chamber with an exit port, using a streak camera. Photographs were taken of the explosion of a 30 mm long, 0.2 mm dia. copper wire (Fig. 1). The wire was exploded at 20 kv. The discharge process was observed in three different stages: 1) plasma discharge from the chamber at a velocity 1.5-2 km/sec; 2) formation of plasmoids, and 3) movement of plasmoids. It was noted that the frictional force between

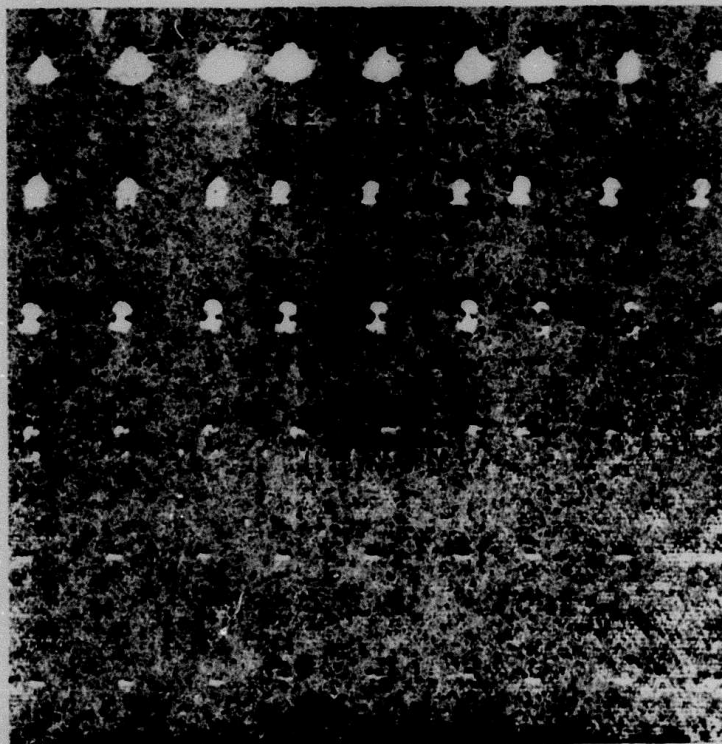


Fig. 1. High-speed photography (43,000 frames per sec) of plasma discharge.

the plasma bunch and medium plays an important part in plasmoid formation. Plasmoid dimensions did not depend on the initial condenser voltage within the 10-50 kv test range. External diameter of plasmoids generated was 20-25 cm and the internal, 10-12 cm. The plasmoid velocity was initially quite high, but quickly decreased to 20-40 m/sec; they also exhibited a pulsating character during movement. It was found that the life-time of plasmoids is directly proportional to the initial condenser voltage. (Fig. 2) and depend on plasmoid quality. During motion in air, they cover

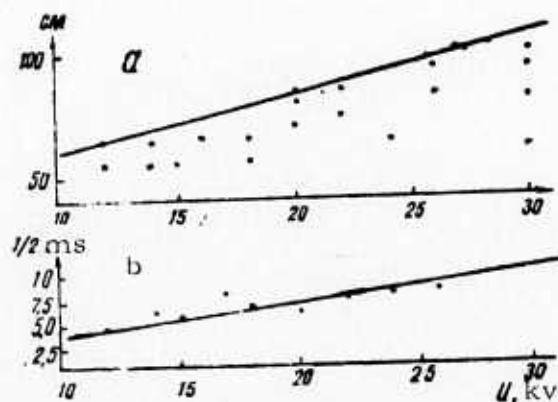


Fig. 2. (a) mean free path and (b) lifetime of plasmoid as a function of initial condenser voltage.

a certain distance, known as mean free path of plasmoid, which is also linearly related to the initial condenser voltage, in the absence of arcs between electrode and chamber walls (Fig. 2a).

The author suggests that it may be possible to obtain plasmoids which may travel hundreds of meters and exist for several minutes, at voltages  $=10^6$  v with corresponding energy. This suggests that ball lightning may be due to plasmoids generated during linear lightning discharges.

Gavrilin, A. I., M. A. Mel'nikov, and  
V. B. Shneyder. Ignition of initiators by  
an electric spark. IN: Sb. Gorennye i  
vzryv, Moskva, Izd-vo Nauka, 1972,  
44-48.

A thermal theory of detonation initiation in inorganic azides from an electric spark is expanded, and used as a model to study processes on the effective boundary surface of local heat sources. In the framework of thermal theory, two equations are derived with three unknowns: flash temperature  $T_*$ , specific power  $\epsilon_1$  of the external source, and ignition time lag  $t_3$ . The equations were used to calculate  $t_3 = f(T_*)$ ,  $t_3 = f'(\epsilon_1)$ , and  $\epsilon_1 = f''(T_*)$ . The temperature  $T_*$ ,  $\epsilon_1$ , and  $t_3 = f'(\epsilon_1)$  were also determined experimentally, and a comparison was made of the experimental and theoretical ignition characteristics. It shows that the  $t_3 = f(T_*)$  calculated from thermal theory agrees with the experimental function better than  $t_3 = f(T_*)$  calculated without allowance for heat losses. The only significant discrepancy between the experiment and thermal theory was observed in  $t_3 = f'(\epsilon_1)$  data. In general a good agreement between the two sets of data confirms the thermal nature of the electric spark-induced detonation of inorganic azides.

Shchirzhetskiy, Kh. A. Characteristics of  
acoustic impulses generated by explosive-  
type phenomena. Akusticheskiy zhurnal,  
no. 2, 1973, 293-296.

A comparative theoretical and experimental determination was carried out of the fundamental acoustical characteristics of an explosive impulse, generated by a pistol shot or a spark gap breakdown. Knowledge of duration  $\tau_1$ , energy  $E$ , and pressure spectrum  $S(\omega)$  of an acoustic impulse is required to analyze echo diagrams. Acoustic power density spectra

$W_i$  in a quarter-octave band were recorded and the corresponding sound power levels  $L_i$  were then calculated. The formulas for  $W_i$  were derived in linear acoustics approximation using either Cremer's or Lamb's model of acoustic explosion. The  $W_i$  formulas were used to calculate  $L_i$ .

Comparison of the theoretical  $L(f)$  functions thus calculated and the experimental  $L(f)$  for impulses generated by a pistol shot and a spark gap breakdown shows that both cited models approximate shock sound with about the same accuracy. For the sake of simplicity, the Cremer model was used to derive the expressions of  $\tau_i$ ,  $E$ , the spectral frequency  $\omega_{\max}$ , and bandwidth  $2\Delta f$ . The cited expressions determine fundamental parameters of explosive-type acoustic impulses, which may be used in measurements of room acoustics.

B. Recent Selections

i. Shock Wave Effects

Akhinyan, Zh. O., and A. G. Bagdoyev. Motion of an elastic half-space due to a shock wave in a magnetic field. IAN Arm, Mekhanika, v. 26, no. 3, 1973, 3-22.

Andriankin, E. I., and M. M. Kononenko. Plane shock wave attenuation during a high-velocity impact. FGiV, no. 4, 1973, 562-566.

Gordeyev, V. Ye., Yu. S. Matveyev, and Ya. K. Troshin. Imitation of detonation spin in nitrogen. DAN SSSR, v. 211, no. 4, 1973, 882-884.

Gurevich, A. V., and L. P. Pitayevskiy. Nonstationary structure of a collisionless shock wave. ZhETF, v. 65, no. 2, 1973, 590-604.

Kanel', G. I., and A. N. Dremin. Electric signals during compression of metal by a shock wave. DAN SSSR, v. 211, no. 6, 1973, 1314-1316.

Naboko, I. M. Gas dynamic phenomenon during expansion of shock-heated gas (flow through slit, orifice). IN: Nauch. tr. In-t mekh. Mosk. un-ta, no. 20, 1973, 53-67. (RZhMekh, 8/73, no. 8B248)

Pereverzev, A. Ye., D. A. Vlasov, and D. Kh. Kulev. Action of shock waves on polymers. ZhPKh, no. 8, 1973, 1847-1849.

Sobolenko, T. M., and T. S. Teslenko. Surface effects in metals after transit of plane shock waves. FGiV, no. 4, 1973, 571-575.

Yeremin, A. V., I. M. Naboko, and A. I. Opara. Total operating time in a shock tube during the study of discharge from an end aperture. TVT, no. 4, 1973, 823-831.

Zaslavskiy, B. I., and R. A. Safarov. Similarity of flows generated during weak shock wave reflections from a rigid wall and a free surface. FGiV, no. 4, 1973, 579-585.

ii. Hypersonic Flow

Dzvonik, L. I. Hypersonic stream-line flow of a three-dimensional body with local shock wave. DAN UkrSSR, no. 8, 1973, 717-721.

Shabanskiy, V. P., and A. P. Shister. Supersonic plasma flow from a rotating source. DAN SSSR, v. 211, no. 4, 1973, 825-828.

iii. Soil Mechanics

Gel'fand, F. M., V. I. Mamayev, D. I. Nenakhov, and Zh. U. Galiyev. Evaluating expansion parameters of detonation products during explosion of a blast-hole charge in a rock massif. IVUZ Gorn, no. 6, 1973, 54-59.

Kharitonov, V. N., and S. N. Pikar. Dynamic strength of brittle bodies with statistical distribution of cracks. IN: Sb. Mekh. i vzryvn. razrusheniye gorn. porod. Kiyev, Izd-vo Nauk, dumka, 1972, 94-98. (RZhMekh, 8/73, no. 8V523)

Koyshigunov, R. A., I. L. Zabudkin, D. T. Zil'berg, et al. Kompleksnaya mekhanizatsiya vzryvnykh rabot na gornorudnykh predpriyatiyakh. [Obzor]. (Broadscale mechanization of blasting operations in mining enterprises. [Review]). Moskva, 1973, 73 p. (KL Dop vyp, 7/73, no. 15204).

Savenko, S. K., A. A. Gurin, and P. S. Malyy. Udarnyye vozdushnyye volny v podzemnykh vyrabotkakh. (Air shock waves in underground mining). Moskva, Izd-vo Nedra, 1973, 152 p. (RZhMekh, 8/73, no. 8B200 K).

Sergeyev, I. T. Wave propagation in highly elastic rock and loose materials. IN: Tr. koordinats. soveshch. po gidrotekhn., no. 80, 1973, 129-131. (RZhMekh, 8/73, no. 8V540).

Yalanskiy, A. A. Investigating the stressed condition and fissuring of sedimentary rock by an ultrasonic method. IN: Sbornik. Mekh. i vzryvn. razrusheniye gorn. porod. Kiyev, Izd-vo Nauk, dumka, 1972, 71-76. (RZhMekh, 8/73, no. 8V524)

Yegorov, P. V., and R. F. Gordiyenko. Effect of fissility on the rock destruction process in a rock-burst focus. IN: Sb. nauch. tr. Kuzbas. politekhn. in-t, no. 48, 1973, 62-65. (RZhMekh, 8/73, no. 8V539)

iv. Exploding Wire.

Bordzilovskiy, S. A., S. M. Karakhanov, and V. V. Polyudov. Electron emission from dynamic heating of wires by a pulsed current. ZhTF, no. 9, 1973, 1987.

v. Equations of State.

Burshteyn, L. M., and V. A. Rabinovich. The equation of state of liquid parahydrogen. IAN B, Seriya fizika-energeticheskikh nauk, no. 3, 1973, 74-82.

Fokin, L. R. Methods of determining parameters of thermal equations of state, taking into account data on phase equilibrium curves. TVT, no. 4, 1973, 750-756.

Gavrilov, S. D. Relation of the equation of state to intermolecular potential. TVT, no. 4, 1973, 886-887.

vi. Miscellaneous Effects of Explosions

Blyumin, M. A., A. M. Blyumina, N. L. Kmitovenko, and Ya. M. Puchkov. Photogrammetric determination of the rock fragment scattering from a large scale explosion. IN: Tr. Sverdl. gorn. in-ta, no. 89, 1972, 24-27. (RZhGeod, 1/73, no. 1. 52. 213).

Blyumina, A. M. Errors in basic elements of stereophotogrammetric filming of an explosion. IN: ibid., 28-33. (RZhGeod, 1/73, no. 1. 52. 214).

Blyumina, A. M. Determining spatial coordinates of fragments in an explosion process according to stereophotogrammetric filming. IN: ibid., 34-38. (RZhGeod, 1/73, no. 1. 52. 215)

Boronin, A. P., Yu. A. Medvedev, and B. M. Stepanov. Unified electric pulse and scattering dynamics of the products of an explosive charge. FGiV, no. 4, 1973, 541-551.

Boyko, I. F., A. A. Vovk, and A. G. Gubarev. Using explosion energy in land reclamation construction. Gidrotekhnika i melioratsiya, no. 7, 1973, 25-28.

Kuznetsov, V. M. Destruction of metallic rings in a plastic state. FGiV, no. 4, 1973, 567-571.

Popov, Ye. I., V. G. Poyarkov, Yu. A. Finayev. Studying the growth rate of pressure during explosion of aluminum powders. IAN B, Seriya fiziko-energeticheskikh nauk, no. 3, 1973, 92-94.

Sonnov, A. P., and Yu. P. Trykov. Calculating explosion-welding parameters of multilayered joints. FiKhOM, no. 4, 1973, 128-133.

### 3. Geoscience

#### A. Abstracts

Komissiya mnogostoronnego sotrudnichestva  
Akademiya nauk sotsialisticheskikh stran. . . ,  
et al. Stroyeniye zemnoy kory tsentral'noy i  
yugo-vostochnoy Yevropy; po dannym vzryvnoy  
seysmologii (Crustal structure of central and  
southeastern Europe; based on explosion  
seismology data). Kiyev, Izd-vo Naukova  
dumka, 1971, 182-284.

The material presented below is a continuation of extracts  
from individually authored chapters and sections of the above monograph.  
The introduction is repeated in this continuation, since there are several  
references to the profiles shown in Figure 1.

## INTRODUCTION

At the 1963 VI Congress of the Carpatho-Balkan Geological Association, its Geophysical Commission passed a resolution to initiate coordinated studies of the deep crustal structure in the Carpatho-Balkan system and adjacent regions. For this purpose the following eight international profiles were planned:

- I. Kharkov - Melitopol' - Black Sea (USSR);
- II. Baturin - Kishinev (USSR) - Brani (Rumania) - Maritsa (Bulgaria);
- III. Ostrog - Dolina - Beregovo (USSR) - Debrecen - Szeged (Hungary) - Dubrovnik (Yugoslavia);
- IV. Debrecen - Kaposvar (Hungary);
- V. Warsaw - Zakopane (Poland) - Kosice (Czechoslovakia) - Debrecen (Hungary);
- VI. Debrecen (Hungary) - Brno - Prague (Czechoslovakia) - Weimar (German Democratic Republic);
- VII. Kaliningrad (USSR) - Poznan (Poland) - Prague (Czechoslovakia);
- VIII. Rostov - Kirovograd - L'vov (USSR) - Swietokrzyskie Mountains (Poland).

In 1966, the European Seismological Commission, at its congress in Copenhagen, established a working group on the explosion seismology projects in Europe.

In 1966, the Commission for Multilateral Collaboration between the Academies of Sciences of Socialist Countries established a working group on deep seismic sounding.

The original program was expanded by adding five more profiles:

- IX. Azov Sea - Black Sea (Nogaysk - Sinop peninsula in Turkey);
- X. Black Sea (Caucasus) - Bulgaria (Varna) - Yugoslavia (Makresh);
- XI. Black Sea (Crimea - Danube River delta) - Rumania (Galati - Vrancea) - Hungary (to the intersection with Profile IV);
- XII. USSR - Rumania - Bulgaria (between Profiles II and III);
- XIII. Southwestern Black Sea - Bulgaria (Burgas - Rhodope Mountains) - Yugoslavia (to the Adriatic Sea).

In addition, many countries (USSR, Yugoslavia, Hungary) planned national profiles in order to study specific geological structures.

The location of the DSS profiles completed by January 1971 are shown in Figure 1.

The field work and interpretation of profile sectors located in the border areas were conducted jointly.

The deep seismic studies were conducted using the technique of continuous profiling to obtain fully correlated systems of time-distance curves for the waves from all main crustal interfaces. Discrete observation systems were employed only at the initial stage and in poorly accessible regions.

The distribution of the completed 13,300 km of profiles is as follows: 1) Bulgaria - 670 km; 2) Hungary - 1200 km; 3) German Democratic Republic - 200 km; 4) Poland - 1050 km; 5) Rumania - 200 km; 6) USSR - 5100 km; 7) Czechoslovakia - 600 km; 8) Yugoslavia - 700 km; and 9) Black and Azov Seas - 3700 km.

It is mentioned that, in recent years, East Germany has been using the "Zemlya" seismic recording system for a large volume of its crustal-study programs.

The present monograph represents the first attempt at summarizing the results of crustal studies in central and southeastern Europe. The monograph includes the description of all international profiles. An attempt is made to determine the correlation between deep and near-surface geological structures, as well as to give an explanation of the evolution of certain geological megastructures.

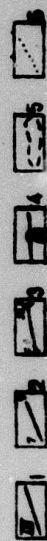
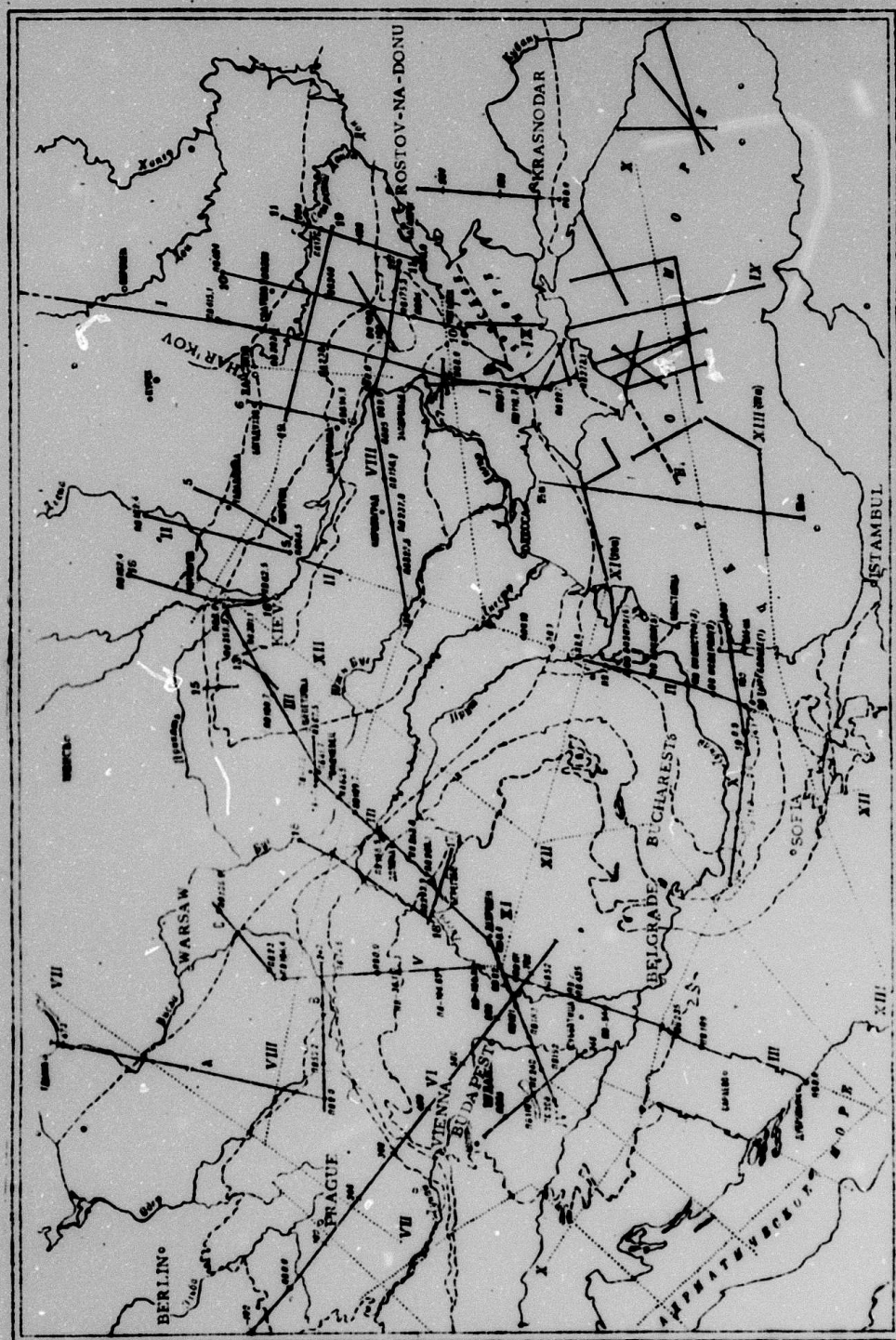


Fig. 1. Location of DSS Profiles in Central and Southeastern Europe.

- 1 - International profiles; 2 - national profiles; 3 - profile end and marker points; 4 - shot points;
- 5 - boundaries of geological regions; 6 - planned profiles.

Czechoslovakian Socialist Republic

Beranek, B. Ya. Weiss, A. Hrdlicka,  
U. Zaunkova, A. Fejfar, A. Dudek, and  
M. Suk.

Crustal studies in Czechoslovakia were conducted along international profiles V, VI and VII (see Fig. 23).

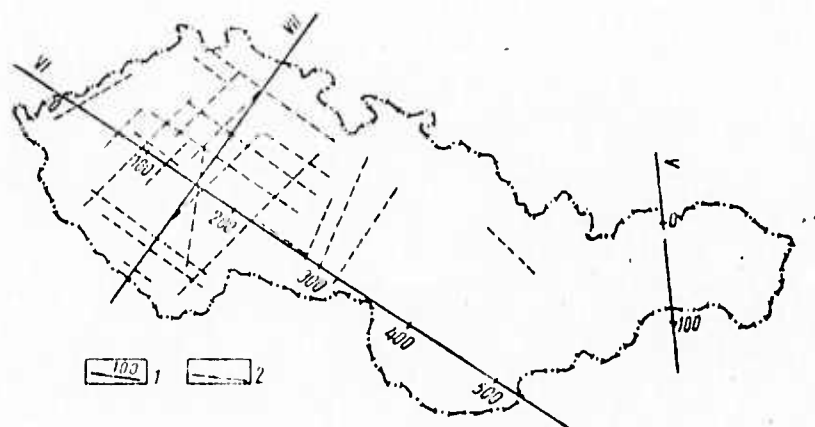


Fig. 23. Location of International Profiles V, VI and VII in Czechoslovakia.

1 - DSS profiles; 2 - high mobility belts (after A. Zatopek)

Profile V crosses the Outer Carpathians (Mahur flysch), a zone of klippen, the Inner Carpathians, and the Slovak karst. Profile VI crosses the Bohemian massif, the Cis-Carpathian foredeep, the Outer and Inner Carpathians, and the Pannonian depression. Profile VII crosses the Bohemian massif.

Seismic observations along profile VI were made using an observing system intended for continuous tracing of the Moho discontinuity using wide-angle reflection data. It was subsequently supplemented in order to record head waves from the Moho discontinuity.

The observing system on the 250-km-long Poland Czechoslovakia-Hungary sector of profile V consisted of two shot points in Germany (164.4 and 74.6), one in Czechoslovakia (36.1), and two in Hungary (106.65 and 169.1).

The seismic instruments used included SS-30/60 CMRW seismic system and SPEN-1 seismometers with a natural frequency of about 10 Hz and NS-3 seismometers with a natural frequency of about 4 Hz. The seismometers were arranged at 100-200 m intervals. The charges were detonated in 40-50-m-deep holes. Large charges (up to 800 kg in the Bohemian massif and 1200 kg in the Carpathians) were detonated in groups spaced 15-20 m apart. Single charges in a group did not exceed 100 kg.

The following wave groups were identified on all profiles:  $P^{oc}$  - associated with interfaces within the sedimentary layer (mostly in the Carpathians);  $P^K$  - associated with the crystalline basement surface and interfaces within the consolidated crust; and  $P^M$  - associated with the Moho discontinuity ( $P_{refl}^M$  - wide-angle reflections and  $P^M$  - head waves).

The velocity distribution in the crust of the Bohemian massif and Carpathians is derived from continuously refracted waves (Kondrat'yev method), reflected waves (Yegorkin method), and by the Wiechert-Herglotz method. The velocity-depth curves for the Bohemian massif and Carpathians are shown in Figure 24.

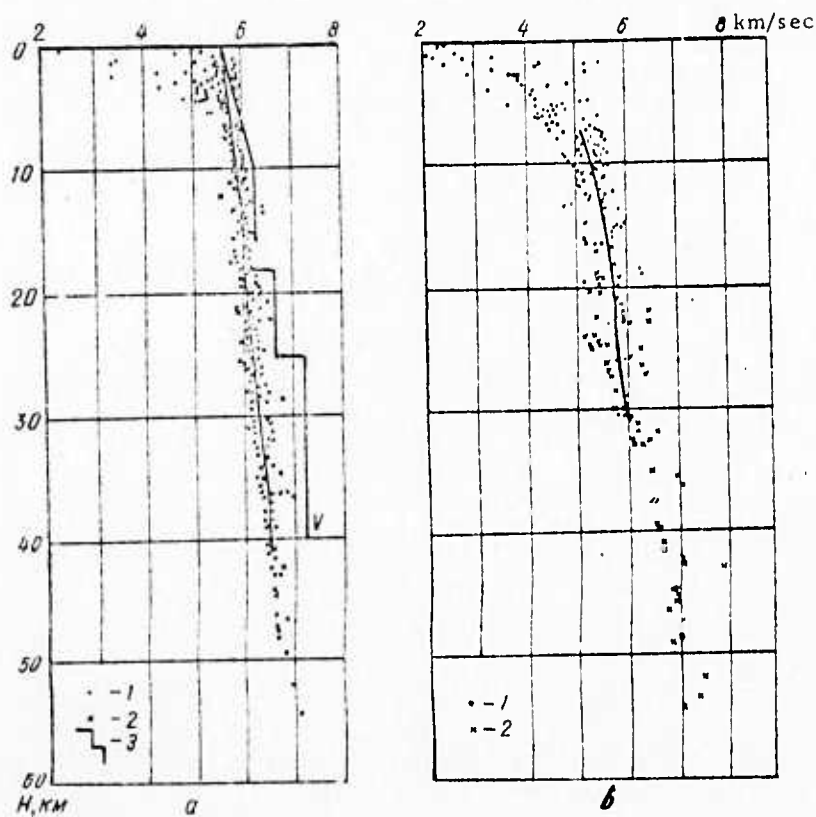


Fig. 24. Velocity-Depth Curves for the Bohemian Massif (a) and Carpathians (b).

1 - Effective velocities determined by the Kondrat'yev method; 2 - the same, determined from reflected waves; 3 - interval velocities.

The effective velocity in the Bohemian massif gradually increases with depth, from 5.6 to 6.5 km/sec. A low velocity zone is observed at a depth of 15 km; its lower limit and velocity are not determined reliably. The velocity distribution in the Carpathians is characterized by high lateral variations (see Fig. 25).

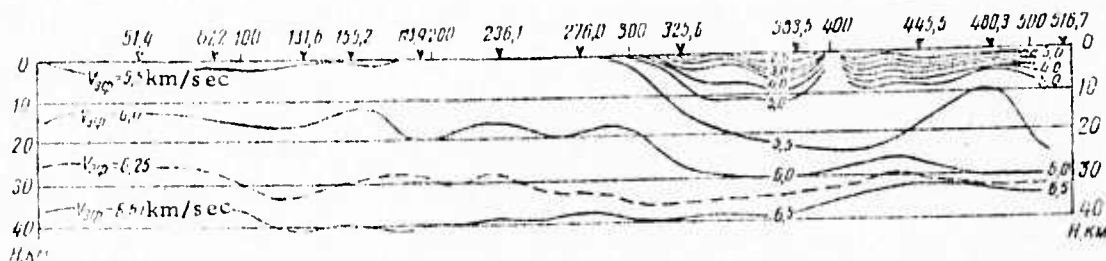


Fig. 25. Velocity Section along Profile VI (in terms of isolines of effective velocity).

The crustal section (see Fig. 26) on the Czechoslovakian sector of international profile VI is inferred from DSS and gravity data.

The average crustal thickness in the Bohemian massif is about 34 km, while it is 28-30 km in the Carpathians. The crust is divided into blocks by abyssal faults. The following abyssal faults are tentatively outlined: in the region of the Doupovske Mountains; between the Central Bohemian Pluton and Moldanubicum; on the eastern border of the Central Pluton; and the faults bounding the Vienna graben. The abyssal fault on the eastern border of the Vienna graben represents a tectonic suture which divides the Outer and Inner Carpathians. Some of the abyssal faults coincide with previously determined mobile zones (see Fig. 23).

The Moho discontinuity forms uplifts in the Doupovske Mountains (29-30 km) and the eastern Moldanubicum. Pronounced depressions are observed in the Central Bohemian Pluton and the western Moldanubicum (38 km). The Moho discontinuity rises southeastward from the Vienna graben (34-35 km) to the Pannonian depression (28 km).

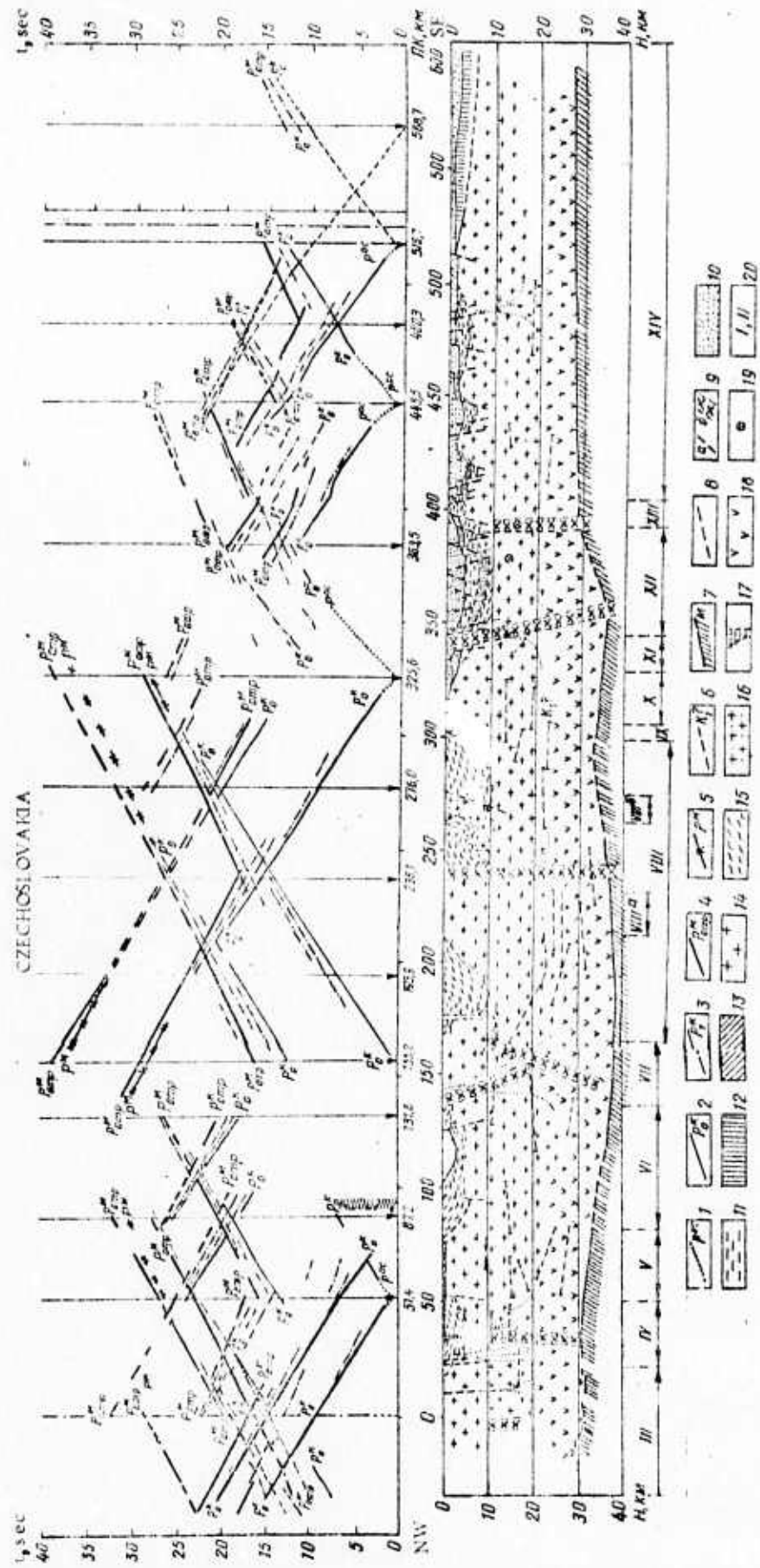


Fig. 26. System of Time-Distance Curves and Seismogeological Section along International Profile VI (territory of Czechoslovakia).

1-5 Time-distance curves for waves from: 1- interfaces within the sedimentary layer; 2- crystalline basement surface; 3- basaltic layer surface; 4- Moho discontinuity, reflected; 5- Moho discontinuity, refracted; 6- assumed Conrad discontinuity; 7- Moho discontinuity; 8- reflection surfaces within consolidated crust; 9a- abyssal faults from geological data; 9b- abyssal faults from DSS data; 10- molasse complex; 11- Flysch; 12- Mesozoic sediments; 13- Paleozoic sediments; 14- granitic layer; 15- crystalline schists; 16- siennites; 17- neovolcanites; 18- basaltic layer; 19- diffraction points; 20- tectonic zones and blocks. (III - VIII - Bohemian massifs: III- Krushe Mountains (Erz Gebirge); IV- Doupovske Mountains; V- Kladno-Rakovnik basin; VI- Barrandien; VII- Central Bohemian Pluton; VIII- Moldanubicum; VIIla- Central Pluton; VIIlb- Trebic massif; (IX - XIII - Carpathians): IX - Moravicum and Brno massif; X- Cis-Carpathian foredeep; XI- Western Flysch Carpathians; XII- Vienna graben; XIII- Pannonian depression.

The Conrad discontinuity is defined presumably from DSS and gravity data. It forms uplifts in the Doupovske Mountains, where a thickened basaltic layer is assumed. Farther southeastward, the Conrad discontinuity has a very complex relief and the relationship between the granitic and basaltic layers varies considerably. Thus, the Conrad discontinuity forms an uplift in the Central Bohemian Pluton and the basaltic layer is thick; in the Central Pluton, it descends, while in the eastern Moldanubicum it again rises (probably to 20 km). In the Vienna graben, the Conrad discontinuity occurs at a depth exceeding 25 km, while in the Pannonian depression it is at 17 km.

Since the entire region east of the abyssal fault at the border of the Vienna graben has an anomalous characteristic, its crustal structure is not clearly determined. According to DSS data, a buried ridge which divides the eastern Alps from the western Carpathians is found in the Carpathian foredeep. Here, the granitic layer surface and the Moho discontinuity are not subsided as much as in the eastern Carpathians or the Alps.

The crustal thickness along profile V (see Fig. 27) increases gradually northward from about 29 km at the Czechoslovakian-Hungarian border. In the region of the Outer Carpathians, the Moho discontinuity lies at a depth of 42 km (a second Moho discontinuity is at about 50 km). An abyssal fault dividing the Outer and Inner Carpathians is assumed in the zone of klippens.

## CZECHOSLOVAKIA

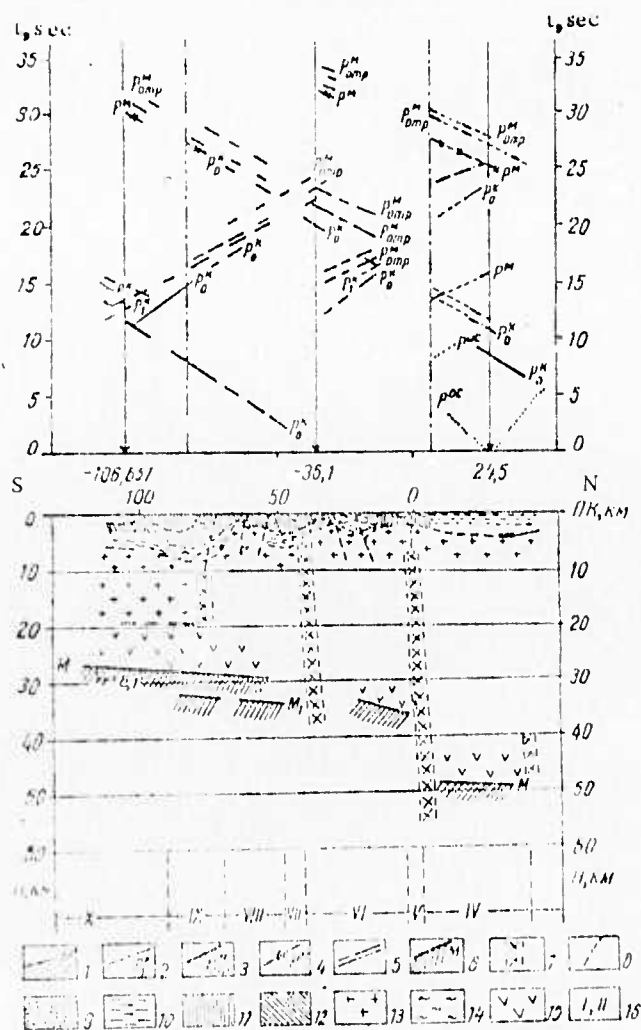


Fig. 27. System of Time-Distance Curves and Seismogeological Section along International Profile V (territory of Czechoslovakia).

Time-distance curves for waves from: 1- crystalline basement surface; 2- basaltic layer surface; 3- Moho discontinuity, reflected; 4- Moho discontinuity, refracted; 5- Interfaces within the consolidated crust; 6- M discontinuity; 7- abyssal faults; 8- faults from geological data; 9- molasse complex; 10- flysch; 11- Mesozoic sediments; 12- Paleozoic sediments; 13- granitic layer; 14- crystalline schists; 15- basaltic layer; 16- tectonic zones and blocks: IV- flysch zone; V- zone of klippen; VI- Inner Carpathians; VII- Severo-Homerske synclinorium; VIII- Spissko-Homerske Mountains; IX- Slovak karst; X- Pannonian depression.

Socialist Federal Republic of Yugoslavia

Prosen, D., B. Milovanovic, and M. Roksandic

Crustal studies in Yugoslavia were conducted along international profile III and national profile Palagruza-Derвента (see Fig. 1).

Profile III in the territory of Yugoslavia crosses the Pannonian depression, the Inner and Outer Dinarides, and terminates in the Adriatic Sea. The Palagruza-Derвента profile crosses the Adriatic Sea (from the Island of Palagruza) and the Dinarides northwest of profile III.

Field work was performed by: 1) continuous profiling on the Yugoslav sector of international profile III and 2) discrete profiling on national profile Palagruza - Derвента.

The seismic instruments used included Texas Instrument 7000 B seismic system and S-36 and M-200 seismometers arranged at 150-m intervals. The charges (100 - 1400 kg) were detonated at sea (50 - 100 m deep) and on land in groups of 25 - 40-m-deep shot holes. The following wave groups were identified:  $P^{OC}$  - associated with interfaces within the sedimentary complex;  $P_o^K$  - associated with the crystalline basement;  $P_{1,2}^K$  - associated with interfaces within the consolidated crust; and  $P^M$  - associated with Moho discontinuity.

The thickness of the crust on the Yugoslav sector of international profile III (see Fig. 28) varies from 22 km in the Pannonian depression to 45 km in the Dinarides. The crust is divided into blocks by abyssal faults. The thickness of the basaltic layer varies from 7-8 km in the Pannonian depression to 20-25 km in the Dinarides. The crust is characterized by roots observed beneath the Dinarides.

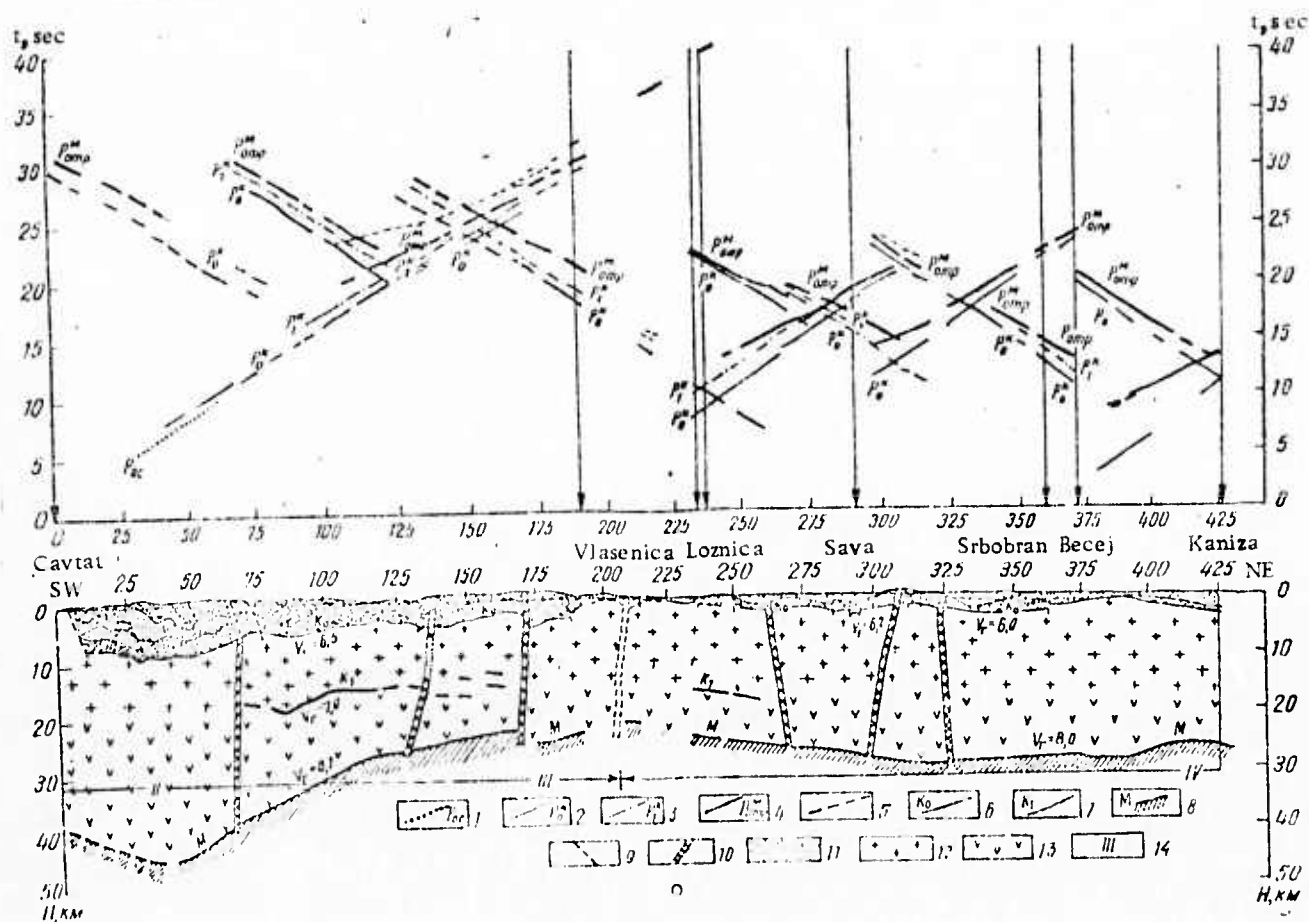


Fig. 28. System of Time-Distance Curves and Seismogeological Section along Profile III (territory of Yugoslavia).

Time-distance curves for waves from: 1- interfaces within the sedimentary layer; 2- crystalline basement surface; 3- basaltic layer surface; 4- Moho discontinuity, reflected; 5- irregular waves; 6- crystalline basement surface; 7- Conrad discontinuity; 8- Moho discontinuity; 9- faults from geological data; 10- abyssal faults; 11- sedimentary layer; 12- granitic layer; 13- basaltic layer; 14- tectonic zones and blocks: II- Outer Dinarides; III- Inner Dinarides, IV- Pannonian depression.

The consolidated crust surface ( $K_0$  interface) gradually rises toward the northwest from a depth of 10 km in the Outer Dinarides to minimum depths in the Pannonian depression (Loznica and Fruska Gora areas). It forms anticlinal and synclinal bends.

The Conrad discontinuity, which is not traced continuously, lies at depths of 16-19 km. The Moho discontinuity rises rapidly from the Outer Dinarides (45 km) to the Foca region. Farther on, it continues rising slowly toward the Pannonian depression where it reaches minimum depth (22 km in the Loznica area).

According to tentative results, the crustal thicknesses determined along national profile Palagruza-Derвента (see Fig. 29) are 52 km in the Outer Dinarides (Livno area), 36 km in the Adriatic Sea basin (near the Island of Korcula), and 30-32 km north of the Dinarides (Kotorvaros area). The thickness of the sedimentary cover varies significantly along the profile, with its maximum value at 16-17 km in the Livno area.

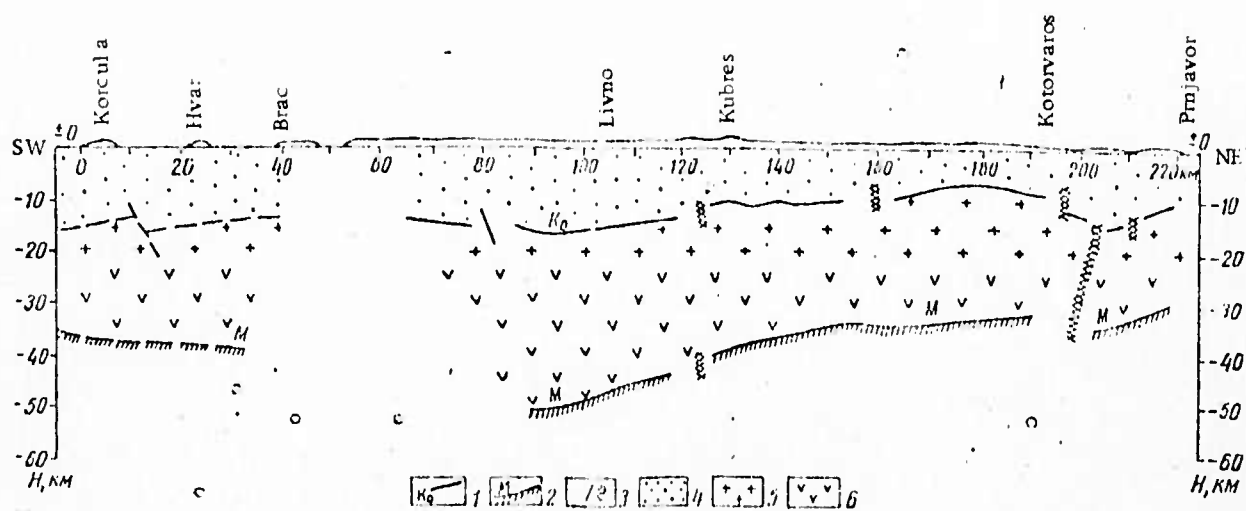


Fig. 29. Seismogeological Section along the Yugoslavian National Profile Palagruza-Derventa.

1- Crystalline basement surface; 2- Moho discontinuity; 3- faults (a- from geological data, b- abyssal); 4- sedimentary layer; 5- granitic layer; 6- basaltic layer.

## Results of Deep Seismic Sounding in the Black Sea

Garkalenko, I. A.

Crustal studies in the western part of the Black Sea basin were conducted along profiles 25 M, 26 M (part of international profile XI), and 27 M (part of international profile XIII). These are located in the immediate proximity of the continental structures of the Carpatho-Balkan region (see Fig. 1).

Submeridional profile 25 M intersects the marginal part of the East European platform, the Scythian plate, and the deep-water portion of the Black Sea basin. Sublatitudinal profile 26 M and 27 M cross the Scythian plate and the deep-water portion of the Black Sea, respectively.

Field work performed in the western part of the Black Sea basin was characterized by very dense observation systems (20 - 40 km-spaced recording points and 1.5 - 2.0-km-spaced shot points) and the generating and recording of seismic waves both at sea and on land. Charges detonated at sea did not exceed 130 kg. At two continental shot points (northern part of profile 25 M), charges of 800 - 1200 kg were detonated in groups of 20 - 40-m-deep shot holes. Recording of seismic waves was made using multichannel seismic system and SPEN-1 and NS-3 seismometers, recording ships, sea bottom seismic instrumentation and radio buoys.

The following wave groups associated with interfaces in the consolidated crust were identified:  $P^K$  - associated with the basement surface and interfaces within the granitic layer;  $P_1^K$  - associated with the Conrad discontinuity; and  $P^M$  - associated with the Moho discontinuity (see Fig. 30).

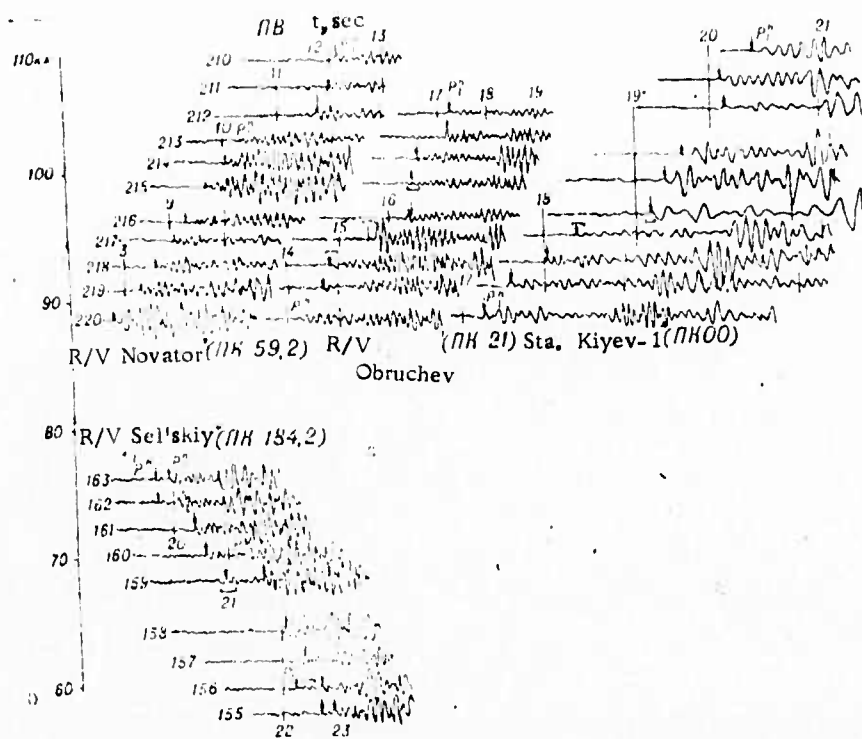


Fig. 30. Seismograms showing  $P^K$ ,  $P_1^K$ , and  $P^M$  phases, recorded in the Black Sea.

The  $P^M$  wave group is traced reliably, both as first and later arrivals, although their recording intervals and travel times differ greatly for the ship and shore recording stations. The intense, well-correlated  $P_{\text{refl}}^M$  waves, recorded as later arrivals by land stations in the shelf zone at distances of 75-85 km with  $v^* = 9.5$  km/sec, are identified as wide-angle reflections. Beyond the critical point, at distances greater than 120-130 km,  $P_{\text{refl}}^M$  and  $P^M$  waves are recorded, the second identified as a head wave.

At sea stations,  $P^M$  waves are recorded as later arrivals at distances of about 130 km (21-22 sec). At 140-150 km, the  $P^M$  waves emerge as first arrivals. They are continuously traced up to 180 km, and are characterized by  $v^* = 6 - 8$  km/sec and insignificant attenuation. They are identified as being head waves.

Velocity distribution along profile 25 M and 26 M was determined by the Chibisov method. The average velocity isolines are shown in Figures 31 and 32. The distribution of effective velocity along profile 25 M accurately reflects the block-layered structure.

The inferred model of the crust along profiles 25 M and 26 M is characterized by block-layered structure. In the regions of the Peri-Black Sea depression and the Black Sea basin, the crustal granitic layer has a reduced thickness while in the deep portion of the Black Sea basin, it thins out even more.

Three large blocks are identified on profile 25 M: the East European platform to the north, and the Scythian plate and Black Sea basin to the south. The crustal thickness in the East European platform is 40 km. The crustal thickness in the Scythian plate lessens to 28 - 30 km, as do the thicknesses of the granitic and basaltic layers. In the transition zone between the Scythian plate and Black Sea basin (between the 190 and 300 km points of the profile), the granitic layer gradually thins out. In the deep-water portion of the Black Sea basin, the 18-km-thick crust consists of sedimentary (10 - 12 km) and basaltic (7 - 9 km) layers. The same crustal thickness is found in the deepwater portion of profile 27 M.

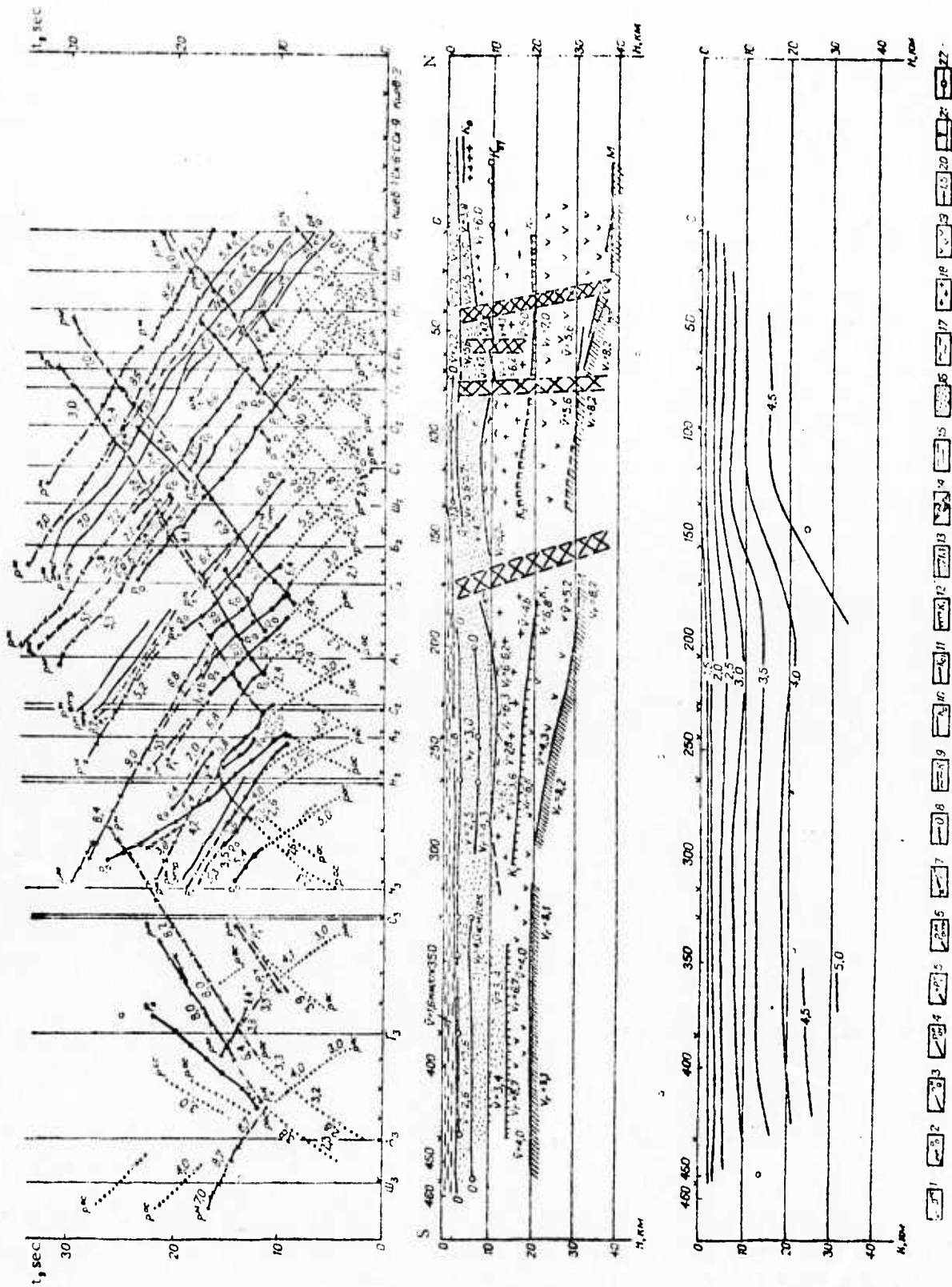


Fig. 31. System of Time-Distance Curves, Seismogeological Sections, and Effective Velocity Isolines along Profile 25 M.

Time-distance curves for waves from: 1- interfaces within the sedimentary layer; 2- Paleozoic basement surface; 3- crystalline basement surface; 4- interfaces within the granitic layer; 5- basaltic layer surface; 6- M discontinuity, reflected; 7- M discontinuity, refracted. Interfaces: 8- interfaces within the sedimentary layer; 9- Paleozoic basement surface; 10- Moho discontinuity; 11- interfaces within the granitic layer; 12- Conrad discontinuity; 13- Moho discontinuity; 14- abyssal faults; 15- water; 16- sedimentary layer; 17- Paleozoic complex; 18- granitic layer; 19- basaltic layer; 20- velocity isolines; 21- receiving points; 22- points where depths were determined.

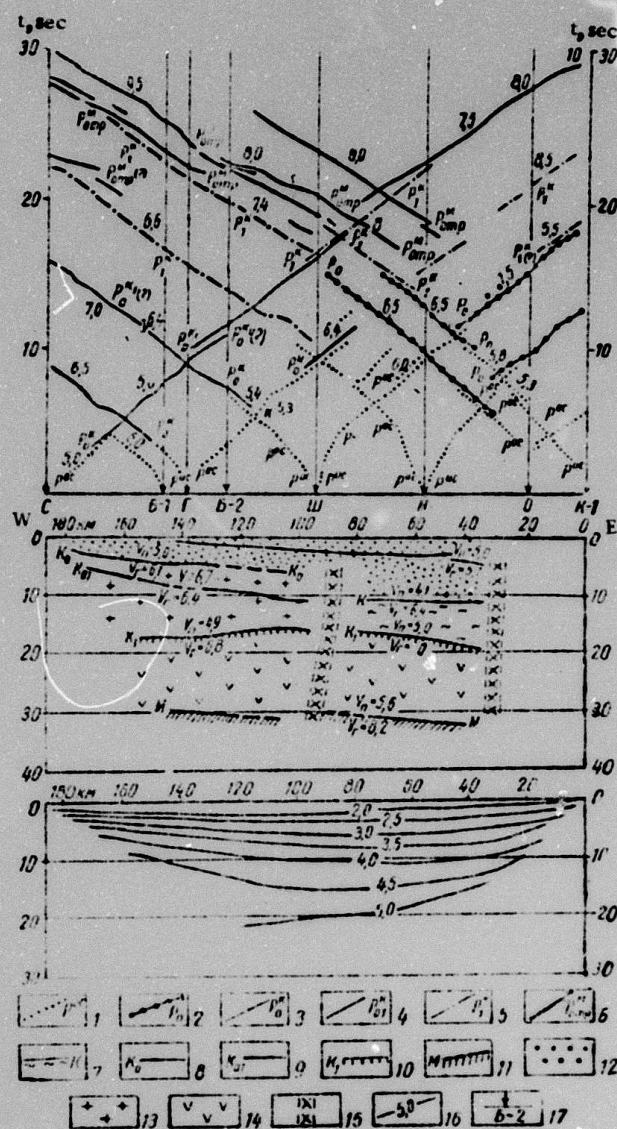


Fig. 32. System of Time-Distance Curves, Seismogeological Section, and Effective Velocity Isolines along Profile XI (26 M).

Time-distance curves for waves from: 1- interfaces within the sedimentary layer; 2- Paleozoic basement surface; 3- crystalline basement surface; 4- interfaces within the granitic layer; 5- basaltic layer surface; 6- M discontinuity, reflected. Interfaces: 7- Paleozoic basement surface; 8- crystalline basement surface; 9- interfaces within the granitic layer; 10- Conrad discontinuity; 11- Moho discontinuity; 12- sedimentary layer; 13- granitic layer; 14- basaltic layer; 15- abyssal faults; 16- velocity isolines; 17- receiving points.

The crust on profile 26 M is divided by the submeridional Odessa abyssal fault zone (between km 80 and 100) into two blocks with different thicknesses of the consolidated crust. The thickness of the consolidated crust is 25 - 27 km west and 18 - 20 km east of the abyssal fault.

Chapter III. Results of deep seismic sounding  
on international profiles.

Minuch, E., K. Posgay (Hungary), Kh. Militser,  
Ch. Knothe (German Democratic Republic), I.  
Uehman (Poland), V. B. Sollogub, A. V. Chekunov  
(USSR), B. Beranek, Ya. Weiss, A. Hrdlicka, A.  
Dudek, M. Zaunkova, M. Suk, A. Fejfar (Czecho-  
slovakia), D. Prosen, B. Milovanovic, M. Roksandic  
(Yugoslavia).

Field work and data interpretation have been completed for  
five out of thirteen international DSS profiles. On some small sectors of  
the profiles, the crustal structure is not uniquely determined, due to complex  
wave field or the inadequacy of the observation systems. The results are  
described for profiles III, V and VI. The results obtained on profile I are  
described in Chapter II of this monograph.

The earth's crust in the regions studied has the following  
general characteristics: In the Pannonian depression the crust is thin ( 25 -  
30 km), while the Moho discontinuity has a rather gentle relief. This region  
of thin crust extends towards the Inner Carpathians (profile V), the buried  
Carpathian extension in Transcarpathia, and the Inner Dinarides (profile III).  
The thickness of the crust increases in all directions outward from the  
Pannonian depression and the structure becomes notably more complex.

Profile III, with a length of 1800 km, begins in the Voronezh  
massif in the north, crosses the Dnepr-Donets aulacogene, the northwestern  
Ukrainian shield, the Volynia-Podolia plate, the Cis-Carpathian foredeep, the  
eastern Carpathians, the Trans Carpathian trough (USSR), the Pannonian  
depression (Hungary, Yugoslavia), the Inner and Outer Dinarides (Yugoslavia),  
and terminates in the Adriatic Sea basin in the south.

The crustal section for profile III is shown in Figure 33.

The crustal thickness varies along the profile from 25 - 27 km in the Pannonian depression to 60-65 km in the Carpathians. The crust is divided into blocks by numerous abyssal faults. The major seismic interfaces are  $K_0$  - the surface of the consolidated crust;  $K_1$  - Conrad discontinuity; and M - Moho discontinuity.

The surface of the consolidated crust is not of the same age and composition along the entire profile. The pre-Riphean crystalline basement of the East European platform is replaced by the Baykalian metamorphosed basement of the eastern Carpathians (in the Cis-Carpathian foredeep). The depth to the basement surface varies along the profile from zero in the Ukrainian shield to a maximum depth of 15 km in the Cis-Carpathian foredeep. In the other tectonic provinces, the following depths are observed: several hundred meters in the Voronezh massif; 4-5 km in the Dnepr-Donets aulacogene; 10-12 km in the Carpathians; 5 - 8 km in the Trans-Carpathian trough; 8 - 10 km in the Pannonian depression; and 10 km in the Outer Dinarides. The basement surface is broken by numerous faults and forms: a graben-like structure in the Dnepr-Donets aulacogene; a deep, narrow syncline in the Cis-Carpathian foredeep; and anticlines in the Carpathians and in the conjunction zone between the Pannonian depressions and the Dinarides (Fruska Gora area in Yugoslavia). The depth to the basement surface in the Adriatic Sea basin is not determined, but it is believed to be no less than 15 km.

The Conrad discontinuity is determined only occasionally. It is broken by many faults, its maximum displacement being 10 km. The Conrad discontinuity occurs at 13-18 km in the Dnepr-Donets aulacogene, forming a gently sloping syncline. In the Ukrainian shield (Korosten Pluton region), it is reliably established that the Conrad discontinuity does not exist, while southwest of the Pluton it occurs at 20 - 24 km. At the fault separating the Ukrainian shield and the Volynia-Podolia plate (indicated by k in Figure 33), the Conrad discontinuity is upthrust to a depth of 12 km. From a depth

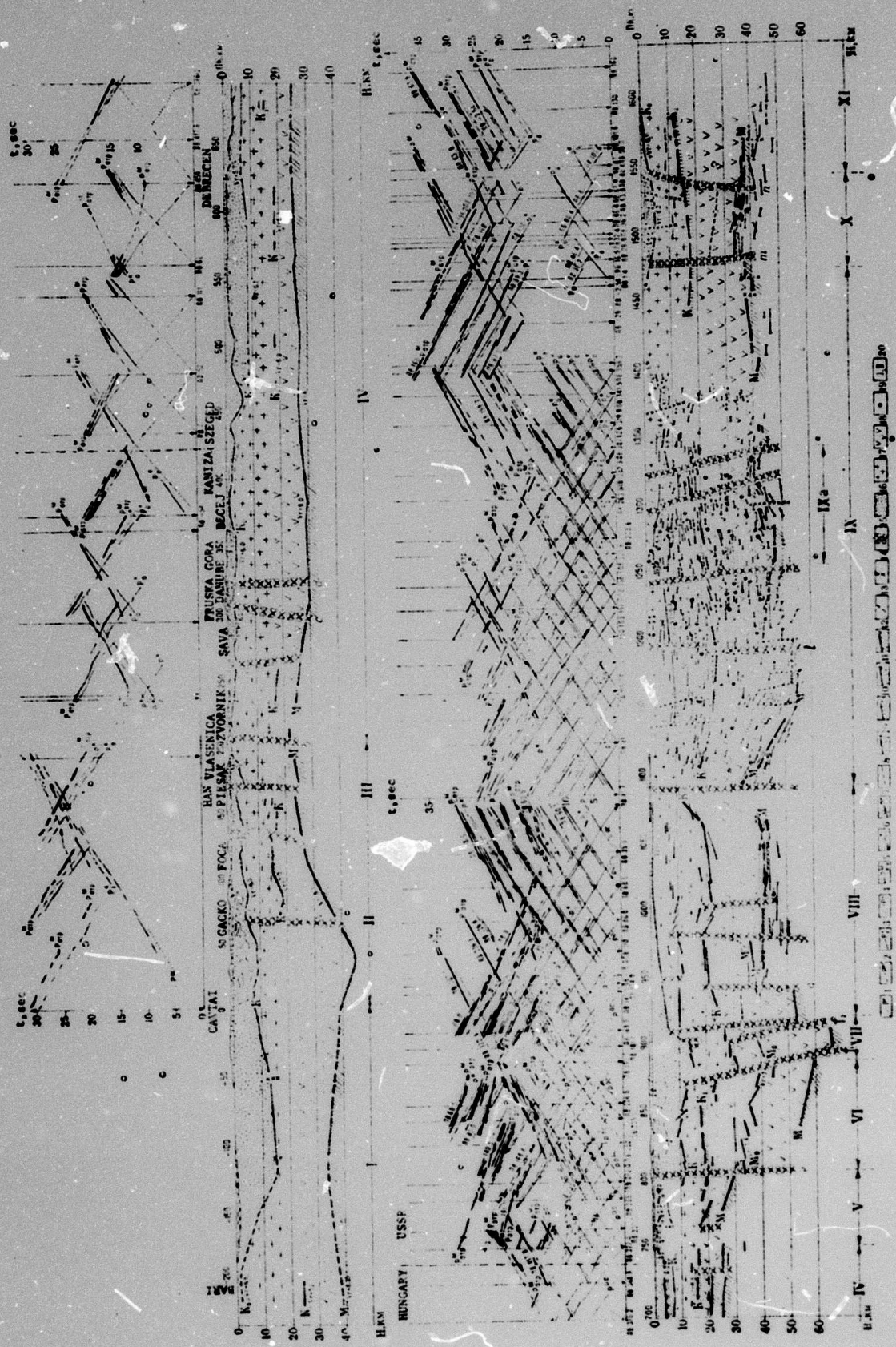


Fig. 33. System of Time-Distance Curves and Seismogeological Crustal Section along International Profile III.

Time-distance curves for waves from: 1- interfaces within the sedimentary layer; 2- Mesozoic-Paleogene folded complex in the Carpathians, continuously refracted; 3- crystalline basement surface, reflected; 4- basaltic layer surface; 5-  $M_0$  interface, reflected; 6- M discontinuity, reflected; 7- M discontinuity, refracted; 8- irregular waves. Interfaces: 9- crystalline basement surface; 10- Conrad discontinuity; 11-  $M_0$ ; 12- Moho discontinuity; 13- faults, from geological data; 14- disjunctive dislocations; 15- abyssal faults; 16- sedimentary layer; 17- granitic; 18- basaltic; 19- diffraction points. 20- Tectonic zones and blocks: I- Adriatic Sea basin; II- Outer Dinarides; III- Inner Dinarides; IV- Pannonian depression; V- Trans-Carpathian trough; VI- Carpathians; VII- Cis-Carpathian foredeep; VIII- Volynia-Podolia plate; IX- Ukrainian shield; IXa- Korosten Pluton; X- Dnepr-Donets aulacogene; XI- Voronezh massif.

of 20 km in the Volynia-Podolia plate, it rapidly subsides stepwise to a maximum depth of 32 km in the Cis-Carpathian foredeep. Where the foredeep joins the eastern Carpathians ( $f_1$ ), it is again upthrust by 10-14 km, thus reaching a depth of 18 - 22 km in the Carpathians. In the Pannonian depression, as in the Carpathians, the Conrad discontinuity lies nearly horizontally at depths of 18 - 20 km. In the Dinarides, as far as is determined, it lies at depths of 18 - 20 km, forming a small synclinal bend.

The Moho discontinuity is characterized by very complex structure. The crustal thickness in the Voronezh massif is 46 - 47 km. The Moho discontinuity in the Dnepr-Donets anlacogene is upthrust at two marginal faults (m and n) so that the crustal thickness is reduced to 35 - 36 km. The average crustal thickness of the Ukrainian shield is about 40 km. However, crustal thickenings of 46 and 55 km are observed within intervals of 200 - 250 km and 100 - 150 km, respectively. At the fault dividing the Ukrainian shield and Volynia-Podolia plate, the Moho discontinuity is displaced. Within the Volynia-Podolia plate, it lies at a depth of about 40 km and starts descending stepwise toward the Cis-Carpathian foredeep, reaching depths of 52 and 65 km in the marginal part of the plate and in the foredeep, respectively. In the eastern Carpathians, the Moho discontinuity rises southwestward. At the fault dividing the eastern Carpathians and the Trans-Carpathian trough, the Moho discontinuity is upthrust by about 25 km, (from a depth of 55 to 30 km). This fault (e) corresponds to the Perip'yeninskiy lineation, which is geologically traced for several hundred kilometers. In the Cis-Carpathian foredeep and the eastern Carpathians, another deep seismic interface ( $M_0$ ) is found at a depth of 35 - 45 km. It is interpreted as an upper (Alpine) Carpathian root. The Moho discontinuity is considered to form the lower, perhaps Lower-Proterozoic, Carpathian root. Near the Soviet-Hungarian border, the Moho discontinuity is not determined decisively. In the Pannonian depression, the Moho discontinuity gradually

descends from 28 to 31 km, with maximum depth confined to the Fruska Gora area. Farther on, toward the Outer Dinarides, it descends rapidly to a depth of 45 km. From the Outer Dinarides to the Adriatic Sea, it rises, thus forming the southward displaced root beneath the Dinarides.

Profile V, 450 km long, begins in the Epi-Paleozoic platform in Poland, crosses the Cis-Carpathian foredeep, the Outer Carpathians (Silesia and Mahur zones), the zone of klippens (Perip'yeninskiy lineation), the Inner Carpathians (Severo-Homerske synclinorium, Spissko-Homerske Rudnyye Mountains, and Slovakian Karst), and terminates in the Pannonian depression.

The tentative crustal section along the profile is shown in Figure 34.

The basement surface ( $K_0$  interface) is determined in Poland, where it lies at a depth of 3 - 4 km and in the Pannonian depression, at 5 km.

The assumed Conrad discontinuity ( $K_1$  interface with  $V_p = 7$  km/sec) is traced only in the Pannonian depression at a depth of 20 km. The Moho discontinuity in the Epi-Hercynian platform and the Cis-Carpathian foredeep (northern part of the profile) lies horizontally. It is displaced from a depth of 40 to 48-50 km. Farther southward, after being upthrust to a depth of 35 km at the Perip'yeninskiy lineation (fault e in Fig. 33), it continues to rise toward the Pannonian depression, where it reaches depths of 25 - 26 km.

The 900-km-long profile VI extends through Germany, Czechoslovakia and Hungary. It crosses the Saxo-Thuringian Variscian zone, the Bohemian massif, the western Carpathians, and the Pannonian depression.

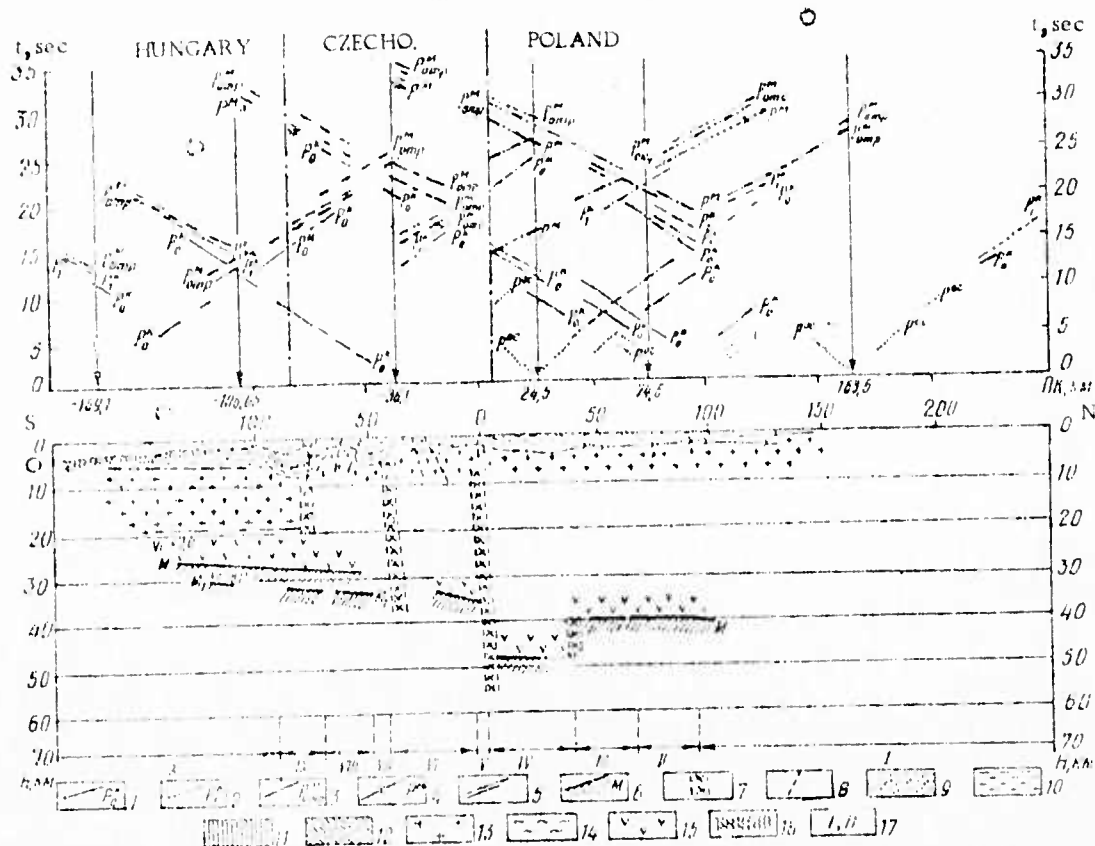


Fig. 34. System of Time-Distance Curves and Seismogeological Crustal Section along International Profile V.

Time-distance curves for waves from: 1- crystalline basement surface; 2- basaltic layer surface; 3- M discontinuity, reflected; 4- M discontinuity, refracted; 5- interfaces within consolidated crust; 6- Moho discontinuity; 7- abyssal faults; 8- faults from geological data; 9- molasse complex; 10- flysch; 11- Mesozoic sediments; 12- Paleozoic sediments; 13- granitic layer; 14- crystalline schists; 15- basaltic layer; 16- folded basement of the Pannonian depression; 17- tectonic zones and blocks: I- Polish Epi-Paleozoic platform; II- Cis-Carpathian foredeep; III- Silesia zone; IV- Mahur zone; V- zone of klippen (Perip'yeninskiy lineation); VI- Paleogene complex of the Inner Carpathians; VII- Severo-Homerske synclinorium; VIII- Spissko-Homerske Rudnyye Mountains; IX- Slovakian Karst; X- Pannonian depression.

The crustal section along the profile is shown in Figure 35.

The depth to the crystalline basement surface ( $K_0$  interface) varies significantly along the profile. While it is exposed in the Bohemian massif, its depth in the Thuringian depression, Vienna graben, and Pannonian depression reaches 10 km. Seismic interfaces within the consolidated crust do not correlate with each other along the profile. Thus, the outlined boundary between the granitic and basaltic layers is considered only as one version of the interpretation.

The Moho discontinuity is the most reliably determined interface on the profile. A maximum crustal thickness of 38 km is observed in the Bohemian massif (the conjunction zone between the Central Bohemian Pluton and Moldanubicum). This suggests that the roots of the Hercynian geosyncline are still preserved. The minimum thicknesses of 27 and 28 km are observed in the Pannonian and East Thuringian depressions, respectively.

The crust along profile VI is divided into blocks by abyssal faults, particularly in the northwestern part of the profile. The following major faults are identified: one dividing the Central German crystalline trough and the eastern Thuringian depression (a); one between the Krusne and Doupovske Mountains (b); the Perip'yeninskiy lineation (f); the Central Bohemian suture (c); and the Pribyslav zone (d).



Fig. 35. System of Time-Distance Curves and Seismogeological Section along International Profile VI.

Time-distance curves for waves from: 1- interfaces within the sedimentary layer; 2- crystalline basement surface; 3- basaltic layer surface; 4- M discontinuity, reflected; 5- M discontinuity, refracted; 6- Conrad discontinuity; 7- Moho discontinuity; 8- reflection surfaces within the consolidated crust; 9a- faults from geological data; 9b- abyssal faults; 10- molasse complex; 11- flysch; 12- Mesozoic sediments; 13- Paleozoic sediments; 14- granitic layer; 15- crystalline schists; 16- siennite; 17- neovolcanites 18- basaltic layer; 19- folded basement of the Pannonian depression; 20- diffraction points. 21- tectonic zones and blocks: I- Central German trough; II- East Thuringian depression; III- Krusne Mountains (Erz Gebirge). IV- Doupovske Mountains; V- Kladno-Rakovnik basin, VI- Barrandien, VII- Central Bohemian Pluton, VIII- Moldanubicum; VIIIa- Central massif; VIIIb- Trebic massif; IX- Morava and Brno massifs; X- Cis-Carpathian foredeep; XI- western flysch Carpathians; XII- Vienna graben; XIII- Lesser Carpathians; XIV- Pannonian depression.

#### Chapter IV. General methodological conclusions.

Sollogub, V. B., and A. V. Chekunov.

Over nearly all the regions of central and southeastern Europe, the following wave groups are recorded during DSS studies:

- 1) waves from interfaces within the sedimentary layer;
- 2) waves from the basement surface and interfaces within the consolidated crust; and
- 3) waves from the Moho discontinuity and interfaces within the upper mantle.

The above wave groups include head waves, waves continuously refracted through a gradient medium, waves reflected both at near vertical and wide angles, diffracted waves, converted waves, and others. Continuously refracted and weakly refracted phases are usually recorded as first arrivals, and reflected phases, as later arrivals.

The uppermost part of the basement is characterized by waves with velocities of 5.8 - 6.2 km/sec which are refracted - weakly refracted phases penetrating the basement. These are traced at distances from 2 - 30 up to 100 - 140 km, depending on the thickness of the sedimentary layer. The vertical velocity gradient in the uppermost basement does not exceed  $0.05 \text{ sec}^{-1}$  and rapidly decreases with depth.

In some regions, particularly in younger plates and median massifs, discrimination of the waves from the basement is very difficult. They have kinematic characteristics similar to wave groups associated with interfaces within the folded-metamorphosed complex overlying the basement, as well as with interfaces within the granitic layer. Reflected phases from the basement surface are recorded only seldom (Donbass and the Thuringian depression). In regions with exposed crystalline basement, converted waves associated with it are recorded. Their dynamic characteristics, to a great extent, depend on the petrological composition of the basement. However, in regions with a thin sedimentary layer (Ukrainian shield, Bohemian massif), waves from interfaces within the granitic layer are very often recorded. In such cases, the wave field is very complex, exhibiting low resolution, and wave correlation is possible only by using dynamic criteria. These waves are associated with discontinuous refraction surfaces with a velocity of 6.3 - 6.8 km/sec. Only locally are phases reflected from these interfaces recorded.

The waves associated with the basaltic layer are identified conditionally, since the Conrad discontinuity is not always a well pronounced interface. There are regions where waves from the Conrad discontinuity are not identified, regions where they are not reliably identified, and regions where these waves are highly recognizable and intense. They are recorded most often at distances of 40 - 60 km with an apparent velocity of 6.8 - 7.2 km/sec. With an increase of distance, they emerge as first arrivals. The recording interval, the dynamic and kinematic wave characteristics, and partly their nature, vary in different regions. For example, in the central part of the Ukrainian shield, in the initial part of the recording interval, they are reflected and in the later part, head waves. In the area of the Korosten Pluton, waves from the Conrad discontinuity are not identified at all.

Waves from the interfaces within the basaltic layer are multi-pulsed and intense, with an apparent velocity of 7.3 - 7.5 km/sec.

The Moho discontinuity over all of central and southeastern Europe (except for the deep-water section of the Black Sea basin) is characterized by intense reflections, which are readily traced from 60 - 80 to 180 - 200 km. Head waves from the Moho discontinuity have poor dynamic expressiveness, and as first arrivals, they are traced only at distances greater than 120 km in Hungary and 200 km in the USSR. Only in the region of the Trans-Carpathian trough are the head and reflected waves from the Moho discontinuity of comparable intensity. Most frequently, waves from the Moho discontinuity are represented by a group of pulses, characterized by interference, an irregular distribution of energy among them, sharp attenuation of some pulses, and the emergence of new pulses. Their waveforms have a "ragged" appearance. The duration of these waves is 0.5 - 1.0 sec and more. In some regions such as Hungary, Czechoslovakia, Germany and the USSR, not one, but two or even more groups of oscillations associated with the Moho discontinuity are recorded. They are separated in time and have identical intensity.

The waves from the major crustal interfaces only locally are simple three- or four-pulse intense oscillations with sustained waveform.

The DSS data obtained in central and southeastern Europe provide evidence that the intricate multi-pulsed deep waves with unsustained waveform reflect the complexity of the structure of the deep interfaces. For example, in the Ukrainian shield and Bohemian massif, with exposed crystalline basement, the deep waves have intricate waveform. On the other hand, in some regions with a thick sedimentary layer, the deep waves have a simple waveform, permitting phase correlation. Thus, the deep interfaces are not sharp boundaries, but finely layered transition zones. The crust-to-mantle transition zone reaches a thickness of 5 km or more. As a

consequence previously used group-wave correlation was abandoned and the emphasis was put on the discrimination of individual waves within a group. The difficulties encountered with this correlation are:

- 1) in the interference zone, it is not always possible to discriminate individual waves over a long distance range;
- 2) the construction of interfaces on the basis of insufficiently long time-distance curves, especially at large incidence angles, has low accuracy; and
- 3) in the interference zones, the time-distance curves of individual waves are distorted.

Furthermore, it appears to be possible to identify (isolate) dislocation zones, using direct and indirect criteria. The difficulties in identifying these zones arise due to the poor velocity differentiation of the consolidated crust and the group character of the deep waves. The poor velocity differentiation causes:

- 1) poor resolution of the records;
- 2) selective emphasis of the horizontal and flat-lying inhomogeneities due to large critical angles ( $65 - 80^\circ$ );
- 3) limited possibilities for the study of the graben-like structures of comparable width and depth;
- 4) low accuracy in locating dislocation zones; and
- 5) low reliability or impossibility of identifying small faults (vertical displacement 200 - 300 m).

The direct criteria for the identification of dislocation zones are:

- 1) interruption of seismic interfaces with or without vertical displacement;
- 2) diffraction of waves; and
- 3) large dip angles of seismic interfaces or individual reflection surface.

The indirect criteria which indicate block crustal structure are:

- 1) changes in the number of seismic interfaces and the thickness of layers;
- 2) changes of the physical properties of interfaces and their structure; and
- 3) changes of refractor and average velocity.

One of the basic results of the DSS studies in central and southeastern Europe is a reconsideration of the previously assumed homogeneous three-layered crustal model. A new concept of an inhomogeneous thin-layered crust with numerous local interfaces has emerged. The interfaces are sometimes concentrated, forming thick transition zones, particularly between the crust and the upper mantle. It has been established that the crust has a complex block-layered structure with different numbers of interfaces within blocks and weak velocity differentiation.

Possibilities for the existence of low velocity zones have been established. It has been further shown that the seismic interface with  $V_r = 6.6 - 7.2$  does not always represent the basaltic layer surface. The boundary between the granitic and basaltic layers is not a distinct interface, but represents a granitic-basaltic mixture. The conclusive criteria for the identification of the basaltic layer is layer velocity.

It was concluded that only continuous, correlated observation systems can provide reliable data on crustal structure and composition. The use of discrete observation system is justified only in the initial stage of investigation and as a complement to continuous observation systems.

Chapter V. Some problems of the structure  
and evolution of the crust.

Subbotin, S. I., V. B. Sollogub, A. V. Chekunov,  
V. Ye. Khain, and V. I. Slavin.

The deep structure of the crust in central and southeastern Europe is summarized, and its qualitative relationship with subsurface geological structures is discussed in terms of a "thick" (greater than 35 - 40 km) and a "thin" (less than 35 - 40 km) crust.

The "thick" crust is confined to the Dinarides, the Carpathians, the Balkanides, the Crimean Mountains, and the Lower-Proterozoic folded regions of the Ukrainian shield. The relief of the Moho discontinuity in the Ukrainian shield is characterized by submeridional uplifts and depressions, its depth varying from 30 to 54 km. The thickening of the crust "roots" is correlated with a region of Lower-Proterozoic folding and the thinning, with a median massif of corresponding age. These "roots" are traced within the Dnepr-Donets aulacogene, the Cis-Carpathian foredeep, and the Outer Carpathians (eastern). Here (profile V), two Moho discontinuities are found at 60 - 65 and about 45 km, respectively. This is explained as a superposition of a submeridional Lower-Proterozoic "root" over a northwest-trending Alpine "root". The Carpathian Alpine "root" is found in clear form on profile V. The "root" beneath the Dinarides has the same amplitude (45 km) as the Carpathian Alpine "root". Less pronounced "roots" are found in Dobruja (Rumania), the Bakony Mountains (Hungary) and the Krusne Mountains between Czechoslovakia and Germany.

Thus, in central and southeastern Europe, the "roots" beneath the mountains are observed almost universally, even though the original mountains are completely absent. The Lower-Proterozoic "roots" are larger than the Alpine "roots", and they, in turn, are larger than the Hercynian "roots".

The "thin" crust (20 - 30 km) is confined to the median massifs (ancient Zaporozh'ye median massif of the Ukrainian shield) and intrageosynclinal coorogenic superposed depressions (Pannonian depression, Black Sea basin, Misian plate).

The crustal thickness, surface relief, Bouguer anomalies, and the hypsometry of the consolidated crust are not uniquely and strictly correlated.

The crust has a block-layered structure. The abyssal faults dividing the crust into blocks represent extensive and rather wide zones with characteristically complex structure. Tectonic sutures dividing the crust of central and southeastern Europe into major structures are observed as follows: between the Bohemian massif and the eastern Carpathians, between the Outer and Inner Carpathians, between the Dinarides and the Pannonian depression, between the East European platform and the Scythian plate, etc.

The Pannonian depression, Misian plate, and Black Sea basin constitute a single region with a thin crust and thin granitic and/or basaltic layers, which is located within the Mediterranean belt of folding. Its marginal sectors submerge into the adjacent folded systems. Along its northern border, large faults are observed (Moho discontinuity displaced by 10 - 20 km) which divide the regions of ancient consolidation from Cimmerian and Alpine geosynclines.

The Ukrainian shield is crossed by extensive submeridional faults (Odessa, Krivoy Rog, etc.).

The evolution of the crust of central and southeastern Europe is seen as a process of the conversion of an ancient platform into an intrageosynclinal superimposed depression (suboceanic crust), as follows: ancient platform (East European platform) → aulacogene and intracratonal trough within a platform (Dnepr-Donets aulacogene and Indol-Kuban trough) → parageosyncline (Donbass) → epigeosyncline and later orogene with foredeeps (Carpathians) → intrageosynclinal superimposed depression concurrent to the orogenic stage (Pannonian depression, Black Sea basin).

The East European platform has simple structure, with about 4 km to the basement surface, 20 - 23 km to the Conrad discontinuity, and 36 - 39 km to the Moho discontinuity. The relief of the Moho discontinuity is smooth. The development of an aulacogene and a pericratonal trough leads to a decrease in the thickness of the consolidated crust and an increase in the sedimentary layer. The basement surface and the Conrad discontinuity are downwarped and, consequently, the granitic and particularly the basaltic layers (Dnepr-Donets aulacogene) or sometimes only the basaltic layer, (Indol-Kuban trough) tend to thin out.

The next link in the evolutionary succession is the intracratonal geosyncline (Donbass), where the sedimentary cover reaches a thickness of 15 - 18 km, embryonal "root" is present, but a foredeep is absent. In the next process of evolution, geosynclines and orogenes (Carpathians) occur, with increased and subsequently dislocated sedimentary cover and relief inverse to that of the Moho discontinuity.

Finally, in the intrageosynclinal depressions which develop on the sites of median massifs, the crustal thickness is reduced to 24 - 26 km, and the granitic (Black Sea) and basaltic (Pannonian depression) layers thin out. Thus, the continental platform in the course of its evolution is converted into a suboceanic structure.

The causes and possible mechanism of the evolution of the central and southeastern European structure are discussed. Several interpretations are presented (hypothesized by Subbotin, Chekunov, and others).

Lursmanashvili, O. V. Regular variation of the occurrence time of earthquakes in some seismically active regions. AN GrugSSR. Soobshcheniya, v. 10, no. 1, 1973, 69-72.

Secular variation of the Earth's position relative to the Sun at the moments of occurrence of major earthquakes is analyzed. The analysis is accomplished for the Kurile-Kamchatka zone ( $M \geq 7\frac{1}{4}$ ) and a zone including Central Asia (excluding Hindu Kush) deep focus earthquakes ( $M \geq 6\frac{1}{2}$ ), Caucasus ( $M \geq 5\frac{3}{4}$ ), Carpathians ( $M \geq 5\frac{1}{2}$ ), and Greece ( $M \geq 7$ ).

It was found that the secular variation of the Earth's position (as well as the position of the seismically active zone) at the moments of occurrence of major earthquakes displays an 11-year periodicity.

Golionko, G. B., N. S. Yefimkin, V. Ye. Zin'kovskiy, and Ye. M. Krestin. Deep geological structure of the northeastern flank of the Voronezh massif and Pachelma trough (from DSS data). Geotektonika, no. 2, 1973, 35-40.

The seismic section along Lipetsk - Ryazan' - Tuma profile, which is a part of the regional DSS profile Black Sea, is described.

The crustal thickness along the profile (see Fig. 1) varies from 49 km in the south to 55 - 56 km in the north. The crust is divided into blocks by deep-seated faults. An interesting feature of the crustal section is the refracting surface with  $V_r = 6.3 - 6.7$  km/sec, which is interpreted to be the

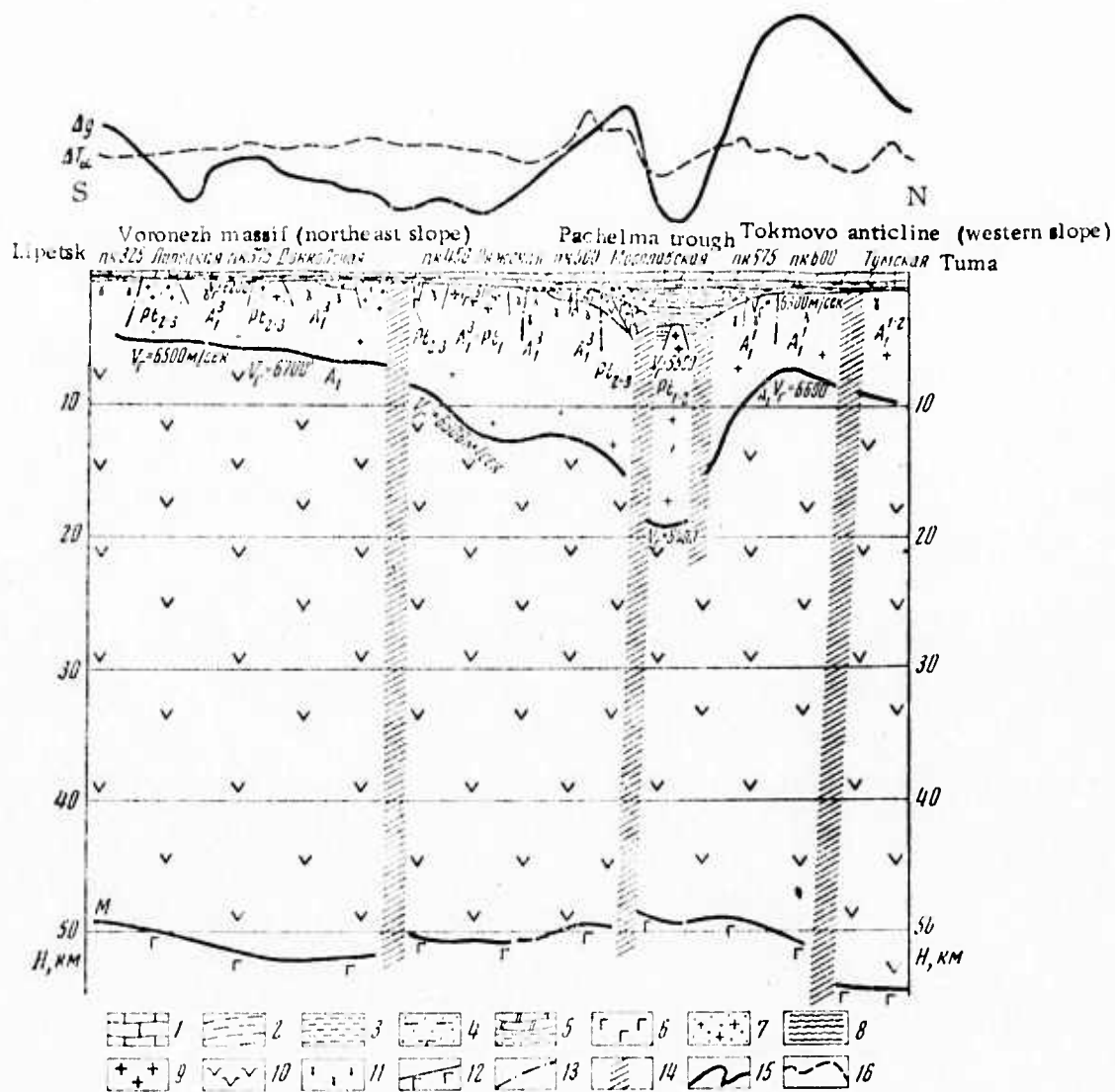


Fig. 1. Seismic-Geological Crustal and Upper Mantle Section along DSS-CMRW Profile Lipetsk - Ryazan' - Tuma.

1-5 - Sedimentary formations; 6-11 - crystalline basement; 12 - Moho discontinuity; 13 - local shallow faults; 14 - deep-seated faults; 15 -  $\Delta g$  curve; 16 -  $\Delta T_{\alpha}$  curve.

surface of the basaltic layer. A similar refracting surface is found over the entire East European platform: in the Ukrainian shield at depths of 1.5 - 3 km; on the northeastern flank of the Belorussian massif at 2 - 3 km; and in the Baltic shield. In areas where this surface lies at shallow depths, positive gravity anomalies are observed. As can be seen from Figure 1, the gravity anomaly along the profile is governed by the relief of this surface. This surface is assumed to represent a "protobasement".

Savarenskiy, Ye. F., N. B. Shoniya, and  
I. R. Yavorskiy. Shear waves from the  
Sarykamysh earthquake, and the focal  
mechanism. IN: GruzSSR. Soobshcheniya,  
v. 70, no. 2, 1973, 321-324.

The focal mechanism of the Sarykamysh earthquake of 5 June 1970 ( $M = 6.6$ ;  $H = 20$  km;  $\phi = 42.5^\circ$  N;  $\lambda = 78.8^\circ$  E) was determined with S polarization angles. The first-motion data from the Abastumani, Iul'tin, Kheys, and Yakutsk stations were used.

The determined direction of motion in the focus, ( $\phi = 193^\circ$  and  $\psi = 57^\circ$ ) agrees with the P nodal solution.

The ratio of  $V_{SV}$  and  $V_{SH}$ , determined using records of five stations at approximately the same latitude, is about 0.99.

#### 4. Particle Beams

##### A. Abstracts

Koval'chuk, B. M., V. V. Kremnev,  
G. A. Mesyats, and Ya. Ya. Yurike.  
Development of a nanosecond surface  
discharge on dielectric with a large  
dielectric constant in gas. ZhPMTF,  
no. 1, 1973, 48-55.

Results are described of experimental investigations on discharges from isolated metallic points touching a dielectric plate (dielectric constant of 100 or more), and from two metallic points with a distance  $l$  between them, one of which touches the plate while the other is offset from it. Test setups for the isolated point and two-point systems are shown in Figs. 1 and 2 respectively. In the single point case, dielectric discs used were

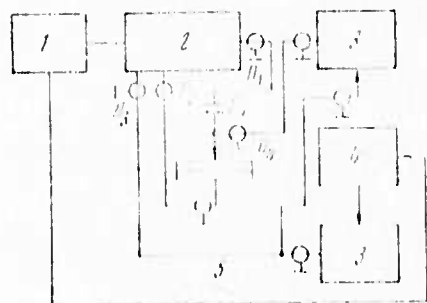


Fig. 1.

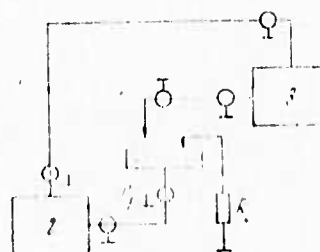


Fig. 2

Test diagram for nanosecond discharge development.

1 - constant voltage source; 2 - generator; 3 - oscilloscope (I2-7); 4 - photomultiplier (FEU-36)

barium titanate, titanium dioxide and steatite ceramics of 10 mm diameter and thickness  $d = 0.5$  mm; for the dual-point case, ceramic plates  $5 \times 6 \times 0.5$  mm<sup>3</sup> were used. Relationships were obtained for discharge propagation rate, time lag and VA characteristics at an exposure of  $\sim 10^{-9}$  sec and voltages up to 1.5 kv of different polarity. The average propagation rate of luminescence during the time  $\leq 3$  nsec was  $10^6$  cm/sec.

It was established that discharge from a negative point is initiated by a field emission current, while from positive points - by autoionization currents. Fundamental principles are outlined for commutators based on the test configurations, using surface discharge with a large number of points. The article includes 7 graphs, one oscillogram and 2 photographs of discharges, taken by electron-optical converter. A detailed description is also given of the experimental procedures.

Volovik, V. D., V. I. Kobizskoy, V. V.  
Petrenko, G. F. Popov, and G. L. Fursov.  
Ionization luminescence of air due to  
relativistic electrons. Atomnaya energiya,  
v. 34, no. 2, 1973, 130-131.

The ionization luminescence of air was investigated as a function of relativistic electron energy under optimal geometrical conditions ( $6 \times 10^{-4}$  ster.  $\times$   $\text{cm}^2$ ). The experiment was conducted in linear accelerators of the Academy's Physicotechnical Institute in Kharkov in the energy range of 20-1400 Mev. The accelerators operated in a pulsed regime with a 50 Hz recurrence frequency. Light produced in the chamber (with dark walls filled with air at normal pressure and room temperature) during transit of the electron beam was recorded by photomultiplier. The luminescence thus recorded was not of individual electrons, but of all electrons in the pulse. This was achieved by placing at the photomultiplier outlet an RC-network with a time constant greater than pulsed current duration. Energetic relationships of luminescence intensity were recorded in different accelerators within above energy range, and all values were referenced to a single current (0.2  $\mu\text{a}$ ) and a single pulse (1.5  $\mu\text{sec}$ ). Results are plotted in Fig. 1, from which it is seen that

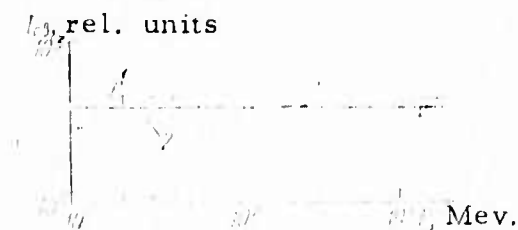


Fig. 1. Relationship of ionization luminescence intensity as a function of primary electron energy.

- 1 - Theoretical curve, according to Moller;
- 2 - ionization loss of electrons in air.

experimental results are in good agreement with the theoretical, calculated according to Moller's formula, which represents the relationship of energy imparted to secondary electrons in the region of maximum excitation cross-section of atoms, as a function of primary electron energy.

Bredikhin, M. Yu., A. I. Maslov, Ye. I. Skibenko, and V. B. Yuferov. Investigating electron heating of a dense beam-plasma discharge in strong magnetic fields. UFZh, no. 2, 1973, 315-317.

Heating conditions were studied of a dense beam-plasma discharge in a strong magnetic field  $H_0$  and high beam power  $W_e$ . Electron temperature of the plasma was measured by an x-ray method and diamagnetic probes. Radial distribution of x-radiation intensity was determined by a tungsten target, inserted in the plasma along a radius. Shf radiation in the

wavelength range  $0.3 \leq \lambda \leq 4$  mm was detected by an indium antimonide sensor. The density of the argon plasma was about  $4 \times 10^{14} \text{ cm}^{-3}$ .

Calorimetric measurements showed that the total loss of electron beam power in passage through the plasma amounted to 50 - 60%. The increase of electron temperature of plasma due to magnetic field intensity at the trap center was proportional to the energy contribution in the plasma (Fig. 1). The heating time was 10-25  $\mu\text{sec}$ . It is shown that electrons in plasma with density  $= 4 \times 10^{14} \text{ cm}^{-3}$  can be heated up to a temperature of 3.5 kev. during beam-plasma discharges; their average energy equals 200-400 ev. Figure 2 shows electron temperature of plasma as a function

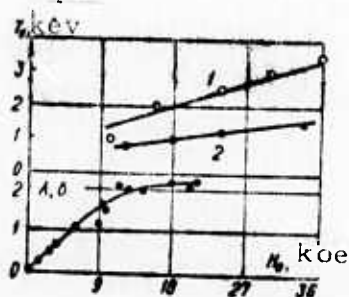


Fig. 1. Relation between electron temp. of plasma and magnetic field intensity at trap center.

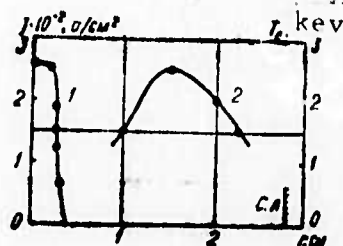


Fig. 2. Relation between electron temp. of plasma and trap radius.

of trap radius, the curves being plotted from the measurements of radial distribution of x-ray intensity.

Kikvidze, R. R., and A. A. Rukhadze.

Theory of oscillation and stability of a  
semiconducting plasma with small number  
of carriers in a strong electric field. IN:  
Trudy Fizicheskogo Instituta AN SSSR, no.  
61, 1972, 3-41.

This is an extensive review of research studies, about 80% of them Soviet, on the title subject. The review covers studies published over the 1949-1970 period. Interest in the reviewed subject is prompted by possibility of electromagnetic wave excitation and amplification from application of a strong electric field to a solid semiconductor.

The review deals mainly with the instability generated by an applied electric field in a solid-state plasma with a small number of carriers  $n < n_{cr}$  ( $n_{cr} \approx 10^{14} - 10^{15} \text{ cm}^{-3}$  for most semiconductors). A number of effects connected with the non-Maxwellian velocity distribution of carriers in such a plasma attracted attention of the authors. Stability characteristics are examined of a spatially-homogeneous; unbounded; and an inhomogeneous, bounded plasma in an electric field. Analysis of the reviewed theory indicates excitation of mainly longitudinal electromagnetic oscillations in the first cited plasma, with a negative current-voltage characteristic. Carrier diffusion stabilizes the oscillations at a wavelength shorter than Debye radius. In a strongly magnetized plasma, either inhomogeneous, unbounded, or homogeneous but bounded, a convection current instability may predominate.

B. Recent Selections

Anosova, L. M., and L. M. Gorbunov. Equilibrium configurations of electron beams in plasma. ZhTF, no. 8, 1973, 1620-1626.

Baksht, R. B., S. P. Vavilov, and M. N. Urbazayev. Luminescence of the side surfaces of a needle cathode in a vacuum diode with explosive emission. IVUZ Fiz, no. 8, 1973, 142-143.

Bogdankevich, L. S., and A. A. Rukhadze. Ob'yemnyye i poverkhnostnyye SVCh volny v plazme i ikh возбуждениye relyativistskimi elektronnyimi puchkami. (Body and surface SHF waves in plasma and their excitation by relativistic electron beams). Moskva, 1973, 36 p. (KL Dop vyp, 7/73, no. 14805)

Khodatayev, K. V. On a propagation characteristic of an electron beam in gas. ZhETF P, v. 18, no. 3, 1973, 184-186.

Kolomenskiy, A. A., V. M. Likhachev, I. V. Sinil'shchikova, and O. A. Smit. Structural characteristics of a heavy-current electron beam during transit through a low-pressure gas. ZhETF P, v. 18, no. 3, 1973, 153-156.

Plyutto, A. A., K. V. Suladze, S. M. Temchin, et al. Ion acceleration by a relativistic electron beam. ZhTF, no. 8, 1973, 1627-1631.

Popovich, V. P., T. A. Novskova, I. F. Kharchenko, and Ye. G. Shustin. Investigating conditions of plasma-beam discharge formation without magnetic field. IVUZ Radiofiz, v. 16, no. 6, 1973, 1109-1117.

Sindinskiy, V. V. The solution of phase-energetic equations of a heavy-current accelerator, taking into account losses in the waveguide walls. ZhTF, no. 8, 1973, 1789-1791.

## 5. Material Science

### A. Abstracts

Vereshchagin, L. F., Ye. N. Yakovlev,  
B. V. Vinogradov, V. P. Sakun, and  
G. N. Stepanov. Transition of diamond  
to the metallic state. ZhETF P, v. 17,  
no. 8, 1973, 422-424.

Previously the authors observed transition of diamond to the metallic state at about 1 Mbar pressure (ZhETF P, v. 16, 1972, 382). In the present paper they give new experimental data on electric resistance  $R$  of diamond as a function of compression force  $F$  at 77 to 600° K (Fig. 1).

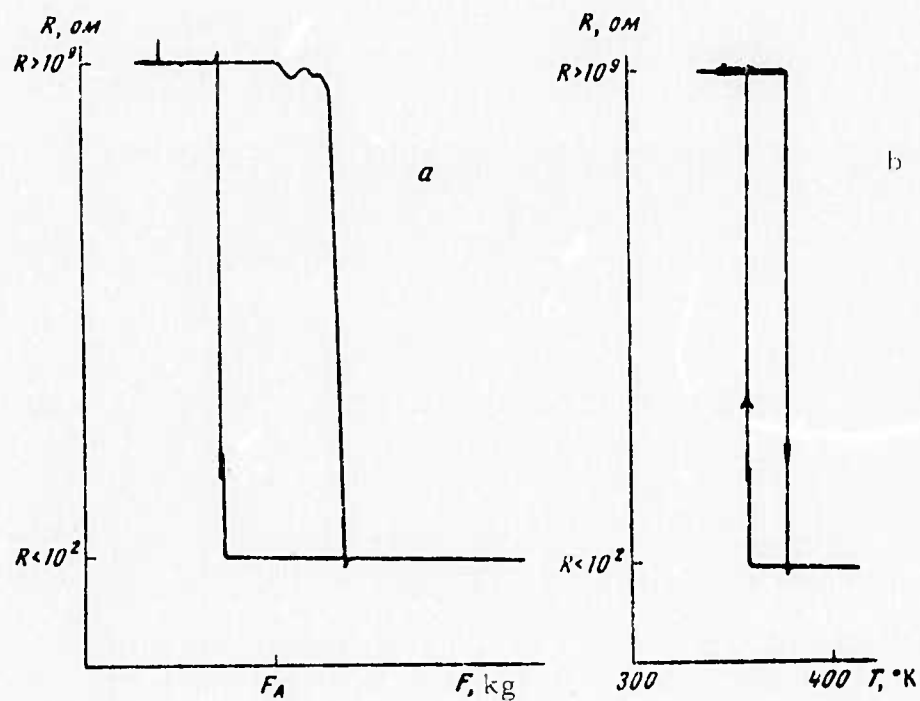


Fig. 1. Electric resistance of diamond versus:  
a- force, b- temperature.

The observed R jump indicates dielectric-to-metal transition in the 20 to 200 kg range of F. The transition occurs at a lower F when T is increased, and vice versa. The R jump on the R(T) curve at a constant F confirms that the  $\partial T / \partial P$  slope of the dielectric-metal equilibrium curve is negative. Transition occurs, as expected, at a higher T when F is decreased. It was concluded from numerical values of F corresponding to the transition that  $(\partial T / \partial P)_{eq} < 0$ . The phase diagrams of F. P. Bundy show that  $(\partial T / \partial P)_{eq} < 0$  is typical of the IV-a group elements of the Periodic Table.

The experiments demonstrate the existence of metastable states, namely a metallic phase in the region adjacent to the equilibrium curve, and a region of stable dielectric phase. In the process of heating the metallic phase at force level  $F_A$  (Fig. 1a), a stepwise increase in R of the system was observed to a value corresponding to dielectric state; continued heating determined transition to the metallic phase.

Vereshchagin, L. F., Ye. V. Zubova,  
V. A. Stupnikov, and Yu. K. Zhukovskiy.  
Modified piston manometer for pressures  
to 100 kbar. PTE, no. 2, 1973, 205-208.

An improved piston manometer is described with automatic recording of pressure to about 100 kbar and temperatures to  $2,000^{\circ}\text{C}$  in a high-pressure chamber. The pressure sensing unit consists of a measuring instrument and a composite piston rod. Compression force is transmitted to a dynamometer and recorded by means of strain gauges and a potentiometer in a two-coordinate system with accuracy within 1%.

The main improvements over an earlier design (PTE, no. 6, 1969, 185) are the decreased load transmitted on the piston rod through the measuring piston, and the ease of assembling and disassembling the manometer. In addition, the high-pressure chamber design includes an arrangement for electrical heating of the sample and an electronic pickup for automatic recording of electric heating capacity; the error of temperature measurement is 0.5%. The cited improvements make it possible to record the data in coordinates of compressive force vs. chamber pressure or electric resistance of a reference metal, or of chamber pressure vs. cell resistance, chamber temperature, or electric heating capacity. This manometer was used to measure, for the first time, pressure during diamond synthesis and to detect the pressure jump of the graphite to diamond transition. Fig. 1 shows a sectional view.

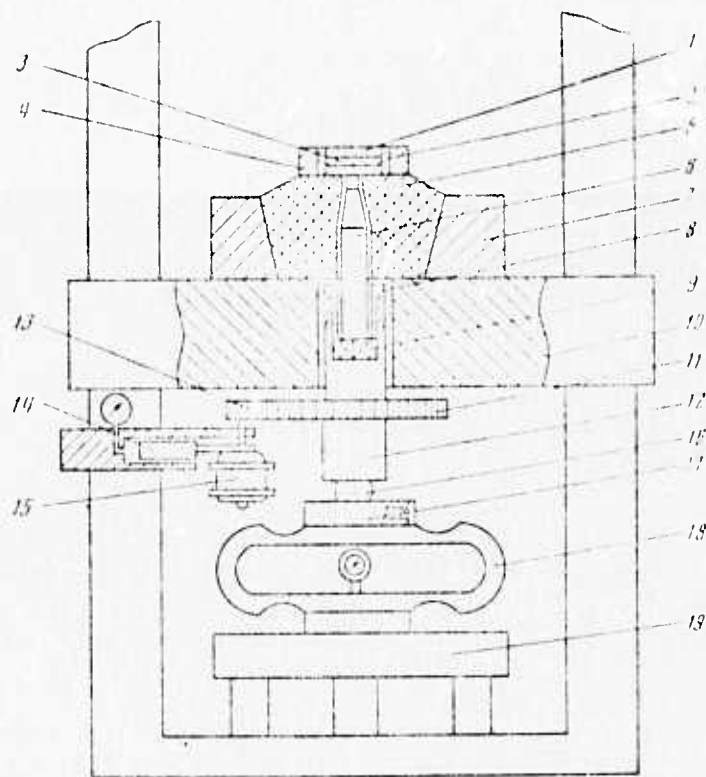


Fig. 1. Piston manometer.

- 1- graphite disc; 2- graphite heater; 3- metal catalyzer;
- 4- catlinite shell; 5- hard alloy die; 6- recording piston;
- 7- steel support collar; 8- collet; 9- hard alloy cylinder;
- 10-press head; 11-gear wheel; 12- steel column; 13- pinion;
- 14- friction torque recorder; 15- drive motor; 16- steel pellet;
- 17- bedplate; 18- dynamometer; 19- adjustable base.

Vereshchagin, L. F., G. L. Aparnikov,  
Ye. V. Zubova, and Yu. K. Zhukovskiy.  
Device for studying solids under high  
pressures with superposed shear stress.  
PTE, no. 2, 1973, 210-212.

An apparatus is described for rapid measurements of critical shear stress  $\sigma$  of solids under pressures to 500 kbar at any plastic strain value, for recording phase transitions, and studying chemical reactions in the solid state. Basically, a thin sample is compressed and rotated between Bridgman anvils. The apparatus consists of a 100 ton four-stage press, a high-pressure unit with a strain generating means, and strain gauges with recorders of pressure and shear stress. The main feature of this device is its unlimited range of plastic strain, owing to the unlimited rotational ability of the plunger dies. The strain gauges convert pressure and shear stress into proportional signals which are recorded in a two coordinate system. Thus, pressure dependence of  $\sigma$  can be analyzed immediately and, for the first time, strain dependence of shear stress can be recorded at a constant pressure. Strain rate can also be varied. Schematics are given of the high-pressure unit and the electric metering circuit.

Kirshenina, I. I., V. S. Mikhaylov, and  
L. N. Fedotov. Change in the structures  
and electrical properties of titanium,  
zirconium and their alloys from high pressures.  
IN: Sbornik. Pretsizionnyye splavy, no. 1,  
Moskva, Izd-vo Metallurgiya, 1972, 151-161.  
(RZhMetallurgiya, 5/73, no. 5I305). (Translation)

Synthesis is reported of the  $\omega$ -metastable phase of Ti and Zr at 9.0-9.5 GN/sq. m (90-95 kbar) and 5.8-6.0 GN/sq. m (58-60 kbar) pressures,

respectively. Quasi-hydrostatic pressures to 100 kbar were attained in a high pressure chamber using a 600 t process. The chamber was equipped with automatic heating and cooling systems. As temperature is increased,  $\alpha \rightarrow \omega$  transition in Ti occurs at a lower pressure, because of the presence of oxygen impurity. It is shown that superconductivity characteristics ( $T_c$  and critical current density) of Ti + 23.5-56 at.%Nb alloys change from the effect of cooling to liquid He temperatures and subsequent treatment by pressure up to 1.5 GN/sq. m (15 kbar). Calculations indicate internal pressure created during alloying of Ti and Zr to be comparable with external hydrostatic pressure of  $\omega$ -phase formation.

Yershova, T. P., and T. S. Lesikhina.

Thermodynamic calculation and experimental study of T-P-C diagram of a Bi-Cd system at pressures up to 25 kbar. IN: Sbornik.

Prob. metalloved i fiz. met., no. 1, Moskva, Metallurgiya, 1972, 14-24. (RZhMetallurgiya, 5/73, no. 5116). (Translation)

The T-P-C phase diagram of the Bi-Cd system under hydrostatic pressure was plotted on the basis of thermodynamic calculations and DTA data. At pressures up to 18 kbar, only lines and nodal points of the diagram shift positions without changing the general pattern. Eutectic temperature decreases slightly ( $dT/dp = 0.6$  degr./kbar). The position of the eutectic point shifts toward decreasing Bi concentrations. At pressures above 18 kbar, high-pressure Bi phases appear and the phase diagram becomes more complex.

Dugladze, G. M., G. Sh. Darsavelidze,  
and G. V. Tsagareyshvili. High-  
temperature internal friction in boron  
fibers. AN GruzSSR. Soobshcheniya,  
v. 70, no. 1, 1973, 141-144.

Measurements of internal friction  $Q$  of boron fibers at temperatures from room to  $700^{\circ}\text{C}$  were made to obtain data on structural imperfections and their effect on properties of the fibers. In most experiments, the commercial grade boron fibers of  $\sim 100\text{ }\mu\text{m}$  dia. deposited on a heated tungsten wire were used. Internal friction was determined by means of a relaxation oscillator with a relative error of 3%. The experimental  $Q^{-1}(T)$  and shear modulus  $G$  versus  $T$  plots exhibit a large  $Q$  relaxation peak at  $380^{\circ}\text{C}$ , and a corresponding deflection in the  $G^2(T)$  plot. An activation energy of relaxation equal to 2.36 eV was determined from shift in the peak position at a different oscillation frequency.

It is shown that the peak height is decreased somewhat by a preliminary heat-treatment of the fiber at  $650$  or  $850^{\circ}\text{C}$ . Irreversible splitting of the  $380^{\circ}\text{C}$  peak in two was observed after annealing at  $1,300$  or  $1700^{\circ}\text{C}$  for 30 min. which indicates significant changes in fiber structure at high temperatures. The degree of oscillation energy damping decreased in  $35\text{ }\mu\text{m}$  fibers. The height and temperature of the  $Q$  peak decreased somewhat in high-purity boron fibers, and even more so in the boron carbide-coated boron fibers. The viscous behavior of fine crystal boundaries under stress is believed to be the mechanism of formation of the  $380^{\circ}\text{C}$  peak on the  $Q^{-1}(T)$  curve for boron fibers.

Turayev, U., and A. A. Vertman. Magnetic susceptibility of transition metals at high temperatures and in the liquid state. Report 1. Magnetic susceptibility of iron, nickel, and cobalt. IAN Tadzh, no. 1, 1973, 50-55.

Experimental data on magnetic susceptibility  $\chi$  of Fe, Ni, and Co at temperatures up to 1800<sup>o</sup> C were obtained for the first time, because of the need for unambiguous information on the structure of their liquid state. A Faraday method was used to measure  $\chi$  with a relative error less than 1-3%. The experimental  $\chi$  versus  $1/T$  curves are shown comparatively with the  $\chi(1/T)$  curves obtained by different authors.

The linearity of the  $\chi(1/T)$  plot of Co in solid and liquid states indicates that  $\chi$  of this ferromagnetic obeys the Curie-Weiss law well in canonical form. Nonrigorous linearity of the  $\chi(1/T)$  plot of Fe points to conformity with Curie-Weiss law within narrow temperature limits only; nonlinearity of the  $\chi(1/T)$  plot of Ni at  $T > 800^{\circ}$  C indicates deviation from the Curie-Weiss at higher temperatures. There is a jump in  $\chi$  on transition to the liquid state in Fe, and a discontinuity of the  $\chi$  polytherm at 1650-1800<sup>o</sup> C. An insignificant change and absence of any jump of  $\chi$  were observed on transition of Co and Ni to the liquid state.

An approximate evaluation of the paramagnetic Curie point and the Curie-Weiss constant indicated absence of any radical change in exchange interaction on melting of Co and Ni. In contrast, the corresponding data for Fe suggest a change of short-range order in liquid iron toward an increase of coordination number.

Lavrenko, V. A., L. A. Glebov, and  
Ye. S. Lugovskaya. High-temperature  
oxidation of chromium boride in oxygen.  
Zashchita metallov, no. 3, 1973, 291-293.

Oxidation of chromium boride ( $\text{CrB}_2$ ) was studied at 500-1200° C and 0.2-740 torr oxygen pressures. Weight increase and scale composition were determined by thermogravimetric, petrographic, and x-ray analysis. Before oxidation the hot-pressed specimens of chemically pure  $\text{CrB}_2$  powder were heat-treated in vacuum. Kinetic curves show that oxidation rate at 740 torr pressure increases sharply above 1150° C. At each temperature, the initially high oxidation rate levels off above a certain critical thickness of oxide layer. Decarburization with CO formation was observed at all temperatures in the cited range, and was accelerated above 1150° C due to decreased carbon diffusion rate. Weight increase at 900° C and 740 torr was smaller in specimens with a higher C content. The oxidation rate at 900° C decreases significantly, when oxygen pressure is decreased. At the same time, the probability of Cr vaporization increases. The scale phase composition varies from a single CrO phase at 500-700° C to two-phase ( $\text{B}_2\text{O}_3$  and  $\text{CrBO}_3$ ) composition at 900° C. Above 1000° C the two phases become intermixed to form a strongly adherent film; a decrease in oxygen pressure also enhances the intermixing of the two phases.

Kornilov, I. I. Relationship of a titanium oxide anomaly to a new structural diagram for a Ti-O system with suboxidation. DAN SSSR, v. 208, no. 2, 1973, 356-359.

Ti, Zr, and Hf manifest anomalies in the rate of their oxidation. A study of these anomalies has revealed that for Hf and Zr, instead of an even decrease of microhardness with respect to the depth of the oxidized layer, at a certain depth of this layer a plateau appears, which is inexplicable from the viewpoint of the theory of metal oxidation according to Wagner's parabolic law. For Zr two such plateaus have been detected, with no deviation from the even decrease of oxygen with respect to layer depth. The presence of such a plateau was recently proven experimentally for titanium (Kornilov, I. I. et al., Zashchita metallov, no. 1, 1973), a basis being thereby provided for an explanation of these phenomena from the viewpoint of the suboxide theory of the oxidation of transition metals, and for the establishment of a relationship between this anomaly and the phase diagram of the Ti-O system.

The total absorption of oxygen during the oxidation of titanium at 700-800° proceeds approximately parabolically. In an investigation of microhardness with respect to the depth of the oxidized layer of titanium there was established, for the first time, a discontinuity in the monotonic decrease of microhardness with respect to the depth of this layer. This was detected during the oxidation of specimens for 1000 hours at 700°, and for 500 hours at 800°. At other oxidation isotherms (600, 900, and 950°), no clearly expressed plateau was detected. A curve of change in microhardness of titanium with respect to the depth of the oxidized layer at 700° is presented in Fig. 1.

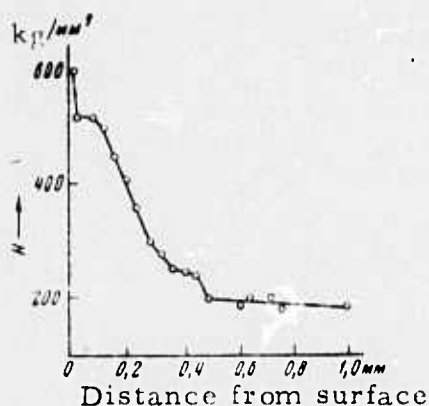


Fig. 1. Curve of microhardness vs. depth of oxygen penetration in the process of titanium oxidation at 700° during 1000 hours.

Two plateau sectors are seen with a constant titanium microhardness value (appr. 500 and 250 kg/mm<sup>2</sup>), which are analogous to two plateaus also established for zirconium. In the author's opinion, the appearance of the plateaus as a result of prolonged oxidation both of zirconium and titanium is connected with the appearance of their suboxides in a medium of alpha-solid solutions.

In Fig. 2 are presented the boundaries of the phase regions of the Ti-O system up to 32 at % and the values of hardness in relation to the composition and structure of alloys of a Ti - O system. Comparison of the curves of microhardness in relation to the composition (Fig. 2B) with the curve of microhardness in relation to the layers of oxidized titanium (Fig. 2A) discloses a definite relationship with the phase diagram of the Ti - O system with suboxides. In the equilibrium diagram (Fig. 2B), the compositions of suboxides Ti<sub>6</sub>O (γ-phase) and Ti<sub>3</sub>O (δ-phase) are characterized by singular minimum points, and on the diagram of titanium microhardness after oxidation (Fig. 2A) these phase regions appear as horizontal plateaus. Thus

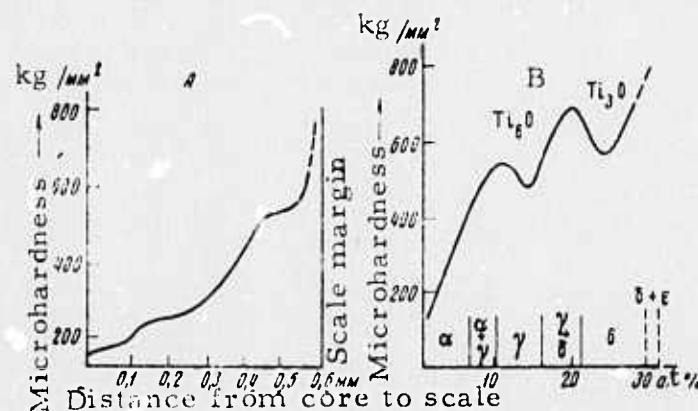


Fig. 2. Change of microhardness from the specimen core to the scale of oxidized titanium at 700° during 1000 hours (A), and change of microhardness due to oxygen concentration in alloys of a Ti - O system in the equilibrium state and the phase regions of this system at 20° (B)

the supposition of the suboxide mechanism of the oxidation of transient metals is confirmed on the basis of the example of titanium oxidation.

Petropavlovskaya, Z. N. High temperature relaxation strength of iron and nickel alloys.  
 MiTOM, no. 1, 1973, 36-39.

Most heat-resistant materials are heterophase, therefore in an investigation of the relaxation properties of heat-resistant steels and alloys, account must be taken of the influence of alloying upon the solid solution and upon the hardening phases. The alloying of solid solutions on the basis of nickel or iron to provide high relaxation resistance must be accomplished by elements which increase the elastic properties of the lattice, and which create heat-resistant hardening phases.

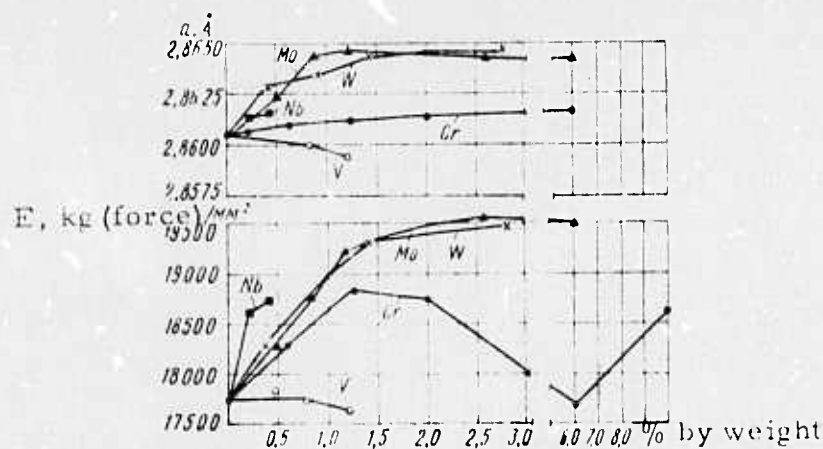


Fig. 1. Relationship of the lattice parameter and the modulus of normal elasticity at  $700^{\circ}$  to the content of alloying elements in solid solutions of nickel:

1. Ni-Cr alloy; Ni-W alloy with 15% Cr and 5% Mo; Ni-W alloy with 15% Cr; 5% Mo and 2% Nb.

In Fig. 1 is shown the relationship of the lattice parameter and the modulus of elasticity of a binary solid solution at  $565^{\circ}$  to the content of various alloying elements of the transition group. It can be seen that when the content of Nb, Mo, W, and Cr is increased up to saturation of the solid solution, a continuous increase of the lattice parameter takes place, and that the lattice parameter increases when vanadium is introduced.

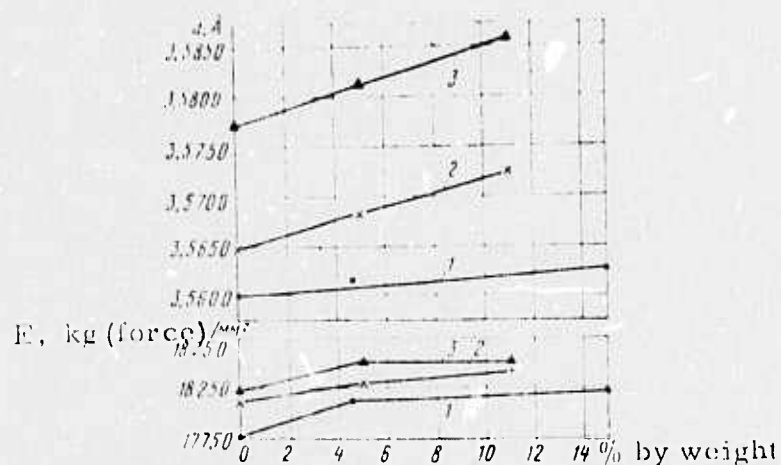


Fig. 2. Relationship of the lattice parameter and the modulus of normal elasticity at  $700^{\circ}$  to the content of alloying elements in solid solutions of nickel:

1 - Ni-Cr alloy; Ni-W alloy with 15% Cr and 5% Mo; Ni-W alloy with 15% Cr; 5% Mo and 2% Nb.

In a set of like curves in Fig. 2 is represented, at 700° C, the change in the elastic properties of solid nickel-base solutions. With the simultaneous alloying of binary nickel-base solutions by up to 15% Cr, up to 5% Mo, and up to 2% Nb, the parameter of the crystalline lattice increases considerably, and as the tungsten content is increased from 0 to 11%, a constant increase of the parameter is observed. The most effective influence upon the elasticity modulus of a nickel-base solid solution is exerted by the addition of 5% W, and with a subsequent increase in the content of W to 11% the elastic forces of the lattice do not increase, although the lattice parameter does increase.

Most effective for the polycomponent alloying of heterophase relaxation-resistant steels and alloys are such elements as niobium, molybdenum, vanadium, and tungsten, which form heat-resistant carbides of the NbC or the  $M_{23}C_6$  type, or intermetallides of the Laves-phase type; most favorable for the polycomponent alloying of nickel-base solid solutions are titanium and aluminum, which facilitate formation of the  $\gamma'$ -phase. Maximum hardening can be obtained at a low content of the alloying elements in comparison to the binary solid solutions. The greatest increase of relaxation resistance is attained with intermetallide and mixed hardening and the least such increase is attained by carbide hardening.

The presence of hardening phases increases the strength and the relaxation resistance only with their dispersed distribution in a solid solution with high elastic properties. In steel with carbide hardening, the average distance between the carbide particles is greater than the distance between intermetallide particles in steel with intermetallide hardening. In the latter case, the relaxation rate decreases sharply with a drop in particle size (and a consequent decrease in the distance between the particles), whereas with very small carbide particles (at an average separation of  $\leq 1.2 \mu$ ) the relaxation rate decreases sharply, due to dissolution of the fine carbides in the relaxation process at 565°.

Lipakis, A. L., A. L. Rusanov, V. V. Korshak, D. S. Tugushi, A. V. Kviklis, and A. N. Machyulis. Ablation of heat-resistant polymers. 3. Thermal oxidative degradation and ablation of poly (N- phenylbenzimidazole). AN LitSSR, Trudy, Seriya B, no. 6, 1972, 159-167.

Thermogravimetric, differential thermogravimetric, and ablation resistance tests are described on the recently synthesized poly (N-phenylbenzimidazole) (PBI-T) which exhibits good mechanical characteristics and high resistance to thermal oxidation. The experimental DTA and DTG curves show that PBI-T burns out completely at  $965^{\circ}\text{K}$  in an air stream. In agreement with theory, the experimental TG curve shows two distinct phases of thermal oxidation, with transition at 10% ablation. It is shown that a substantial char layer forms during the most intensive ablation in the  $850\text{-}925^{\circ}\text{K}$  range. Transition from the initial to a quasistationary ablation always occurs at the same value of specific mass loss ( $\sim 0.35\text{ kg/m}^2$ ), regardless of temperature. The mass ablation rate increases sharply when stagnation temperature of the air stream is increased from  $875$  to  $900^{\circ}\text{K}$ . This increase is explained in terms of weakening of the char layer by concurrence of thermal degradation and mechanical destruction. The authors conclude that PBI-T is more ablation-resistant than the poly(azophenylene) or phenolformaldehyde-base compositions.

Turchanin, A. G., Ye. A. Guseva, and  
V. V. Fesenko. Thermodynamic properties  
of refractory carbides at temperatures from  
0-3000° K. 3. Zirconium carbide. Poroshkovaya  
metallurgiya, no. 3, 1973, 47-50.

The equation

$$C_p = D\left(\frac{435}{T}\right) + E\left(\frac{750}{T}\right) + 1.0 \cdot 10^{-4} \cdot T + 1.5 \cdot 10^{-5} \cdot T^{3/2} \text{ [cal/mole. deg]}. \quad (2)$$

where D and E are Debye and Einstein functions, was derived for heat capacity  $C_p$  of ZrC using the method described by the authors in earlier publications, together with the available experimental  $C_p$  data at low temperatures. Equation (1) describes the cited data in the 100-350° K range to an accuracy of the order of 1.5%. Comparison of deviations of numerous experimental and reference  $C_p$  data at high temperature from  $C_p$  calculated from (1) shows that the calculated  $C_p$  (T) curve averages fairly well the experimental  $C_p$  data in the 300-3000° K range. Thus, Eq. (1) can be used to calculate  $C_p$  of ZrC in the 100-3000° K range. Fundamental thermodynamic functions of ZrC in the 0-3000° K range were calculated using  $C_p$  values estimated by means of (1). The tabulated functions are estimated to be accurate within about 2%.

Litvin, Yu. A., V. P. Butuzov, E. M.  
Nikiforova, and S. I. Futergendler.  
Growing diamond crystals in whisker and  
platelet form. Kristall, no. 2, 1973, 435-  
436.

Diamond whiskers a few hundred microns in length and up to  
50  $\mu$  in diameter, and platelets, e. g., 50 x 200 x 600  $\mu$ , were grown on a

synthetic diamond single crystal substrate from a metal-carbon system under ultrahigh pressures. Both formations are shown to be prismatic single crystals. They grow as isolated small crystals, in linear rows or in groups. Late diffraction studies established a parallel orientation of both formations relative to the substrate. Growth direction coincides with the  $\langle 110 \rangle$  orientation of C-C bonds. Crystal habit and morphology were determined. The whiskers grew also on the (100) face of the substrate. It is concluded that growth of both whiskers and platelets is the result of the substrate medium interaction under highly nonisothermic conditions. In this case dissolved carbon is transferred to the growth site exclusively by diffusion.

Cisowski, J., and W. Zdanowicz. Electrical properties of  $\text{Cd}_3\text{As}_2$  under high pressure. APP, v. A43, no. 2, 1973, 295-299.

Electrical resistivity  $\rho$  and Hall coefficient data are given and discussed to clarify the controversial band structure of the semiconductor  $\text{Cd}_3\text{As}_2$ . The experimental data were obtained with both polycrystalline and single crystal samples under 1 to 12 kbar hydrostatic pressures  $p$  in the 300-450° K range. Electron concentration in the samples varied from  $1.8 \times 10^{18}$  to  $7.7 \times 10^{18} \text{ cm}^{-3}$ .

The Hall coefficient was found to be practically independent of  $p$  and  $T$  in all samples but one. The experimental  $\rho$  versus  $p$  plots at 300-450° K show that  $\rho$  increases linearly with increase in  $p$ , at a rate inversely proportional to electron concentration. The  $p$  dependence pattern of  $\rho$  is independent of temperature. Temperature dependence of Hall mobility determined at 1 bar, 5, and 10 kbar pressures is given as  $\mu = A \times T^{-\alpha}$ , where  $A$  is a function of  $p$ . The cited data suggest that a single Kane-type conduction band is a reasonable model for  $\text{Cd}_3\text{As}_2$  semiconductor.

Fabrikov, M. Ye. Device for controlling isolated mobile cylindrical (bubble) magnetic domains. Otkr izobr, no. 13, 1973, no. 372579. (Translation).

The title device is composed of a thin magnetouniaxial crystal and a source of constant magnetic shift field. The purpose of the invention was to increase data recording density and response speed of the device. To this effect, a light source with a modulator and a projection unit are incorporated into the device and a photoresistive layer with electrodes is placed above the crystal. The projection unit is placed between the modulator and the photoresistor layer.

Mints, R. I., T. M. Petukhova, and V. M. Segal'. Structure of a metallic fragment of lunar material. MITOM, no. 1, 1973, 2-3.

A study is made of a metallic fragment of lunar material retrieved by the "Luna-16" space station. The composition of the lunar fragment was established to comprise Fe + 5.5% Ni + 0.6% Co. No carbon was detected. At least 90% of the particles is an alpha-solid solution. On the basis of the chemical and phase composition, the fragment appears to constitute a low-nickel octahedrite.

Metallographic study disclosed, in one of the sections, a subgrain with a martensite of dendritic morphology, with evidence of Neumann bands. The observed morphological, structural, and crystallographic features permit the dendritic martensite of the lunar nickel iron to be referred to the group of athermous martensites.

It was established that phase conversion took place at about  $600^{\circ}\text{C}$ ; such heating under conditions of the lunar surface could occur as a result of the inelastic impact of micrometeorites. However it was impossible to construct a consistent model of phase conversion in a lunar particle on the basis of the composition, morphology, and the assumed kinetics. It may be assumed that the dendritic martensite in the lunar fragment is a result not of  $\gamma \rightarrow \alpha$  transition, but of  $\alpha_2 \rightarrow \alpha$  transition, i.e., it was formed from a distorted body-centered cubic lattice. Additional verification is required from lunar specimens and on the basis of model alloys.

Brylov, S. A., and G. N. Martynov.

Resistance of crystals to mechanical effects.

IVUZ Geol, no. 1, 1973, 133-137.

The authors investigate the causes of the formation of crack nuclei in crystals, which must be studied at the level of the crystalline-lattice structures, on the basis of dislocation theory. The dislocation density was measured by selective etching of Iceland spar ( $10^4\text{ cm}^{-2}$ ), topaz ( $10^3\text{ cm}^{-2}$ ), beryllium ( $3 \times 10^2\text{ cm}^{-2}$ ), and piezo quartz ( $80-90\text{ cm}^{-2}$ ). It was found that the mineral with the highest plasticity had the greatest dislocation density (Iceland spar), and the most brittle one was piezo quartz.

To ascertain the conditions of intactness of crystals when they are acted upon by dynamic loads, experiments were conducted on the effect of various harmonic oscillations upon the behavior of dislocations in crystals. Crystals of Iceland spar were glued onto metal plates having different natural frequencies (400, 1000, 2000, and 5000 Hz). Oscillations were excited in the plates with the duration of their action upon the crystals and the energy of the action being in all cases identical. Study of the etched crystals showed that during high-frequency oscillations (5000 Hz), dislocations in the crystals

accumulate along specific directions (barriers). Such an accumulation is known to lead to the formation of cracks in a crystal. During low-frequency oscillations (400 Hz), accumulation of the dislocations was not observed, except at an approximately doubled oscillation energy.

To determine the effect of individual pulses on the process of crack formation in crystal, a series of experiments was conducted on an installation for the testing of transparent materials. Beryllium crystals were acted upon by excitation pulses of different duration and, consequently, of different spectral composition. The shape of the driving pulse, and the moment of appearance of the crack, were registered by means of a special photo sensor. Fig. 1 shows pulses of varied duration and energy, and the corresponding spectral densities.

An analysis of the acting pulses of all three series of experiments (Fig. 1, a, b, c) showed that during the action of short pulses (up to 3 millisecc), pulse no. 3, with an energy of  $0.85 \text{ joules/cm}^2$ , is the destructive one. For 6-millisecc pulses no. 3 is also the destructive one, but its density is  $1.10 \text{ joules/cm}^2$ . The spectra of the destructive pulses of all three series are shown together in Fig. 1, d, showing the spectrum of the destructive pulse of series c to have the narrowest frequency band.

The tests confirm the relatively greater damage effect of higher frequencies, or higher harmonics of pulsed loads; hence pulsed excitation should have a reasonably narrow spectral spread to avoid damage to the crystal.

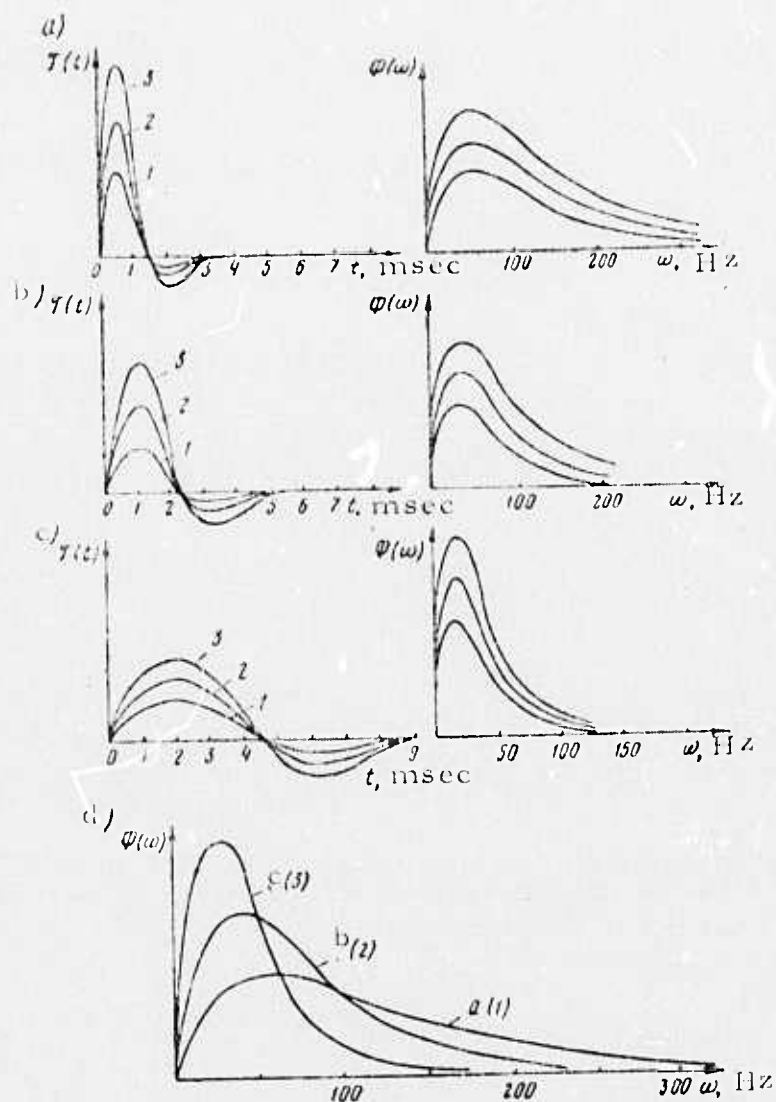


Fig. 1. Pulses of varied duration and energy, and the corresponding spectral densities.

Umanskiy, E. S., L. I. Tuchinskiy, V. V. Krivenyuk, and V. Ya. Fefer. Creep and long-term strength of molybdenum fiber-reinforced titanium. Problemy prochnosti, no. 1, 1973, 24-27.

In a study of the laws governing the creep and long-term tensile strength of combined materials, tests were conducted on titanium reinforced with continuous filaments of molybdenum, oriented along the tension axis. The creep and long-term strength characteristics during tensile load were determined under vacuum. Titanium compositions were studied having the following content of Mo filaments, by volume: 8, 22, and 38% as well as pure VT-10 titanium. The test specimens, consisting of titanium foils 0.08 mm thick, on which was wound a molybdenum wire 0.08 mm in diameter, were obtained under vacuum.

Results of tests of titanium foils, molybdenum wire, and compositions with the indicated components, conducted for long-term strength at 550° C, are shown in Fig. 1. According to the data a power-law relationship

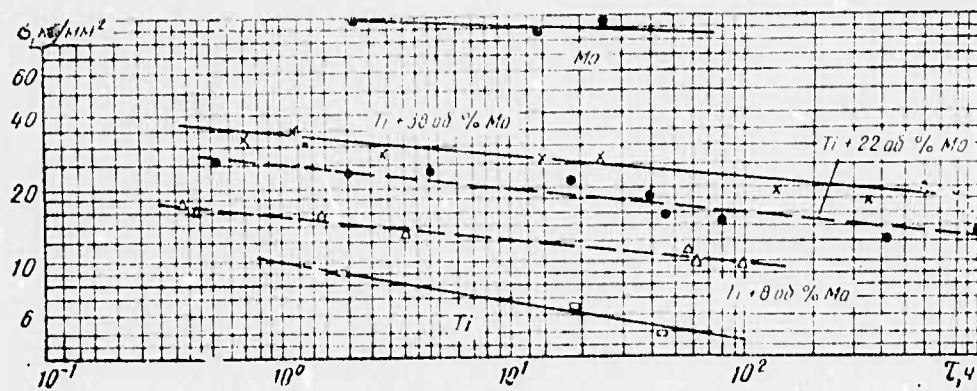


Fig. 1. Load vs. strength for Ti and Ti alloys.

exists between the load and the long-term strength for the titanium-molybdenum composites and its components. Analysis of the creep curves leads to the conclusion that in compositions with a molybdenum content by volume of 22% and above, the plasticity characteristics are essentially the same. The long-term strength of the composition, in relation to the volumetric content of molybdenum filaments, is subject to the law of additivity. The reinforcement of titanium by molybdenum filaments results in a considerable increase of strength; thus, at a longevity of  $t = 1$  hour, from  $10 \text{ kg/mm}^2$  for pure titanium the strength increases to  $15.5 \text{ kg/mm}^2$  for a composition containing 8% Mo by volume, and to  $34 \text{ kg/mm}^2$  for a composition containing 38% Mo by volume.

Bogdanov, A. G., I. I. Cheremisin, V. S. Rudenko, and B. P. Baranov. Failure of quartz single crystals from heating to high temperatures in a vacuum. NM, no. 2, 1973, 323-324.

Experiments were conducted to establish causes for the failure of quartz single crystals during heating in a vacuum to  $1300-2000^\circ \text{C}$ , and to ascertain the conditions under which they can be heated to such temperatures without breakdown.

Specimens of single-crystal quartz of various types - synthetic crystals (No. 4, 5) and a natural crystal from a deposit in the far northern Urals (No. 17) -- were ground into cylinders with a diameter and height of about 7 mm, such that the crystallographic axis  $c$  corresponded with the axis of the cylinder. Heating and subsequent cooling of the crystals was done in a vacuum of  $1-2 \times 10^{-5}$  torr at a rate of 6 degrees/min within the temperature range of  $20-800^\circ \text{C}$ , and at 14 degrees/min for higher temperatures.

Microscopic study of specimens subjected to this heat treatment revealed acute differences in their macrostructure. Investigation showed that a change of parameters  $a$  and  $c$  of hexagonal quartz shows no anomalies in the temperature range from 800 to 1600° C and is insignificant in amount. It is obvious that the small thermal expansion of  $\alpha$ -quartz cannot be the cause of its failure at high temperatures. It was noted that a definite relationship exists between the heat resistance of various quartz crystals at high temperatures and the initial content of water in them.

The cited quartz specimens were subjected to diffusion annealing for 48 hours at 1250° C. After annealing, specimen No. 5 broke down completely and proved to be totally unsuitable for spectrography. Specimens No. 4 and 17 manifested no visible macroscopic defects. Specimens that had been subjected to diffusion annealing were subjected to microstructural analysis after heating to 1400° C by the usual program, with a subsequent temperature increase to 1700° C within the space of 150 seconds and with cooling from 1700 to 1400° C within the same period of time. As a result of heating, specimens No. 5 and 17 broke down, although to a different degree, while specimen No. 4 (a synthetic crystal with the minimal initial water content), manifested, under microscopic observation, only the finest of internal flaws, linearly grouped by separate "tunnels" parallel to the  $c$  axis.

Uvarov, V. V., and V. N. Samokhvalov.

Heat and mass transfer during liquid  
evaporation from capillary-porous bodies  
immersed in hot air flow. IVUZ Mashinostroyeniye, no. 2, 1973, 68-72.

An analysis is made of the results of an experimental investigation of external heat and mass transfer for the case of the evaporation of a liquid from a capillary-porous body, where the evaporation surface is depressed within the material. The experimental stand on which this investigation was conducted is briefly described. Research was conducted primarily on foam polyvinyl formal (FPVF). The coefficients of heat and mass transfer were determined on the basis of the difference of the partial vapor pressures or the temperature difference between the air outside the boundary layer and the surface of the material.

Criterial equations are presented for longitudinal and frontal flow of air about the body.

The process of adiabatic evaporation during longitudinal flow about a porous body was studied at an air velocity of 0.8 - 12.4 m/sec; the air temperature at the intake was 100-160°C, the absolute air humidity at the intake was 4 - 40 g/kg. The total evaporated fluid comprised 3.5 - 15.5 kg/m<sup>2</sup> hour. The length of the evaporation surface in the direction of movement of the air was adopted as the determining dimension. Processing of results of the experiment for FPVF in relative coordinates in relation to the injection factor manifested good agreement of experimental results with the theory.

A study of the process of adiabatic evaporation during frontal flow was conducted with distributive grids of varied configurations. The air velocity at the grating apertures varied from 1.9 to 25 m/sec; the remaining parameters were the same as for longitudinal flow. The moisture collection comprised 4-28 kg/m<sup>2</sup> hour. The velocity of the air flowing out of the nozzles was adopted as the determining velocity, and the distance between the grating and the surface of the material was adopted as the determining dimension. Processing of the experimental data was conducted in the conventional manner in relation to the geometric parameters of the nozzles.

With calculation of the process of heat and mass transfer on the basis of mean parameters, the schemes for calculation of the adiabatic and nonadiabatic processes of evaporation become identical, and therefore the relationships used for adiabatic evaporation were used in the case of nonadiabatic evaporation as well.

Three possible limit cases of the process may be considered :  
1) the surface temperature of the material ( $t_s$ ) is greater than the temperature of the evaporation surface ( $t_e$ ), then the moisture content of the air on the surface of the material ( $d_s$ ) is equal to the moisture content of the evaporation surface ( $d_e$ ) since condensation is absent in the layer between the surface of the material and the evaporation surface; 2)  $t_s = t_e$ , then  $d_s = d_e$ ; 3)  $t_s < t_e$ , then  $d_s < d_e$ , since the vapor of the fluid condenses and, consequently,  $d_s$  should be sought as the point of intersection of  $t_s$  with the saturation line.

Results of calculations of the process of nonadiabatic evaporation, taking into account heat transfer from the heat carrier and the evaporation surface and using the equations recommended for adiabatic evaporation, have coincided with the experimental data to within  $\pm 10 - 15\%$ .

Regel', V. R., and A. I. Slutsker. All-Union conference on microanalysis of polymer fracturing. (Leningrad, 14-16 June 1972). MP, no. 1, 1973, 185-186.

The conference was convoked by the Scientific council on problems of solid state physics at the Presidium of the Academy of Sciences, USSR and the laboratory of the physics of strength of the Physicotechnical Institute imeni A. F. Ioffe, Academy of Sciences, USSR (Leningrad) headed by academician S. N. Zhurkov. Participating in the conference were about 180 scientific researchers from 24 cities of the USSR. Sixty-seven reports were presented.

The Conference was divided into three sections: a) elementary acts of polymer destruction; b) submicroscopic (nucleating) cracks; microscopic and macroscopic (main) cracks; c) questions pertaining to the relationship between polymer destruction and deformation. A brief discussion on these topics is included.

## B. Recent Selections

### i. High Pressure Research

Adadurov, G. A., V. V. Gustov, V. S. Zhuchenko, M. Yu. Kosygin, and P. A. Yampol'skiy. Transformation of shock compression into isentropic compression. FGiV, no. 4, 1973, 576-579.

Apayev, T. A., and A. M. Kerimov. Experimental study of cyclohexane density at high pressures and temperatures. ZhFkh, no. 8, 1973, p. 2144.

Baturin, V. Ye., Yu. D. Klebanov, B. V. Rozanov, and V. N. Sumarokov. Investigating characteristics of cold and hot molding of powdered blanks. Poroshkovaya metallurgiya, no. 8(128), 1973, 10-14.

Bordzilovskiy, S. A., and S. M. Karakhanov. Emf source parameters in a shock-compressed copper-nickel couple. ZhTF, no. 9, 1973, 1979-1986.

Bychkov, Yu. F., Yu. N. Likhanin, and V. A. Mal'tsev. Physical properties of the  $\omega$ -phase of zirconium. FMiM, v. 36, no. 2, 1973, 413-414.

Gol'dshteyn, V. Ya., M. A. Smirnov, and E. S. Atroshchenko. Structural changes from heating of shock loaded silicon iron. FMiM, v. 36, no. 2, 1973, 352-357.

Gural'nik, E. Kh., L. Yu. Maksimov, G. G. Mukhin, and V. Ye. Slobtsov. Increase in plasticity of molybdenum after hydrostatic compression. FikHOM, no. 4, 1973, 89-92.

Klochkov, I. S., and N. D. Manachinskiy. Ignition of hexogene by heated wires at 1000-13,000 kg/cm<sup>2</sup> pressures. FGiV, no. 4, 1973, 510-515.

Kositsyn, V. P., T. M. Platova, and I. Ye. Khorev. Phase transitions in low-carbon steel at high pressures. FiKhOM, no. 4, 1973, 143-146.

Martin, G., and E. Hegenbarth. The effect of hydrostatic pressure on the ferroelectric phase transition of CdTiO<sub>3</sub> ceramics. PSS(a), v. 18, no. 1973, K151-K153.

Shekhter, B. I., and L. A. Shushko. Shock adiabats of some layered plastics. FGiV, no. 4, 1973, 599-601.

Simakov, G. V., M. A. Podurets, and R. F. Trunin. New data on compressibility of oxides and fluorides, and on a hypothesis of Earth's homogeneous composition. DAN SSSR, v. 211, no. 6, 1973, 1330-1332.

Vdovkin, G. P., A. N. Dremin, S. V. Pershin, and I. D. Shevalevskiy. Transformation of meteoritic substance in experiment's on shock compression at 500-1000 kbar pressures, generated by an explosion. FGiV, no. 4, 1973, 535-541.

ii. High Temperature Research

Baranov, V. M., V. G. Bukatov, and O. S. Korostin. Temperature dependence of elasticity constants of vanadium carbides. NM, no. 8, 1973, 1362-1364.

Dombrovskiy, L. A., and N. N. Ivenskikh. Radiation of a homogeneous plane-parallel layer of spherical particles. TVT, no. 4, 1973, 818-822.

Guzman, I. Ya., Yu. N. Litvin, Ye. V. Putrya, Ye. I. Tumakova, and A. V. Fedotov. Oxidation of silicon nitride, silicon oxynitride,  $Al_2O_3$  - and SiC-base oxynitride binders. IN: Tr. Mosk. khim-tekhmol. in-ta. im. D. I. Medvedeva, no. 72, 1973, 76-78. (RZhKh, 17/73, no. 17M59).

Konkin, A. A. Uglerodnyye i drugiye zharostoykiye voloknistyye materialy. (Carbon and other heat-resistant fibrous materials). Izd-vo Khimiya. (NK, 37/73, to be published early in 1974).

Korshunov, I. G., V. Ye. Zinov'yev, P. V. Gel'd, V. S. Chernyayev, A. S. Borukhovich, and G. P. Shveykin. Thermal diffusivity and thermal conductivity of titanium and zirconium carbides at high temperatures. TVT, no. 4, 1973, 889-891.

Kozlov, L. F., and V. G. Mizak. Approximate integration of the equations of a laminar boundary layer on a porous heat-insulated surface in a compressible gas with suction. IN: Gidromekhanika. Resp. mezhved. sb., no. 23, 1973, 26-40. (RZhMekh, 8/73, no. 8B613).

Levitskiy, V. A., N. N. Shevchenko, Yu. Khekimov, and Ya. I. Gerasimov. Studying interactions of strontium oxide and strontium tungstate with zirconium at high temperatures in hydrogen or in vacuum. DAN, v. 211, no. 4, 1973, 916-919.

Mikhaylov, Yu. A., and Yu. T. Glazunov. An approximate method of solving two-dimensional problems of heat- and mass-transfer. IAN Lat, Seriya fizicheskikh i tekhnicheskikh nauk, no. 4, 1973, 45-52.

Mohamed Salakh Sifani. Experimental study of the temperature field in porous bodies during evaporation with intensification. IN: Sb.

Protsessy perenosa energii i veshchestva pri nizk. temperaturakh v vakuume. Minsk, 1973, 186-205. (RZhMekh, 8/73, no. 8B643)

Nemets, I. I., A. I. Nestertsov, G. V. Kukolev, et al. Effect of Al-containing components on the phase alloying of periclase ceramics.

NM, no. 8, 1973, 1399-1403.

Petrak, D. Numerical computation of convective heat exchange between spherical particles and gas flow. IN: Sb. Teplo- i massoperenos, v. 9, pt. 2, Minsk, 1972, 27-44. (RZhMekh, 8/73, no. 8B623)

Poluboyarinov, D. N., I. G. Kuznetsova, and Ye. P. Sadkovskiy. A method of manufacturing refractory products from boron nitride powder. Author's certificate, USSR, no. 357185, published January 25, 1973. (RZhKh, 15/73, no. 15M62 P)

Poluboyarinov, D. N., A. S. Metushevskiy, D. M. Karpinos, V. M. Grosheva, Ye. P. Mikhachuk, and A. S. Vlasov. A refractory material. Author's certificate, USSR, no. 357183, published January 25, 1973. (RZhKh, 15/73, no. 15M40 P).

Rasin, O. G., V. I. Krivtsun, and V. A. Krivonos. A method of calculating convective heat exchange on nonisothermic evaporation surfaces. IN: Sb. Protsessy perenosa energii i veshchestva pri nizk. temperaturakh v vakuume. Minsk, 1973, 175-179. (RZhMekh, 8/73, no. 8B645).

Rud', Yu. V., and K. V. Sanin. Investigating the electrical conductivity of CdSe single crystals at high-temperatures. UFZh, no. 8, 1973, 1377-1383.

Usov, P. G., V. I. Vereshchagin, V. A. Amelina, and N. V. Sobora. Synthesis and baking of  $\text{MgAl}_2\text{O}_4$  at lowered temperatures. IN: Sb. tr. molodykh uchenykh. Tomsk. politekhn. in-t., no. 1, 1973, 98-101. (RZhKh, 17/73, no. 17M50).

Vasil'yeva, I. A., and I. S. Sukhushina. Thermodynamic properties of vanadium oxides of the  $\text{V}_n\text{O}_{2n-1}$  ( $n = 4$  and  $7$ ) series at high temperatures. ZhFKh, no. 8, 1973, 2083-2084.

Vasil'yeva, I. A., and I. S. Sukhushina. Thermodynamic properties of  $\text{V}_3\text{O}_5$  at high temperatures and at  $298.15^\circ\text{K}$ . IN: ibid., 2085-2086.

Vasil'yeva, I. A., I. S. Sukhushina, and R. F. Balabayeva. Thermodynamic properties of vanadium oxides of the  $\text{V}_n\text{O}_{2n-1}$  ( $n = 5$  and  $8$ ) series at high temperatures. IN: ibid., 2162.

Yurevich, F. B., and V. M. Kaptsevich. A nonstationary method of separating radiative and convective components of a heat flux during a complex heat exchange. IAN B, seriya fiz.-energ. nauk., no. 1, 1973, 84-85. (RZhMekh, 8/73, no. 8B616)

Zen'kovskiy, A. G., and S. I. Gertsyk. Radiative heat exchange in a plane layer of an absorbing medium. IN: Sb. tr. Mosk. vech. metallurg. in-t., no. 12, 1972, 273-276. (RZhMekh, 8/73, no. 8B615)

### iii. Miscellaneous Material Properties

Akulichev, V. A., and V. A. Bulanov. Tensile strength of liquid hydrogen. ZhETF, v. 65, no. 2, 1973, 668-672.

Arkhipov, S. M., V. A. Kaz'minskaya, V. I. Kidyarov, and P. L. Mitnitskiy. Effect of  $\text{HIO}_3$  on lithium iodate crystallization during evaporation of water solutions. IAN SO SSSR, seriya khim. nauk, no. 9, 1973, 39-43.

Berlyant, S. M., and A. A. Gavlovskiy. Physicomechanical properties of  $\gamma$ -irradiated tetrafluoroethylene + vinylidenefluoride copolymers. Plasticheskiye massy, no. 8, 1973, 9-11.

Grishin, A. M., and E. A. Kaner. Giant quantum oscillations of Rayleigh sound waves in metals. ZhETF, v. 65, no. 2(8), 1973, 735-750.

Gunayev, G. M., I. G. Zhigun, T. G. Sorina, and V. A. Yakushin. Shearing strength of composites based on whiskerized fibers. MP, no. 3, 1973, 492-501.

Korshak, V. V., D. P. Kunchuliya, and N. I. Bekasova. Synthesis and study of poly(m-carboranylenehydrazides) and poly(m-carboranylene-1, 3, 4-oxadiazoles). Vysokomolekulyarnyye soyedineniya, v. (A)15, no. 8, 1973, 1731-1736.

Korzo, V. F., and V. Ya. Chebotarenko. Radiation-stimulated electrical conductivity of quasiamorphous layers of pyrolytic carbon-alloyed chromium. FiKhOM, no. 4, 1973, 34-37.

Kuznetsov, N. P., M. I. Bessonov, and N. A. Adrova. Studying strength and relaxation characteristics of a polyimide. Vysokomolekulyarnyye soyedineniya, v(A)15, no. 8, 1973, 1886-1892.

Rafikov, S. R., I. V. Zhuravleva, R. S. Ayupova, et al. Investigating aging processes in carboran-containing polyarylates. Vysokomolekulyarnyye soyedineniya, v(A)15, no. 8, 1973, 1706-1712.

Samodurova, I. D., and A. S. Sonin. Investigating the domain structure of p-azoxyanisole liquid crystal by means of light diffraction. FTT, no. 8, 1973, 2359-2362.

Vinogradova, S. V., N. A. Churochkina, Ya. S. Vygodskiy, and V. V. Korshak. Synthesis and properties of mixed cardiac polyimides. Vysokomolekulyarnyye soyedineniya, v. (A)15, no. 8, 1973, 1713-1717.

Zaytseva, L. L., M. I. Konarev, A. I. Sukhikh, et al. Obtaining molecular cermets from pertechnetates of rare-earth elements and yttrium. NM, v. 9, no. 8, 1973, 1423-1426.

iv. Superconductivity

Abrikosov, A. A., and V. M. Genkin. The theory of optical Raman scattering in superconductors. ZhETF, v. 65, no. 2, 1973, 842-847.

Babenko, B. F., F. A. Vodopyanov, Yu. F. Dushin, et al. A 900 Mev superconducting isochronous cyclotron. IN: Tr. Radiotekhn in-ta. AN SSSR, no. 11, 1972, 90-99. (RZhElektr, 9/73, no. 9A278)

Likharev, K. K. Nonlinear properties of granular superconducting films. FTT, no. 8, 1973, 2524-2527.

Likharev, K. K., and V. K. Semenov. Effect of fluctuations on the SHF impedance of superconducting point contacts. RiE, no. 8, 1973, 1757-1759.

Litvinov, V. N. Superconducting accelerating resonators with variable frequency tuning. IN: Radiotekhn. in-ta. AN SSSR, no. 11, 1972, 148-156. (RZhElektr, 9/73, no. 9A274)

Menke, Kh., and Yu. A. Shishov. Sverkhprovodyashchaya peremychka. (A superconducting bridge). Dubna, 1973, 11 p. (KL, 34/73, no. 27936)

Serdyuk, A. D., and I. I. Fal'ko. Spin-lattice relaxation of a two-band superconductor, taking into account the interband scattering of electrons by phonons. FMiM, v. 36, no. 2, 1973, 427-429.

Soldatov, V. P., V. I. Startsev, T. I. Vaynblat, and Yu. G. Kazarov. Issledovaniye nizkotemperaturnoy plastichnosti sverkhprovodyashchikh splavov Pb-Sb. (Investigating low-temperature plasticity of superconducting Pb-Sb alloys). Khar'kov, 1972, 15 p. (KL Dop vyp, 7/73, no. 15244).

Tagintsev, Yu. F. An experimental superconducting quadrupole lens with 1 kg/cm magnetic field gradient and a 65 mm aperture. IN: Tr. Radiotekhn. in-ta. AN SSSR, no. 11, 1972, 142-147. (RZhElektr, 9/73, no. 9A273)

Troitskiy, A. M. Optimizing the winding geometry of a superconducting inductive energy storage device. IN: Tr. Radiotekhn. in-ta. AN SSSR, no. 11, 1972, 138-141. (RZhElektr, 9/73, no. 9A272)

Vasenko, S. A. Detecting electromagnetic radiation by superconducting point contacts. RiE, no. 8, 1973, 1694-1697.

Vodopyanov, F. A., and Yu. F. Tagintsev. A superconducting synchrotron with mechanically shifting time-independent magnetic field. IN: Tr. Radiotekhn. in-ta. AN SSSR, no. 11, 1972, 111-120. (RZhElektr, 9/73, no. 9A279)

Zel'dovich, A. G., and Yu. A. Shishov. Termostatirovaniye sverkhprovodyashchikh magnitov s vnutrenney stabilizatsiyey bez podvoda geliya k obmotke. (Thermostatic control of superconducting magnets with internal stabilization, without helium supply to the winding). Dubna, 1973, 7 p. (KL, 34/73, no. 27926).

v. Epitaxial Films

Adonin, A. S., N. G. Ryabtsev, and L. N. Mikhaylov. Studying temperature and concentration dependences of epitaxy and etching of gallium arsenide in an open chloride system. IN: Sb. Khimiya i khim. tekhnol. Moskva, 1972, 363-365. (RZhKh, 16/73, no. 16B551)

Bolkhovityanov, Yu. B., R. I. Bolkhovityanova, and P. L. Mel'nikov. The dependence of GaAs film morphology on liquid epitaxy conditions. NM, no. 8, 1973, 1320-1324.

Ikonnikova, G. M. Effect of magnetic field on epitaxial growth of gallium arsenide. IN: Dokl. 19-y Nauch. -tekhn. konf. posvyashch. dnyu radio. Tomsk, 1972, 25-29. (RZhKh, 15/73, no. 15B553)

Malkin, G. M., V. Ye. Grigor'yev, and A. A. Tumanov. Etching and growth of Ge in a flow system with cyclic diffusive mass-transfer. NM, no. 8, 1973, 1427-1428.

Postnikov, V. S., V. M. Iyevlev, I. V. Zolotukhin, and G. S. Rodin. Growing  $\text{LiNbO}_3$  epitaxial films. NM, no. 8, 1973, p. 1455.

Zavadskiy, V. A., V. I. Kuznetsov, and V. A. Mokritskiy. Reducing the dislocation density in GaP epitaxial layers. NM; v. 9, no. 8, 1973, 1443-1444.

## 6. Atmospheric Physics

### A. Abstracts

Vas'kov, V. V., and A. V. Gurevich.  
Parametric excitation of Langmuir  
oscillations in the ionosphere by a strong  
r-f field. IVUZ Radiofiz, no. 2, 1973,  
188-198.

The authors note that parametric instability in plasma occurs when the amplitude of the E-field of the r-f wave exceeds some threshold value  $E_t$  which depends on the concentration of plasma, the temperature and collision frequency of electrons, and ion temperature. In the present article the specific conditions for parametric instability of an ionospheric region in the neighborhood of the point of reflection of an ordinary radio wave are analyzed. The incident e-m waves excite ion-acoustic oscillations in the plasma with frequency  $\Omega$ , and Langmuir oscillations with frequency  $\Omega \pm \omega$ . On the basis of dispersion equations for the excitation of oscillations and other considerations, equations are derived for determining two types of plasma instability-the periodic instability with  $\Omega \neq 0$ , and aperiodic instability with  $\Omega = 0$ . Both types of instability are analysed, a formula for determining the minimal threshold field  $E_t^2$  is obtained, and the conditions establishing the domain for the minimal value  $E_t$  are derived.

The dependences of minimal threshold field  $E_t$  on altitude in the ionosphere during the night and day hours and at various longitudes are presented graphically. Since at  $E > E_t$  the parametric instability develops in the vicinity of the field maxima, the formula for the number of maxima and the amplification coefficients are derived and their dependence on altitude is

graphically shown. Finally, the effective threshold radiation power above which parametric excitation of the ionosphere sets in is determined and its dependence on  $\omega$  during the day and night hours is demonstrated.

Semenova, V. I. Effect of collisions on e-m wave propagation in plasma formed by a moving ionization source. IVUZ Radiofiz, no. 12, 1972, 1793-1800.

The effect is studied of charged particle collisions on the propagation of monochromatic plane e-m waves in a plasma formed by a moving ionization source. For determining the electromagnetic field in a plasma, which varies according to an exponential law, Maxwell's equations and the equation of electron motion are used. The equation for determining the frequency of the transmitted wave is derived. Using the approximate solutions of these equations, formulas are derived defining the attenuation of e-m waves in plasma behind the ionization front, with the following limitations: 1) The collision frequency of charged particles is small; 2) The collision frequency is high as compared to the frequency of the incident wave or the Langmuir frequency of plasma electrons.

From analysis of the obtained results, conditions are defined under which the collisions have little effect upon the propagation of waves behind the ionization front. Strong collisions in plasma behind the ionization front signify that the characteristics of the formation of charged particles at the front become unimportant and the electromagnetic field behind the front, as in the case of the stationary medium motion, can be determined from the basic parameters  $\epsilon$  and  $\delta$  (dielectric permeability and conductivity) of the plasma. The fields behind the ionization front in the limiting case for which the propagation velocity of the ionization front is near the velocity of light ( $V_0 \rightarrow c$ ), are also established.

Armand, S. A. Deformation of a Gaussian electromagnetic wave beam in a nonuniformly stratified nonlinear medium. RiE, no. 1, 1973, 1-8.

The propagation of a Gaussian beam of e-m waves in a nonhomogeneous, nonlinear medium is analyzed, under the assumption that the linear part of the dielectric permeability is a monotonic function of a space coordinate  $z$ . A qualitative analysis of this problem was carried out, first on the basis of evident physical considerations and then on the basis of a nonlinear parabolic-type wave equation solution. For obtaining this solution the concept of a "thin" beam was introduced and the solution was analyzed in the subcaustic region. The procedure is described how the approximate solution of this equation using the methods of numerical analysis can be obtained. On the basis of obtained results it established, that a cylindrically-symmetric Gaussian beam transforms into an elliptic in media with a regular gradient. The formation of ellipticity due to action of refraction during self-focusing the beam does not converge into a point as in the case of a homogeneous medium. Two separate regions are originated where  $\underline{a}$  (the radius of a beam in the  $\{z, y\}$  plane) and  $\underline{b}$  (the radius of a beam in a plane perpendicular to  $\{z, y\}$  plane) assume minimum values. In these regions the beam takes on an elliptical form with large eccentricities and major semi-axes located in perpendicular planes. The locations of these regions along the beam axes are determined. The eccentricity of the ellipse, which characterizes the profile of a beam and depends on the field intensity, is analyzed.

Berger, V. K. Reflection of e-m waves from heterogeneous anisotropic plasma layers (normal incidence). GiA. no. 1, 1973, 173-177.

The normal incidence of an electromagnetic wave propagating along the coordinate  $z$ , upon a layer of plane-laminated inhomogeneous (along the  $z$ -axis) anisotropic plasma, is considered. The equation describing the e-m field of such a medium is taken in the form

$$\frac{d^2 E_\mu}{dz^2} + \frac{\omega^2}{c^2} \sum_{\nu=1}^2 A_{\mu\nu} E_\nu = 0, \quad (1)$$

where indices  $\mu$  and  $\nu$  assume values 1, 2 and correspond to coordinates  $x$  or  $y$ . The coefficients  $A_{\mu\nu}$  are expressed in terms of  $H_0$  - the constant magnetic field,  $e$ ,  $m$ ,  $N$  - the charge, mass and concentration of electrons respectively,  $\nu_{\text{eff}}$  the effective frequency of electron collisions with molecules and  $\phi$  - the angle between the magnetic field  $H_0$  and wave vector of an incident wave. The solution of Eq. (1) is sought in the form

$$E_\mu = \sum_{m=0}^{\infty} E_\mu^{(m)} \alpha^m \quad (2)$$

where  $\alpha \equiv \omega/\nu_{\text{eff}}$

The coefficients of Eq. (1) also are expanded in infinite series in powers of  $\alpha$  which together with values from (2) are substituted into Eq. (1). By equating the coefficients of terms with various powers of  $\alpha$  to zero, a system of equations for various approximations of the e-m field of the wave in the plasma layer is derived.

A complete solution of the system describing the e-m field in a plasma layer is presented. The conditions under which the solution is convergent are established. Expression for the first approximation of the wave transmission coefficient as well as expressions for polarization coefficients of the incident, reflected and transmitted waves are derived. The author notes that the results obtained can be used to analyze wave reflections from nonuniformities in the lower atmosphere.

Kaufman, R. N. Propagation of LF electromagnetic waves in the Earth-ionosphere waveguide. GiA, no. 1, 1973, 68-73.

The propagation of low frequency e-m waves in a spherical waveguide located near the ground and surrounded by an inhomogeneous isotropic ionosphere is analysed. It is assumed that the complex permeability is a linear function of the ionosphere radius vector ( $\epsilon = \epsilon(\mathbf{r})$ ), and the geomagnetic field is neglected. Determination of the e-m field components E and H and of the structure of the magnetic field is based on the analytic solution of a corresponding boundary value problem for the Hertz function differential equation, which is obtained from Maxwell's equations. The Hertz function within the waveguide and in the ionosphere is sought in the form of infinite series in terms of spherical Bessel functions and radial functions. The coefficients of expansions are determined from boundary conditions. The derived series are found to converge very slowly. To increase the rate of convergence the Watson transform (G. N. Watson, Proc. Roy. Soc., 1919, 95A, 546) was applied. After this transformation, the expansions of the Hertz function in series in normal waves (modes) converge more rapidly, so that only a few terms are necessary to calculate the Hertz function with sufficient accuracy. From the Hertz function the e-m field components can be readily calculated. Numerical estimates of the width of the reflecting and of the skip layers are derived on the basis of experimental data.

Getmantsev, G. G., G. P. Komrakov,  
V. P. Ivanov, I. V. Popkov, and V. N.  
Tyukin. Results of Cosmos-381 measure-  
ments of inhomogeneities in electron  
concentration of the ionosphere.  
Kosmicheskiye issledovaniya, no. 2,  
1973, 335-338.

Electron concentration and its inhomogeneities in the atmosphere were measured by Cosmos-381, which was launched on December 2, 1970, using a HF impedance probe. Electron concentration was determined by measuring change in capacitance of the recording probe depending on variations of the ionospheric dielectric constant at a frequency  $f \approx 3$  MHz. Measurements were recorded 29 times during flights (29 revolutions) over a portion of ground with longitudes from  $-70^\circ$  east to  $+70^\circ$  west and from  $74^\circ$  to  $40^\circ$  mean latitude. Graphs are plotted of electron concentration for two discrete regions: region 1 -  $40^\circ$  to  $60^\circ$  latitude and region 2 -  $60^\circ$  to  $74^\circ$  latitude. It was noted that the increase in average concentration for region 1 was from  $8 \times 10^{-3}$  (size of inhomogeneity,  $L = 1-2$  km) to  $4 \times 10^{-2}$  ( $L = 40-70$  km) during daytime, and from  $3.5 \times 10^{-3}$  (1-2 km) to  $2.2 \times 10^{-2}$  (15-40 km) at night. For region 2, the concentration increase during day was from  $5 \times 10^{-3}$  (1-2 km) to  $3.6 \times 10^{-2}$  (40-70 km), and during night - from  $4.4 \times 10^{-3}$  (1-2 km) to  $9.2 \times 10^{-3}$  (15-40 km). Graphs for occurrence probability of inhomogeneous electron concentrations show that in region 1 the probability of inhomogeneity occurrence for electron concentrations of size 1 to 40 km is nearly identical, and does not depend on  $L$  during day; but at night it shows a maximum for size 1 to 5 km. For region 2, maximum inhomogeneity occurrence is noted for electron concentration of size 2 to 5 km during day as well as night. The probability of inhomogeneity occurrence decreases for electron concentrations of size below 1 km and greater than 40 km.

Zavorotnyy, V. U., and V. I. Tatarskiy.  
Quantum fluctuations of photon flux from  
propagation in free space and in a diffraction  
pattern. ZhETF, v. 61, no. 2, 1973, 453-462.

Statistical characteristics of the number  $V_{\Sigma T}$  of photons traversing a surface of area  $\Sigma$  during a sufficiently long time  $T$ , in free space is considered. The mean value  $\langle V_{\Sigma T} \rangle$ , the mean-square value  $\langle (\Delta V_{\Sigma T})^2 \rangle$ , and three-dimensional correlation functions of  $V_{\Sigma T}$  for coherent monochromatic and thermal radiation sources are established, using the expression for operator  $V_{\Sigma T}$  derived earlier (Tatarskiy, ZhETF, 63, 1968, 2077). The ratio  $\langle (\Delta V_{\Sigma T})^2 \rangle / \langle V_{\Sigma T} \rangle$  for  $R \ll \lambda$  and  $R \gg \lambda$ , where  $R$  is the radius of circular area  $\Sigma$  and  $\lambda$  is the operating wavelength, are analyzed. It is shown that in the former case the ratio differs significantly from a Poisson distribution, but in the second case does correspond to the Poisson law.

The basic statistical characteristics for the fluctuation of the number of photons in a free space derived by use of operator  $V_{\Sigma T}$  coincide with corresponding characteristics for photocounts. Statistical characteristics of  $V_{\Sigma T}$  ( $\langle V_{\Sigma T} \rangle$  and  $\langle (\Delta V_{\Sigma T})^2 \rangle$ ) in the case of optical diffraction by a rectangular aperture are also established using a scalar approximation. The solution obtained by the Kirchhoff method in the Fraunhofer region of diffraction is taken as an approximate solution. The statistical characteristics derived differ from the characteristics obtained in a free space. The ratio  $\langle (\Delta V_{\Sigma T})^2 \rangle / \langle V_{\Sigma T} \rangle$  in the diffraction case differs significantly from the Poisson distribution law.

Bukatyy, V. I., N. V. Kozlov, and  
S. S. Khmelevtsov. Determining  
microstructures of freely falling aerosols  
by an optical method. IVUZ Fiz, no. 3,  
1973, 105-107.

Preliminary laboratory data are given on drop-size spectra of stabilized artificial fogs. The data were obtained by measuring transparency of the free-falling aerosol to a collimated beam from a He-Ne laser at  $0.63 \mu$  and a  $5'$  divergence. The time-dependent transparency data thus obtained were used to calculate drop-size distribution function  $F$  and the function  $N = F/k$  of the counting particle concentration, where  $k$  is the volumetric coefficient of attenuation. Calculations were based on the Mie scattering theory and Stokes' precipitation law. Limitations of the method are discussed.

The  $N$  versus particle size data obtained by the cited method are compared with  $N$  data from microphotographs of the aerosol probes picked up by a trap simultaneously with the scattering signal recordings. The two sets of data are shown to be in satisfactory agreement. Thus, the study confirms the reliability of the optical method of drop-size spectra determination in a stabilized artificial fog.

Borovoy, A. G., B. V. Goryachev, B. N.  
Denchik, and B. A. Savell'yev. Fluctuations  
in light flux propagating in a dispersive  
medium. IVUZ Fiz, no. 3, 1973, 101-102.

Laser beam intensity fluctuations in scattering media were studied in the laboratory, and the experimental results are compared with theory. In the experiment the schematically presented intensity of a He-Ne laser ( $\lambda = 0.63 \mu$ ) beam forward-scattered by a milk or lycopodium solution

was recorded photometrically at different optical thicknesses  $\tau$  of the scattering medium, and different distances  $L$  from the solution-containing cell to the detector. The standard deviations  $\sigma$  of the measured signal plotted versus  $\tau$  are shown to be in satisfactory agreement with the theoretical  $\sigma$  over the entire measured range of  $\tau$ , but only at  $L$  values which satisfy the condition of Fraunhofer diffraction. It is shown that in agreement with theory, the relative  $\sigma$  value decreases when the diameter of the detector aperture is increased. The experimental data show that propagation of a collimated beam in a scattering medium is always accompanied by fluctuation phenomena.

Ovsyannikov, V. A., and A. M. Romanov.

Signal-to-noise ratios in lidar systems.

OMP, no. 1, 1973, 11-14.

General calculations of signal-to-noise ratio in optical ranging system are developed in this article. Expressions are derived for the generalized signal-to-noise ratios  $\mu(\alpha)$  at the output of an optimum optical signal detector against a background of white, hyperbolic and mixed receiver noises. Also, expressions for the transfer function of the optimal filter, the signal spectrum, and the variance of the noise at the output of such a filter are derived, on the basis of which the maximal real signal-to-noise ratio  $\rho$  is obtained, from computer calculations. Graphs of  $\sqrt{\mu}$  and  $\sqrt{\rho}$  as functions of receiver time delay for the cases of white and hyperbolic noise are presented. In the case of mixed noise the corresponding expressions for  $\mu(m)$  and  $\rho(m)$  are also derived. The results derived could be used for optimal selection of parameters for a lidar system with a slow time constant detector.

Bochkov, D. S., B. N. Denchik, and  
B. A. Savel'yev. On the propagation  
laws of spatially-confined radiation flux  
in a dispersive medium. IVUZ Fiz,  
no. 3, 1973, 103-105.

Dependence was studied experimentally of the applicability limit  $\tau_{\text{lim}}$  of Bouguer's law on the laser beam optical diameter  $\Delta$  and scattering phase function  $\eta$ , and of the degree of polarization  $R$  and intensity  $J_2$  of the scattered laser beam, on the optical distance  $\tau$  from the beam axis. The optical depth at which  $J_1$  of the incident beam equals  $J_2$  of the forward-scattered beam was considered as  $\tau_{\text{lim}}$ . A He-Ne laser ( $\lambda = 0.63 \mu$ ) beam, with  $\Delta = 0.6-2.4$  and divergence  $\alpha = 3.5$  and  $5'$ , and a polystyrene suspension with Mie parameter  $\rho = 2.8$  and  $3.8$  or artificial fog with  $\rho = 30$  were used in the  $\tau_{\text{lim}}$  experiments.

The experimental  $\tau_{\text{lim}}$  plots show a shift of  $\tau_{\text{lim}}$  towards lower values with an increase in  $\Delta$  or  $\rho$ . The linear  $\tau_{\text{lim}}$  versus  $\eta$  dependence is approximated by  $\tau_{\text{lim}} = 10-2.4 \log \eta$  for different dispersive media. A laser beam with  $D = 20$  mm and  $\alpha = 5$  min in an artificial fog with rms scatter diameter  $= 6\mu$  was used in the  $R$  and  $J_2$  experiments. The experimental plots show that at  $\tau < 10.5$ ,  $J_2$  decreases sharply with increase in  $\tau_r$ , and at  $\tau = 27$  the  $J_2$  decrease is smooth. The same pattern was observed in  $R$  variations versus  $\tau_r$ . The observed phenomena are interpreted in terms of predominantly single or multiple scattering.

Khinrikas, K. V., and V. N. Afinogenov.

Depolarization of laser radiation in an optical channel. IVUZ Radioelektr, no. 12, 1972, 1501-1506.

A discussion is given of the effect of turbulent atmosphere on polarization in open optical communication lines, consisting of transmitting antenna with directing mirror, the atmosphere, and a receiving optical antenna. An expression is derived for determining depolarization at various points of the directing mirror. It was found that factors responsible for depolarization include inaccurate incidence of the beam on the mirror center, asymmetrical intensity distribution, mirror imperfections and fluctuations in incident angle of the laser beam. A turbulent atmosphere causes fluctuations in intensity and angle of incidence, and flickering of the beam, which in turn cause polarization fluctuations at the receiving antenna.

An experiment was conducted for investigating depolarization effects on an optical communication line with a path length of 5.2 km; the transmitter was a type LC-36 He-Ne laser operating at  $\lambda = 0.63 \mu$  and the receiver was an FEU-51 photomultiplier. Depolarization of the output laser radiation was -37 db, while at the receiver with a Cassegrainian antenna the depolarization was -25 to -17 db. The author points out that the depolarization effects can be decreased by using long-focus collecting elements at the receiving end. At the transmitting end depolarization does not cause signal fluctuations, and if necessary, it may be compensated as a constant background noise.

Andreyev, S. D., V. Ye. Zuyev,  
L. S. Ivlev, M. V. Kabanov, and Yu.  
A. Pkhalagov. Spectral transmission  
characteristics of atmospheric haze in the  
visible and infrared range. FAiO, no. 12,  
1972, 1261-1267.

The spectral transmission of atmospheric haze was measured in the wavelength range of  $0.56 - 12 \mu$ , during summer-autumn 1970 in the Tomsk region. Measurements were made with a single-beam method over a 3.5 km long path. The receiver-recorder device consisted of two channels: a) spectrometric for obtaining a relative transmission spectrum of the atmosphere in the  $1-12 \mu$  range with an accuracy of  $0.05-0.12 \mu$ ; and b) photoelectric, for measuring absolute transparency at four intervals of the visible and near infrared wavelength range with centers at  $0.59$ ,  $0.69$ ,  $0.83$ , and  $1.06 \mu$ . Optical measurements were conducted by standard meteorological observations and microstructural measurements, which were taken at 4 points over the path by means of Petryanov filters and PRV-IM blowers. During sampling, the volume of aerosol particles deposited in a filter of  $18 \text{ cm}^2$  area within 30 min was 600 liters. The coefficient of aerosol attenuation was determined on the basis of microphysical measurements of concentration and particle distribution. Calculated results are compared with those of optical measurements, and are found to be in good agreement. The authors note that microphysical results of the present work agree well with those obtained previously near Ryl'sk during summer-autumn periods in 1967-69. (Ivlev, L. S., et al. Problem of the stability of aerosol particle distribution according to size in the surface boundary layer. IN Sb: Problemy fiziki atmosfery, no. 8, LGU, 1970; Ivlev, L. S., et al. Measuring atmospheric aerosol distribution. IN: Sb. Problemy fiziki atmosfery, no. 6, LGU, 1968). The daily variation in the aerosol particle distribution function according to size and countable concentration is similar. The variation of particle distribution function according to size is nearly independent of the atmospheric relative humidity.

Vereshchaka, A. I., Yu. V. Popov, and  
V. P. Smirnov. A phase DME using a CO<sub>2</sub>  
laser. OMP, no. 1, 1973, 63-64.

A phase optical range finder using a CO<sub>2</sub> laser is described,  
the block diagram of which is shown in Fig. 1. A type OKG-15 CO<sub>2</sub> laser

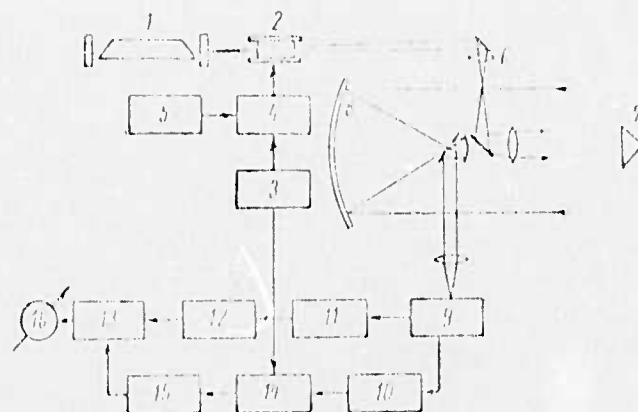


Fig. 1. Block diagram of DME.

1 - OKG-15 laser; 2 - modulator; 3 - HF oscillator;  
4 - filter; 5 - constant bias source; 6 - transmitting  
optics; 7 - reflector; 8 - receiving optics; 9 - photo-  
receiver; 10 - heterodyne; 11 - I-f amplifier with AGC;  
12 - phase inverter; 13 - phase detector; 14 - mixer;  
15 - I-f amplifier; 16 - null indicator.

(1) is used at  $\lambda = 10.6 \mu$  and power output = 1 watt. Laser radiation is modulated at a frequency  $f_{\text{mod}} = 5 \text{ MHz}$  by modulator (2), which is fed by h-f voltage from generator (3) through filter (4). The modulator operates on a quarter-wave constant voltage bias from supply (5). The modulated beam is transmitted by optics (6) over the measured distance to reflector (7), where the beam is reflected back to the receiving optics (8) and photoreceiver (9).

The optical sensor used is a Te-Cd-Hg photocell operating at liquid nitrogen temperature. An alternating voltage of frequency  $f_g = 5.25$  MHz from heterodyne (10) is applied to the cell, and a frequency mixing takes place between modulated radiation frequency and heterodyne frequency, giving a difference frequency  $f_{pr} = 250$  KHz. The heterodyne voltage at the photocell is held constant at 1 v and the constant mixing voltage equals 1.2 v. The i-f signal carrying range information from the photoreceiver after amplification by (11) enters phase detector (13), to which a reference signal of the same i-f is simultaneously applied from mixer (14) through amplifier (15). The unknown distance is determined by phase difference  $\Delta\phi$  between the reference and radiated signals. The accuracy of the above range finder was found to be within  $\pm 10$  cm, i.e.  $\sim 1^\circ$  (Fig. 2). It was

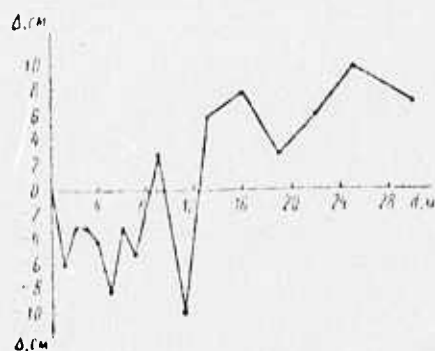


Fig. 2. Distance measurement error vs. range.

concluded that under complex meteorological conditions a reflector area of  $30 \text{ cm}^2$  is adequate to measure ranges of 10 km or more.

## B. Recent Selections

### i. Optical Transmission

Al'pert, Ya. L. Rasprostraneniye elektromagnitnykh voln i ionosfera (Electromagnetic wave propagation and the ionosphere). 2nd edition, Moskva, Izd-vo nauka, 1972, 563 p.

Arshinov, Yu. F., V. A. Donchenko, V. Ye. Zuyev, V. V. Kostin, and I. V. Samokhvalov. Experimental study on attenuation and backscatter of laser radiation at  $\lambda = 2.36$  and  $0.63 \mu$  by artificial fog and haze. IVUZ Fiz, no. 6, 1973, 62-67.

Banakh, V. A., V. L. Mironov, and T. V. Myshkina. Mean intensity of an asymmetrical optical beam in a turbulent atmosphere. FAiO, no. 5, 1973, 539-543.

Donchenko, V. A., M. V. Kabanov, G. G. Matviyenko, and I. V. Samokhvalov. Correlation between total scatter and backscatter indices in artificial fog and haze. IVUZ Fiz, no. 6, 1973, 133-135.

Gavrilenko, V. G., and N. S. Stepanov. Spectra of waves propagating through a turbulent stream. RiE, no. 6, 1973, 1105-1110.

Genin, V. N., and M. V. Kabanov. On viewing extended objects through a turbulent atmosphere. IVUZ Fiz, no. 7, 1973, 84-89.

Gurvich, A. S., and V. V. Pokasov. Frequency spectra of strong fluctuations in laser radiation through a turbulent atmosphere. IVUZ Radiofiz, no. 6, 1973, 913-917.

Gusev, V. D., N. A. Makhmutov, and A. Khuri. Solving the ray equation by an excitation method. RiE, no. 8, 1973, 1715-1717.

Gusev, V. D., B. I. Polyakov, and V. V. Fadeyev. Measuring spectral fluctuation of laser radiation propagating through a model turbulent atmosphere. RiE, no. 5, 1973, 934-939.

Ivlev, L. S. Form of dimensional spectra of aerosols in the surface boundary layer. DAN SSSR, v. 210, no. 2, 1973, 335-338.

Khmelevtsov, S. S., and R. Sh. Tsvyk. Experimental study on intensity fluctuations of light in a turbulent atmosphere. IVUZ Fiz, no. 6, 1973, 130-131.

Kovalev, V. A. A method for determining atmospheric transparency. Author's certificate no. 390401, assigned Nov. 1, 1971. Otkr izобр, no. 30, 1973, 138.

Manuylova, R. O., and G. M. Shved. Calculating transmissivity functions in strata for inclined beams in a spherical atmosphere. FAiO, no. 7, 1973, 769-770.

Prishivalko, A. P. Using attenuation and backscatter indices to determine particle concentration and parameters of size distribution. ZhPS, v. 19, no. 2, 1973, 320-331.

Prishivalko, A. P. Correlation between optical scatter or attenuation indices and the microstructural parameters of a polydisperse scattering medium. FAiO, no. 5, 1973, 552-556.

Romanov, G. S., and V. K. Pustovalov. Illumination of a cloudy atmosphere containing water droplets by intense monochromatic radiation. ZhPS, v. 19, no. 2, 1973, 332-339.

Sorokin, S. A., and V. P. Shak. Stabilizing an optical beam in an absorbing medium. M., In-t problem mekhaniki, AN SSSR. Preprint no. 21, 1972, 11 p. (KI. Dop vyp., 4/73, no. 7931).

Strelkov, G. M. Coefficient of absorption of laser radiation by water aerosols. RiE, no. 7, 1973, 1493-1496.

Tishchenko, A. A. Study of laser propagation and diagnostics of a randomly nonuniform troposphere. IVUZ Fiz, no. 7, 1973, 45-50.

Zuyev, V. Yel., G. M. Krekov, and A. I. Popkov. Numerical experiments in laser probing of aerosol strata in the atmosphere. FAiO, no. 7, 1973, 770-774.

## ii. Geomagnetic Pulsations

Afanas'yeva, L. T., and O. M. Raspopov. Characteristics of the polarization of Pi 2 pulsations in the auroral and subauroral regions. IN: Sb. Geomagnit. i ionosfer. vozmushcheniya v vysokikh shiroтах, L., Nauka, 1973, 131-136. (RZhGeofiz, 7/73, no. 7A275)

Aksenov, V. V. Spherical analysis of  $S_q$  variations. IN: Sb. Probl. geol. i metody geokhim. i geofiz. issled, Novosibirsk, 1972, 122-130. (RZhGeofiz, 7/73, no. 7A255)

Aksenov, V. V. Spherical and spatial analysis of periodic geomagnetic variations. IN: ibid., 139-149. (RZhGeofiz, 7/73, no. 7A256)

Aleksandrov, A. P., L. L. Van'yan, V. I. Dmitriyev, and A. A. Kozhevnikov. Propagation of directional hydromagnetic waves in plasma, magnetized by a curvilinear field. IN: Sb. Issled. po geomagnet., aeron., i fiz. solntsa, no. 24, Irkutsk, 1972, 30-36. (RZhGeofiz, 4/73, no. 4A274)

Aleksandrov, M. S., Z. M. Bakleneva, N. D. Gladshteyn, V. P. Ozerov, A. V. Potapov, and L. T. Remizov. Fluktuatsii elektromagnitnogo polya Zemli v diapazone SNCh (VLF fluctuations in the geomagnetic field). Moskva, Izd-vo nauka, 1972, 195 p. (RZhF, 5/73, no. 5Zh203)

Al'perovich, L. S., M. N. Berdichevskiy, L. L. Van'yan, and Ye. B. Kocharyants. Geomagnetic pulsations with maximum intensity at middle latitudes. GiA, no. 3, 1969.

Antonova, Ye. Ye., B. A. Tverskoy, and F. Z. Feygin. Characteristics of hydromagnetic wave propagation in a slowly varying magnetic field. GiA, no. 6, 1972, 1074-1081.

Babushnikov, M. S. Geomagnetic stud. s. IN: Sb. Vopr. fiz. okolozemn. prostranstva i zemn. nedr Belorussii, Minsk, Nauka i tekhn., 1972, 13-27. (RZhGeofiz, 7/73, no. 7A259)

Barsukov, V. M., L. L. Van'yan, and M. I. Pudovkin. On the possibility of auroral electron acceleration by electric field pulsations. GiA, no. 3, 1972, 568-569.

Beneze, P., E. Florian, and J. Saiko. Dynamic processes in the ionosphere during the geomagnetic storm of February 2, 1969. Acta geodact., geophys. et montanist., Acad. sci. Hung., v. 7 (1-2), 1972, 137-146.

Bol'shakova, O. V., and A. V. Gul'yel'mi. Penetration of hydromagnetic waves into the polar cap from the magnetosphere tail. GiA, no. 3, 1972, 569-571.

Bol'shakova, O. V., and O. V. Khorosheva. Zonal character of some micropulsation excitations at a geomagnetic pole. GiA, no. 2, 1973, 344-346.

Bondarenko, A. P., A. I. Vilinskiy, and A. M. Shilova. Correlations among geomagnetic field variations in the Carpathian region. DAN Fizika zemli, no. 10, 1972, 95-96.

Buldyrev, V. S., A. A. Kovtun, and Fam Van Chi. A magneto-acoustic resonator of Pc 2 oscillations in the terrestrial magnetosphere. GiA, no. 1, 1973, 136-142.

Davydov, V. M. Propagation of low-frequency hydromagnetic pulsations over nonorthogonal force lines of the main geomagnetic field. IN: Sb. Issled. po geomag., aeron. i fiz. Solntsa, no. 23, Moskva, 1972, 217-224. (RZhGeofiz, 8/72, no. 8A367)

Davydov, V. M. Method of determining longitudinal magnetospheric conductivity from pulsations of the Pi-2 type. DAN SSSR, v. 208, no. 5, 1973, 1071-1073.

Davydov, V. M. Frequency and geometrical probing of the magnetosphere using long-period hydromagnetic pulsations. IN: Sb. Issled. po geomag., aeron. i fiz. Solntsa, no. 24, Irkutsk, 1972 43-62. (RZhGeofiz, 5/73, no. 5A204)

Degtyarev, V. I., and T. P. Zhukova. PCA-type absorption and Forbush decreases during April 11-18, 1969. IN: Sb. Issled. po geomag., aeron. i fiz. Solntsa, no. 18, Moskva, Izd-vo nauka, 1971, 248-252. (RZhGeofiz, 3/72, no. 3A305)

Dobes, K., K. Prikner, and J. Strestik. Processing rapid variation records of the geomagnetic field by computer. Geofys. sb., no. 18, 1970 (1972), 335-348. (RZhGeofiz, 5/73, no. 5A240)

Dobes, K., J. Strestik, and K. Prikner. Numerical calculation of frequency-time displays using amplitude-time records. Studia geophys. et geod., v. 15, no. 3, 1971, 331-339. (RZhGeofiz, 4/72, no. 4A259)

Dubrovskiy, V. G., and S. A. Kramarenko. On the spectral distribution of mean variations in geomagnetic field intensity. IAN TurkSSR, Ser. fiz-tekhn. i geol. nauk, no. 6, 1971, 100-104.

Fel'dshteyn, Ya. I. Variations in various magnetospheric parameters during substorms, based on aurora oval dynamics. IN: Sb. Geofiz. issled. v zone pol'yarn. siyaniy, Apatity, 1972, 65-73. (RZhGeofiz, 7/72, no. 7A298)

Fel'dshteyn, Ya. I. Magnetic field variations in interplanetary space and near the Earth's surface. VAN, no. 8, 1973, 15-27.

Feygin, F. Z., and V. L. Yakimenko. The mechanism of generation and development of pearls with cyclotron instability of the outer proton region. GiA, no. 4, 1969.

Feygin, F. Z., and V. L. Yakimenko. Fine structure of Pc 1 micropulsations. GiA, no. 3, 1970, 558-560.

Feygin, F. Z., and V. L. Yakimenko. IPDP as a source of proton stream instability. GiA, no. 4, 1971, 665-668.

Gasset, G., A. I. Zhulin, F. Cambou, Kh. D. Kanonidi, N. G. Kleymenova, O. M. Raspopov, A. Seint-Marc, and J-P. Treilhou. Auroral electron modulation and geomagnetic pulsations during the March 8, 1970 storm. GiA, no. 6, 1972, 1059-1066.

Geomagnetizm i vysokiye sloi atmosfery. T. 1. (Geomagnetism and the upper atmospheric layers. Vol. 1). Moskva, 1972, 220 p.

Gokhberg, M. B., V. N. Bogayevskiy, L. L. Van'yan, and A. Ya. Pozner. The inverse problem of a magnetospheric resonator. DAN SSSR, v. 197, no. 6, 1971.

Gokhberg, M. B., V. I. Karpman, and O. A. Pokhotelov. On a nonlinear theory of pearl evolution. DAN SSSR, v. 204, no. 4, 1972, 848-850.

Gogatishvili, Ya. M. The tendency for repetition of geomagnetic field pulsations. GiA, no. 4, 1969.

Gogatishvili, Ya. M. Variation in frequency of appearance of geomagnetic pulsations with the level of geomagnetic and solar activity. GiA, no. 1, 1969.

Gorbachev, L. P., and Yu. N. Savchenko. Propagation of a hydromagnetic pulse in the ionospheric channel. GiA, no. 1, 1972, 71-76.

Gudkova, V. A., O. M. Raspopov, L. L. Van'yan, L. A. Geller, Yu. A. Kopytenko, and V. V. Privalov. Regularities in amplitude distribution of geomagnetic pulses over a meridional profile. GiA, no. 6, 1971, 1123-1125.

Gul'yel'mi, A. V. On the theory of diagnosing the concentration of a plasma density by dispersion of hydromagnetic whistlers. GiA, no. 1, 1969.

Gul'yel'mi, A. V. A magnetosonic channel under the plasmosphere arch. GiA, no. 1, 1972, 147-150.

Gul'yel'mi, A. V., T. A. Plyasova-Bakunina, and R. V. Shchepetnov. Relation of the period of Pc 3,4 geomagnetic pulsations with near-Earth space parameters. GiA, no. 2, 1973, 382-384.

Gul'yel'mi, A. V., and O. V. Bol'shakova. Diagnostics of the interplanetary magnetic field from ground observations of Pc 2-4 micropulsations. GiA, no. 3, 1973, 535-537.

Hallo, L., M. Tatrallyay, and J. Vero. Experimental results with characterization of geomagnetic pulsations. Methods of characterizations used. Acta geodact., geophys. et montanist., Acad. sci. Hung., v. 7(1-2), 1972, 155-166.

Hessler, V. P., R. R. Heacock and V. A. Troitskaya. Micro-pulsations at the geomagnetic poles. Antarct. J. U.S., v. 6, no. 5, 1971, 226-227. (RZhGeofiz, 6/72, no. 6A258)

Hessler, V. P., R. R. Heacock, and V. A. Troitskaya. Micro-pulsations at the geomagnetic poles. Antarct. J. U.S., v. 7, no. 5, 1972, 157-158. (RZhGeofiz, 5/73, no. 5A226)

Isayev, S. I. Polyarnnyye siyaniya i protsessy v magnitosfere Zemli (Polar aurorae and processes in Earth's magnetosphere). Leningrad, Izd-vo nauka, 1972, 244 p. (LC-VKP)

Issledovaniya po geomagnetizmu, aeronomii i fizike Solntsa. Sbornik statey (Studies on geomagnetism, aeronomy and solar physics. Collection of articles). No. 26, SO AN SSSR, 1973, 286 p. (KL, 23/73, no. 17515)

Kalisher, A. L., and E. J. Matveyeva. Estimating resonant proton diffusion of Pc 1 from ground observations. GiA, no. 4, 1971, 739-741.

Kanonidi, Kh. D. A special type of geomagnetic pulsation. GiA, no. 2, 1972, 365-366.

Kiselev, B. V., O. M. Raspopov, and B. I. Rezhnev. Correlation of IPDP-type geomagnetic pulsations with drift of plasma irregularities in the magnetosphere. GiA, no. 1, 1973, 132-135.

Kapel'zon, A. A., and I. M. Vilenskiy. Problem of the propagation of atmospheric whistlers in the ionosphere. IN: Sb. Vopr. issled. nizhn. ionosfery, Novosibirsk, 1972, 28-31. (RZhGeofiz, 6/73, no. 6A291)

Kiziriya, L. V. On the polarization character of Pi 2 geomagnetic pulsations. IN: Tr. In-t geofiz. AN GruzSSR, no. 28, 1972, 64-69. (RZhGeofiz, 3/73, no. 3A271)

Konecny, M. Occurrence of Pc 1 and Pc 2 pulsations at Novolazarevskaya Station (Antarctica), and comparison with Budkov Observatory data. IN: Geofys. sb., no. 18, 1970(1972), 349-362. (RZhGeofiz, 5/73, no. 5A230)

Korsunova, L. P. Effect of geomagnetic excitations on the nocturnal E-region at midlatitudes. GiA, no. 5, 1973, 835-839.

Koshelevskiy, V. K., O. M. Raspopov, and G. V. Starkov. Correlation of Pi 2 geomagnetic pulse parameters with processes in the auroral zone. GiA, no. 5, 1972, 886-891.

Likhter, Ya. I., O. A. Molchanov, V. M. Chmyrev, V. A. Rapoport, V. Ya. Trakhtengerts, and V. A. Cherepovitskiy. Modulation in spectra and amplitude of VLF signals in the magnetosphere. IN: Proc. Joint Symp. of COSPAR, IAGA and URSI: Critical problems of magnetospheric physics. Madrid, May 11-13, 1972 (to be published in Space Research XIII, Akad. Verlag, Berlin, 1973)

Likhter, Ya. I., Ya. P. Sobolev, F. Jiricek, and P. Triska.  
Early results from VLF experiments in the Intercosmos 5 satellite.  
IN: *ibid.*

Likhter, Ya. I. Peculiarities of VLF propagation in the outer ionosphere, based on observational data of the Cosmos-3 and -5 satellites. IN: Sb. X. Vses. konf. po rasprostr. radiovoln. Tezisy dokl. Sekt. 3. Moskva, Nauka, 1972, 137-139. (RZhGeofiz, 11/72, no. 11A238)

Lipatov, A. S. Questions on hydromagnetic wave propagation in the terrestrial magnetosphere. IN: Tr. XV and XVI nauch. konf. Mosk. Fiz.-tekh. in-ta, 1979-1970. Seriya mat. Ch. 1. Dolgoprudnyy, 1971, 81-89. (RZhGeofiz, 7/72, no. 7A297)

Liperovskiy, V. A., and S. A. Mart'yanov. Fading of hydromagnetic waves in a turbulent plasma. GiA, no. 2, 1973, 311-317.

Lyatskiy, V. B. Interpretation of pearls by the Cerenkov radiation from proton beams. IN: AN SSSR. Polyarnyy geofizicheskiy institut. Geofizicheskaya yavleniya v avroral'noy zone. (Geophysical phenomena in the auroral zone). Leningrad, Izd-vo nauka, 1971, 141-155.

Lyatskiy, V. B. Shock wave in the magnetosphere tail as a cause of the active phase of a magnetospheric substorm. GiA, no. 6, 1971, 1038-1048.

Lyatskiy, V. B., and Yu. P. Mal'tsev. Effect of longitudinal currents on excitation in the polar cap. GiA, no. 1, 1972, 83-87.

Magnitskiy, B. V., and B. A. Tverskoy. Vertical currents at conjugate points. GiA, no. 4, 1972, 708-711.

Mal'tsev, Yu. P. Propagation of hydromagnetic waves in the Earth's magnetosphere and ionosphere. IN: AN SSSR. Polyarnyy geofizicheskiy institut. Geofizicheskiye yavleniya v avroral'noy zone. Leningrad, Izd-vo nauka, 1971, 173-182.

Mal'tsev, Yu. P. Resonant oscillations of the magnetosphere. IN: Sb. Morfol. i fiz. polyarn. ionosfery. Leningrad, Izd-vo nauka, 1971, 75-79. (RZhGeofiz, 3/72, no. 3A310)

Mal'tseva, N. F., and V. P. Selivanov. Analysis of dynamic spectra of IPDP micropulsations, observed simultaneously at a longitudinal chain of observatories. GiA, no. 3, 1972, 575-578.

Matveyeva, E. T., A. L. Kalisher, and B. V. Dovbnya. Physical conditions in the magnetosphere and interplanetary space during excitation of Pc 1 geomagnetic pulsations. GiA, no. 6, 1972, 1125-1127.

Matveyeva, E. T., V. A. Troitskaya, and A. V. Gul'yel'mi. Long-term statistical forecast of the activity of Pc 1 type geomagnetic pulsations. Planet. and Space Science, no. 5, 1972, 637-638. (RZhGeofiz, 11/72, no. 11A284)

Namgaladze, A. N. Observations of short-period oscillations of the geomagnetic field at Kaliningrad. GiA, no. 4, 1970.

Prikner, K., J. Strestik, and K. Dobes. Frequency analysis of geomagnetic beat-type pulsations in the Pc 3 range. Stud. geophys. et geod., no. 3, 1972, 262-270. (RZhGeofiz, 2/73, no. 2A223)

Roldugin, V.K., B. N. Belen'kaya, and N. F. Mal'tseva. Electric field in the ionosphere during pulsating aurorae. GiA, no. 5, 1971, 813-818.

Raspopov, O. M., V. A. Troitskaya, L. N. Baranskiy, B. N. Belen'kaya, V. K. Koshelevskiy, L. T. Afanas'yeva, J. Roke, and O. Fambitokoyya. Spectral properties of Pi 2 geomagnetic pulsations along a meridional profile. GiA, no. 5, 1972, 892-896.

Raspopov, O. M. Development of geomagnetic pulsations during a substorm. IN: Sb. Issled. po geomagn., aeron. i fiz. Solntsa. Moskva, Nauka, no. 23, 1972, 235-245. (RZhGeofiz, 8/72, no. 8A366)

Raspopov, O. M., L. T. Afanas'yeva, B. V. Kiselev, and G. A. Loginov. Magnetosphere dynamics and geomagnetic pulsations of the Pc 5 type. GiA, no. 1, 1972, 150-153.

Repin, I. Conjugate points. Komsomol'skaya pravda, 23 June 1973, p. 4.

Sedova, F. T. Some characteristics of Pc 1 occurrence at mid-latitudes. IN: Sb. Geofiz. issled. territorii Ukrainy. Kiyev, Izd-vo naukova dumka, 1972, 8-14. (RZhGeofiz, 7/73, no. 7A271)

Sobolev, Ya. P. The electric field in the magnetosphere under quiet conditions, based on ground observations of atmospheric whistlers. GiA, no. 2, 1973, 379-382.

Strestik, J., K. Prikner, and K. Dobes. Daily variation in parameters of beat-type Pc-3 (BPc 3) pulsations. Stud. geophys. et geod., no. 1, 1973, 27-35. (RZhGeofiz, 5/73, no. 5A234)

Tashkinova, L. G., and B. A. Tverskoy. Oscillations of DP-1 and DP-2 current systems. GiA, no. 3, 1972, 573-575.

Troitskaya, V. A., A. V. Gul'yel'mi, O. A. Bolshakova, E. T. Matveyeva, and R. V. Shchepetnov. Indices of geomagnetic pulsations. Planet. and Space Sci., no. 6, 1972, 849-958. (RZhGeofiz, 2/73, no. 2A222)

Van'yan, L. L., M. B. Gokhberg, and L. A. Abramov. The effect of the lower ionosphere on propagation of hydromagnetic waves guided by the geomagnetic field. GiA, no. 4, 1970.

Van'yan, L. L., L. A. Abramov, M. B. Gokhberg, N. A. Deniskin, L. V. Kiziriya, N. A. Lagova, and Yu. G. Turbin. On polarization of geomagnetic pulsations. GiA, no. 6, 1971, 1061-1064.

Van'yan, L. L., and M. B. Gokhberg. On the excitation of magnetospheric resonators. GiA, no. 3, 1972, 492-497.

Van'yan, L. L., Yu. G. Turbin, and L. A. Abramov. On polarization of Pc 5 pulsations. GiA, no. 3, 1972, 498-502.

Van'yan, L. L., L. M. Zelenyy, A. A. Kozhevnikov, and V. A. Yudovich. Hydromagnetic waves in a finite-conductivity plasma. GiA, no. 4, 1973, 730-734.

Vinogradov, P. A., V. N. Vinogradova, and T. Gorin. Diurnal variation in the direction of the polarization axis of Pc 1 pulsations. GiA, no. 3, 1970, 557-558.

Vinogradova, V. N. Classification of micropulsations of the Earth's electromagnetic field. GiA, no. 2, 1970, 371-373.

Vinogradova, V. N. Variations in Pc 1 occurrence rate at mid-latitudes. GiA, no. 3, 1970, 501-504.

Zagulyayeva, V. A., and A. A. Kashin. The correlation of horizontal component variations of the geomagnetic field with drift in the ionosphere. IN: Sb. Ionosfern. issledovaniya, no. 21, Moskva, Izd-vo nauka, 1972, 15-18. (RZhGeofiz, 5/73, no. 5A180)

Zelenkov, V. Ye. Parameters of ionospheric inhomogeneities and geoelectromagnetic field variations. IN: ibid., 26-33. (RZhGeofiz, 5/73, no. 5A181)

Zelenkova, L. V., I. N. Men'shutina, and M. I. Pudovkin. Two types of geomagnetic field pulsation at the polar cap. GiA, no. 5, 1973, 955-958.

Zhmur, L. Ye. Effect of collisions on ion-acoustic waves under outer ionospheric conditions. GiA, no. 5, 1973, 825-828.

Zhigalov, L. N., and N. N. Zhigalova. Space-time distribution of magnetic activity during magnetic storm periods. IN: Tr. Arkt. i antarkt. NII, no. 310, 1972, 114-125. (RZhGeofiz, 3/73, no. 3A266)

Zhigalova, N. N. On electrojet displacement during geomagnetic disturbances. IN: Sb. Probl. Arktiki i Antarktiki. Leningrad, Gidrometeoizdat, no. 40, 1972, 120-123. (RZhGeofiz, 10/72, no. 10A246)

iii. Miscellaneous

Afraymovich, E. L., A. D. Kalikhman, and V. A. Korolev. Investigation of ionospheric heterogeneous structures using a dynamic spectral analysis technique. IN: Sb. Issled. po geomagnetizmu, aeron. i fiz. solntsa. no. 21. Irkutsk, 1972, 31-54. (RZhGeofiz, 5/73, no. 5A59)

Afraymovich, E. L., A. D. Kalikhman, and V. A. Korolev. Investigation of ionospheric heterogeneous structures using a dynamic spectral analysis technique. 2. Features of the envelope as a function of time. IN: *ibid.*, 55-76. (RZhGeofiz, 5/73, no. 5A60)

Afraymovich, E. L., A. D. Kalikhman, and V. A. Korolev. Investigation of ionospheric heterogeneous structures using a dynamic spectral analysis technique. 3. Space-time analysis. IN: *ibid.*, 77-88. (RZhGeofiz, 5/73, no. 5A61)

Afraymovich, E. L., A. D. Kalikhman, V. A. Korolev, and V. A. Rybin. Investigation of ionospheric heterogeneous structures using a dynamic spectral analysis technique. 4. Features of the envelope as a function of frequency. IN: *ibid.*, 89-103. (RZhGeofiz, 5/73, no. 5A62)

Afraymovich, E. L., G. M. Kudelin, and B. V. Troitskiy. Interference methods of determining time periods and vertical parameters of wave-like disturbances in the  $F_2$  layer. IN: *ibid.*, 104-113. (RZhGeofiz, 5/73, no. 5A63)

Andreyev, G. A., V. M. Kuznetsov, and V. E. Tseytlin. Method of determining structural characteristics of the fluctuations in refractive index of the atmosphere. Author's certificate, USSR, no. 390423, dated October 18, 1971. (Otkr. izobr., 30/73, p. 142)

Andrianov, V. A., and V. I. Vetrov. A method of calibrating for ultra-short wave refraction measurements in the surface boundary layer. RiE, no. 5, 1973, 1053-1057.

Apparatura i metody obrabotki radioastronomicheskikh nablyudeni. (Apparatus and methods of processing radioastronomical observations). Riga, Izd-vo Zinatne, 1972, 127 p. (LC-VKP)

Belov, S. V., L. P. Gorbachev, and Yu. N. Savchenko. Generating a directional hydromagnetic signal by pulsed acoustic waves in a nonisentropically conducting medium. GiA, no. 5, 1973, 818-824.

Bezruchenko, L. I., M. I. Belen'kiy, and S. P. Tikhomirov. Study of the lower ionosphere by a partial reflection method. GiA, no. 3, 1973, 521-523.

Danilov, A. D. Current problems of aeronomy. VAN, no. 7, 1973, 45-57

Dzhordzhio, N. V., L. G. Ol'dekop, and N. I. Fedorova. Measuring auroral ionization at high latitudes with the Cosmos-348. GiA, no. 3, 1973, 437-441.

Gershman, B. N., and G. I. Grigor'yev. Current instability of atmospheric gravitational waves. GiA, no. 4, 1973, 604-609.

Grib, S. A. Questions on the interaction of solar wind shock waves with Earth's magnetosphere. GiA, no. 5, 1973, 788-793.

Gurevich, A. V., et al. Nelineynaya teoriya rasprostraneniya radiovoln v ionosfere. (Nonlinear propagation theory of radio waves in the ionosphere). Moskva, Izd-vo Nauka, 1973, 272 p. (RBL, 5/73, no. 604)

Gvelesiani, A. I., and A. G. Khantadze. Nonstationary distribution of charged particles in the upper atmosphere. GiA, no. 3, 1973, 514-516.

Imyanitov, I. M., et al. Elektrichestvo oblakov (Electricity of clouds). Leningrad, Izd-vo Gidrometeoizdat, 1971, 93 p. (LC-VKP)

interpretatsiya i ispol'zovaniye sputnikovykh dannykh v analize i prognoze pogody. (Interpretation and use of satellite data in the analysis and forecasting of weather). Leningrad, Izd-vo Gidrometeoizdat, 1971, 162 p. (LC-VKP)

Ionosfera i solnechno-zemnyye svyazi. (The ionosphere and the sun-earth link). Alma-Ata, Izd-vo Nauka, 1973, 160 p. (LC-VKP)

Kazantsev, A. N., V. A. Danilin, and V. I. Chivilev. Radio wave absorption during vertical probing of the ionosphere. GiA, no. 3, 1973, 523-526.

Kotik, D. S., and V. Yu. Trakhtengerts. On the decay interaction of VLF waves with the Earth's magnetosphere. GiA, no. 5, 1973, 871-877.

Krymskiy, G. F., and I. A. Transkiy. On shock wave propagation in an interplanetary medium. II. GiA, no. 5, 1973, 777-781.

Lukashkin, V. M., and K. Ye. Chernin. Correcting radiometric data for pattern width and orientation of the receiving antenna. IN: Sb. Problemy arkt. i antarkt, no. 41, 1973, 101-102.

Modelirovaniye teploobmena atmosfery. (Modelling heat exchange of the atmosphere). Moskva, Izd-vo Gidrometeoizdat. Mosk. otdeleniye, 1972, 65 p. (LC-VKP)

Nagorskiy, P. M. Plasma instability in front of a fast-moving body in the ionosphere. GiA, no. 4, 1973, 631-634.

Naklonnoye zondirovaniye ionosfery. (Slant probing of the ionosphere). Leningrad, Izd-vo Gidrometeoizdat, 1972, 269 p. (RZhF, 9/73, no. 9Zh172 K).

Radioaktivnost' atmosfery. (Radioactivity of the atmosphere). Moskva, Izd-vo Gidrometeoizdat, Mosk. otdeleniye, 1972, 144 p. (LC-VKP)

Rybin, V. A. Determining vertical parameters of wave-like ionospheric disturbances. GiA, no. 4, 1973, 670-673.

Schwarz, E. Occurrence of long-range ionospheric propagation in the VLF range. Gerlands Beitr. Geophysik, v. 82, no. 2, 1973, 107-110.

Shashun'kina, V. N. Gravitational waves in the F region of ionosphere. IN: Sb. Ionosfernyye isslednovaniya, no. 21. Izd-vo Nauka, 1972, 154-162.

Sheftel', V. M., and S. P. Chernysheva. Excitation exchange between magnetically conjugate regions of the ionosphere. GiA, no. 5, 1973, 937-938.

Sitnov, Yu. S., and M. N. Fatkullin. On the theory of magnetically-conjugate transport of cold plasma in the low-latitude outer ionosphere. Kozmich. issled., no. 3, 1972, 459-461.

Sorokin, V. M., and G. V. Fedorovich. Propagation of MHD waves along the lower ionospheric boundary. GiA, no. 5, 1973, 866-870.

Stotskiy, A. A. Large-scale phase fluctuations during radiowave propagation in a turbulent atmosphere. RiF, no. 8, 1973, 1579-1583.

Toplygin, I. N. Propagation and attenuation of magnetohydrodynamic waves in interplanetary space. IN: Sb. IV Leningr. mezhdunar. seminar "Edinoobraziye uskoreniya chastits v razlich. masshtabakh kosmosa, 1972". Leningrad, 1972, 267-292. (RZhMekh, 7/73, no. 7B180)

Tulinov, V. F., Yu. M. Zhuchenko, V. A. Lipovetskiy, G. F. Tulinov, and V. M. Leygin. Soft electron fluxes in the upper atmosphere of the polar region. GiA, no. 3, 1973, 513-514.

Naklonnoye zondirovaniye ionosfery. (Slant probing of the ionosphere). Leningrad, Izd-vo Gidrometeoizdat, 1972, 269 p. (RZhF, 9/73, no. 9Zh172 K).

Radioaktivnost' atmosfery. (Radioactivity of the atmosphere). Moskva, Izd-vo Gidrometeoizdat, Mosk. otdeleniye, 1972, 144 p. (LC-VKP)

Rybin, V. A. Determining vertical parameters of wave-like ionospheric disturbances. GiA, no. 4, 1973, 670-673.

Schwarz, E. Occurrence of long-range ionospheric propagation in the VLF range. Gerlands Beitr. Geophysik, v. 82, no. 2, 1973, 107-110.

Shashurkina, V. N. Gravitational waves in the F region of ionosphere. IN: Sb. Ionosfernyye isslednovaniya, no. 21. Izd-vo Nauka, 1972, 154-162.

Sheftel', V. M., and S. P. Chernysheva. Excitation exchange between magnetically conjugate regions of the ionosphere. GiA, no. 5, 1973, 937-938.

Sitnov, Yu. S., and M. N. Fatkullin. On the theory of magnetically-conjugate transport of cold plasma in the low-latitude outer ionosphere. Kozmich. issled., no. 3, 1972, 459-461.

Sorokin, V. M., and G. V. Fedorovich. Propagation of MHD waves along the lower ionospheric boundary. GiA, no. 5, 1973, 866-870.

Stotskiy, A. A. Large-scale phase fluctuations during radiowave propagation in a turbulent atmosphere. RiF, no. 8, 1973, 1579-1583.

Toptygin, I. N. Propagation and attenuation of magnetohydrodynamic waves in interplanetary space. IN: Sb. IV Leningr. mezhdunar. seminar "Edinoobraziye uskoreniya chastits v razlich. masshtabakh kosmosa, 1972". Leningrad, 1972, 267-292. (RZhMekh, 7/73, no. 7B180)

Tulinov, V. F., Yu. M. Zhuchenko, V. A. Lipovetskiy, G. F. Tulinov, and V. M. Feygin. Soft electron fluxes in the upper atmosphere of the polar region. GiA, no. 3, 1973, 513-514.

Tulinov, V. F., and V. V. Tulyakov. Corpuscular radiation and radio wave absorption in the polar region. IN: Tr. Tsentr. aerol. observ., no. 1, 1972, 29-32. (RZhGeofiz, 5/73, no. 5A70)

Turbulentnost' pogranichnogo sloya atmosfery i yeye primeneniye v prikladnykh zadachakh. (Turbulence of the atmospheric boundary layer and its applications). Moskva, Gidrometeoizdat, Mosk. otdeleniye, 1972, 164 p. (LC-VKP)

Van'yan, L. L., and A. S. Debabov. A three-dimensional current system of substorms, with allowance for mutual effects of magnetically conjugate regions in the ionosphere. GiA, no. 5, 1973, 951-952.

Vasil'yev, G. V., Yu. M. Agafonnikov, V. M. Bednazhevskiy, et al. The B-2 apparatus for measuring radiowave absorption simultaneously at two frequencies by a pulse (Al) method. IN: Sb. Ionosfern. issledovaniya. no. 21. Moskva, Izd-vo Nauka, 1972, 90-92. (RZhGeofiz, 5/73, no. 5A65)

Vergasova, G. V., and N. A. Chernobrovkina. On the cause of the presence of double reflections in ionograms. IN: Sb. Issled. po geomagnetizmu, aeron. i fiz. solntsa. no. 21. Irkutsk, 1972, 114-119. (RZhGeofiz, 5/73, no. 5A64)

Vershinin, Ye. F., Yu. N. Gorshkov, Ye. A. Ponomarev, V. Yu. Trakhtengerts, and V. I. Shapayev. Low-energy electrons in the ionosphere as a new source of electromagnetic waves in the VLF range. DAN SSSR, v. 210, no. 3, 1973, 563-566.

Vershinin, Ye. F., Yu. N. Gorshkov, Ye. A. Ponomarev, V. Yu. Trakhtengerts, and V. I. Shapayev. VLF wave generation in the ionosphere close to the low-frequency plasma resonance. 1. GiA, no. 4, 1973, 615-623.

Vilenskiy, I. M., and V. V. Plotkin. Reflection of powerful radio waves from the lower ionosphere. IVUZ Radiofiz, no. 6, 1973, 886-891.

Voprosy eksperimental'noy fiziki atmosfery. (Problems in experimental physics of the atmosphere). Leningrad, 1972, 177 p. (LC-VKP)

Yastrebov, A. A. Theory of the disturbance of the lower ionosphere by a metallic body. IN: Tr. Tsent. aerol. observ., no. 111, 1972, 35-43. (RZhGeofiz, 5/73, no. 5A80).

Yastrebov, A. A. Disturbance of a dense plasma by a moving charged body in the lower atmosphere. IN: ibid., 44-52. (RZhGeofiz, 5/73, no. 5A81).

Zhulina, Ye. M. One of the possible anomalous paths of short-wave propagation at high latitudes. GiA, no. 3, 1973, 449-454.

A. Abstracts

Melent'yev, V. V., and Yu. I. Rabinovich.

Methods of laboratory measurements of radiation properties in the centimeter band.

IN: Trudy Glavnoy geofizicheskoy observatorii, no. 291, 1972, 3-8.

Direct laboratory measurement of centimeter wave return from various terrestrial surfaces was made feasible by a method introduced by the authors, which is analyzed in this paper. Emissivity data for terrestrial surfaces are used in interpreting remote sensing measurements of the atmosphere and underlying surfaces by satellite and airborne microwave measurements of meteorological characteristics. For this purpose, exact measurement of the emission coefficient  $\alpha_s$  of the underlying surface is important.

The laboratory arrangement for the  $\alpha_s$  measurement (Fig. 1)

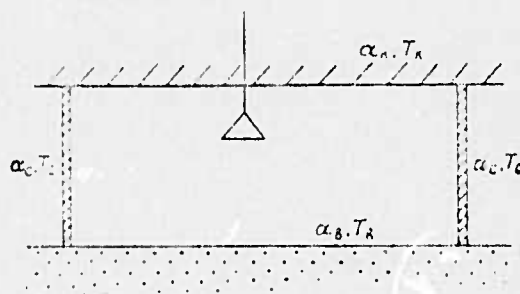


Fig. 1. Diagram of the experimental arrangement for measuring emissivity of terrestrial surfaces.

consists of a closed cavity formed by two superposed parallel planes and totally-reflecting lateral walls. The bottom of the cavity is formed by the surface studied and the top is alternately formed by a black body and a perfect reflector. A horn antenna positioned above the surface receives an emission

$\alpha_B T_B$  from the surface and the reflected emission  $\alpha_K T_K$  from the top. Formulas are derived for the r-f return  $T$  received by the antenna and for the emissivity  $\alpha_B$  which is a function of r-f brightness temperatures of the cavity with the top formed by a black body ( $T_1$ ) and a perfect reflector ( $T_2$ ). Two independent measurements of  $T_1$  and  $T_2$  thus give  $\alpha_B$  of the surface. The accuracy of the method is governed by the black body emissivity and its thermodynamic temperature  $T_K$ . The accuracy expressed as  $(T_1 - T_2)$  and error ( $\delta\%$ ) values in measurements of the  $\alpha_s$  of a water surface at  $290^\circ \text{K}$  are shown (Fig. 2) as an illustration of the method.

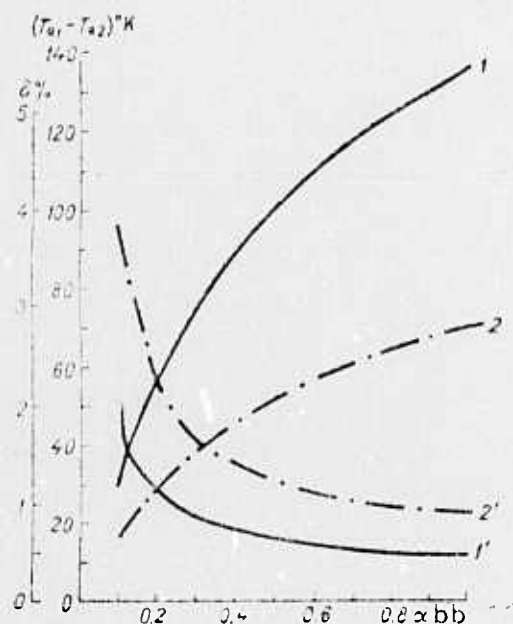


Fig. 2. Measured contrast (1, 2) and experimental error (1', 2') versus black body emissivity: 1, 1' - at  $T_{K1} = 500^\circ \text{K}$ , 2, 2' - at  $T_{K1} = 400^\circ \text{K}$ .

The accuracy is significantly lower when the contrast ( $T_1 - T_2$ ) is smaller; contrast is increased when  $\alpha_{bb}$  is higher. A formula is given to calculate the relative error  $\Delta\alpha_b/\alpha_b$  of a single measurement. The error analysis indicates that measurement accuracy is a function of the wavelength used and the surface type.

Melent'yev, V. V., and Yu. I. Rabinovich.

Measuring emission coefficients of a water  
surface covered with foam and organic films.

IN: Trudy Glavnoy geofizicheskoy laboratorii,  
no. 291, 1972, 9-13.

In a contribution to oceanographic studies by passive microwave techniques, the authors measured the emission coefficient  $\epsilon$  of a salt water free surface and surfaces covered with foam or organic layers. The laboratory arrangement used for the  $\epsilon$  measurements is described in the preceding abstract.

The experimental  $\epsilon$  data for a free surface were plotted versus surface temperature (10-40° C) and water salinity (0-40‰) and are found to be in general agreement with theory. The most notable deviation from theory was observed above 25-30° C. The average  $\epsilon$ , measured at  $\lambda = 3.2$  cm and 20-24° C on a foam covered surface was  $0.862 \pm 0.008$  for egg white and  $0.893 \pm 0.005$  for detergent foams. Comparison of the data with foam bubble diameter distribution curves led to the conclusion that  $\epsilon$  decreases when the total bubbles per unit volume increases and the probable bubble volume decreases. The average  $\epsilon$  measured at  $\lambda = 3.2$  cm and 18-24° C, on a water surface covered with a thin kerosene or oil film was  $0.410 \pm 0.006$  and  $0.471 \pm 0.008$  respectively. The film thickness is considered to be a decisive factor in the study of film properties on a sea water surface. The study supports the feasibility of evaluating ocean pollution and foaming by using a microwave emission techniques.

Melent'yev, V. V., and Yu. I. Rabinovich.

Results of laboratory measurements of  
emission coefficients of natural surfaces.

IN: Trudy Glavnoy geofizicheskoy observatorii,  
no. 291, 1972, 14-17.

Emission coefficient  $\epsilon$  measurements of various land surfaces were made to provide realistic data for interpretation of airborne and satellite microwave observations of underlying land surfaces. The laboratory arrangement used described in an earlier abstract in this issue. Tabulated experimental  $\epsilon$  data (Table 1) display  $\epsilon$  variations within a wide range (0.742-0.961), wider than in the IR band. The emissivity of sand, for example, is strongly reduced in the presence of water. Deviation from average  $\epsilon$  is also diminished because the experimental error in  $\epsilon$  is greater for surfaces with higher emissivity. Variations in surface emissivity versus wavelength are illustrated by the example of dry and wet sand (Fig. 1). The decrease in  $\epsilon$  of wet sand

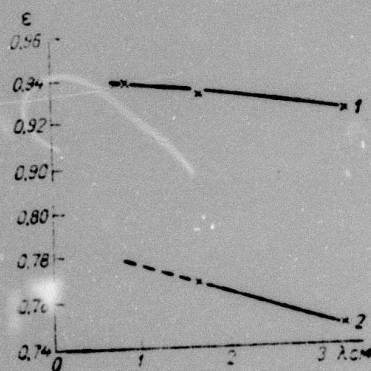


Fig. 1. Emission coefficient vs. wavelength for dry (1) and wet (2) sand.

with an increase in  $\lambda$  is less steep than that of dry sand. The decrease in  $\epsilon$  of the grass cover is related to changes in the Rayleigh roughness factor.

Table 1

Surface	Brief description	Wavelength, cm	Emission coefficient	Surface temperature °C	Number of runs.
dry sand	sandy soil, smooth surface, 25 cm thick layer	3.2	0.927 ± 0.015	25.5 ± 1.5	40
		1.6	0.933 ± 0.015	19 ± 1	41
		0.8	0.939 ± 0.007	15.5 ± 1	53
wet sand	sandy soil, smooth surface, water-saturated sand, 25 cm thick layer	3.2	0.749 ± 0.008	24 ± 2	39
		1.6	0.769 ± 0.010	19.5 ± 1	23
grass cover	15-20 cm high grass, 20 cm. thick soil layer	3.2	0.935 ± 0.008	27.5 ± 2	58
		1.6	0.961 ± 0.009	22 ± 2	37
crushed stone	coarse limestone 25 cm. thick	3.2	0.877 ± 0.011	22 ± 2.5	81
slate	undulating, several layers, 15 cm thick	3.2	0.742 ± 0.012	24 ± 3	71
slag	coarse, 4-6 cm. average size, 25 cm. thick layer	3.2	0.787 ± 0.008	23.5 ± 3	65
timber	pane, 10 cm thick	3.2	0.878 ± 0.008	20 ± 0.5	23
foliage	birch branches, 25 cm thick.	3.2	0.882 ± 0.011	16.5 ± 1	47

Melent'yev, V. V., Yu. I. Rabinovich,  
and G. G. Shchukin. Airborne measure-  
ments of return from a disturbed sea  
surface. IN: Trudy Glavnoy geofizicheskoy  
observatorii, no. 291, 1972, 34-39.

Experimental data are given on polarized r-f ( $\lambda = 0.8 - 3.2$  cm) return  $T_B$  from a sea surface under varying state of disturbance. The data can then be used to measure sea state conditions. The horizontally ( $T_{BH}$ ) and vertically ( $T_{BV}$ ) polarized return was measured radiometrically from an IL-18 aircraft 300 m. over the Caspian Sea. The experimental procedure was described earlier by Rabinovich et al (Trudy GGO, no. 235, 1970). Sea state was defined by the wave height  $h$ . The plots of  $T_{BH}$  versus the view angle  $\theta$  show that at  $h = 0.5$  m,  $T_{BH}$  decreases when  $\theta$  is increased from 0 to 75 degrees. The decrease of  $T_{BH}$  also depends on  $\lambda$ . The effect of  $h$  on  $T_{BH}$  at  $\lambda = 1.6$  cm and simultaneously measured  $T_{BH}$  and  $T_{BV}$  at  $\lambda = 3.2$  cm. is shown in Figs. 1 and 2, respectively. Curves 3-5 in Fig. 1 show a  $8-10^\circ$  K

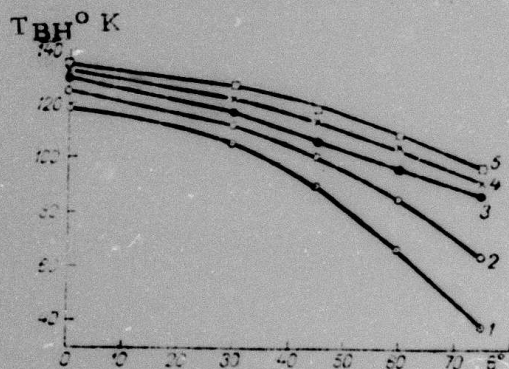


Fig. 1. Brightness temperature of disturbed sea versus view angle at  $\lambda = 1.6$  cm.

1- curve calculated without allowance for atmosphere, 2- with allowance for atmosphere, 3-  $h = 0.5$ , 4-  $h = 2.0$ , 5-  $h = 3-3.5$  m.

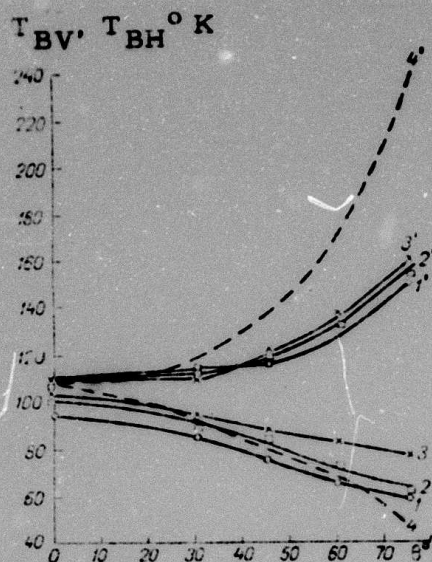


Fig. 2. Brightness temperature of disturbed sea versus view angle at  $\lambda = 3.2$  cm. for vertically (1'-4') and horizontally (1-4) polarized emissions:

1 -  $h = 0.5$ , 2 -  $h = 1.5$ , 3 -  $h = 2$ , and 4 -  $h = 0$  m.

increase in sea  $T_{BH}$  with the increase in wave  $h$ . The contribution of the atmosphere is significant. Comparison of theoretical  $T_{BH}$  for a smooth surface (curve 2) with the experimental  $T_{BH}$  of a disturbed surface (3-5) shows that the contribution of disturbance averaged 10-25° K. Fig. 2 shows that  $T_{BH}$  increases with an increase in  $h$ , but  $T_{BV}$  variations do not follow a definite pattern. Dependence of r-f return on sea roughness is clearly shown by a decrease in polarization  $P\%$  calculated at  $\lambda = 3.2$  cm. with an increase in  $h$  from 0.5 to 2 m. Airborne microwave emission measurements over the salt-saturated Kara-Bogaz-Gol Bay revealed waters of the  $T_{BH}$  and  $T_{BV}$  variation patterns inverse of those usually observed for unsaturated solutions of increased salinity. The feasibility was demonstrated of evaluating sea state from airborne measurements at  $\theta > 60$  degrees, based on r-f return build-up with increases in wave height.

Martsinkevich, L. M., and V. V. Melent'yev.  
Centimeter band return from a disturbed sea  
surface. IN: Trudy Glavnoy geofizicheskoy  
 observatorii, no. 291, 1972, 24-33.

Formulas are derived for determining the state of sea surface by microwave radiometry using an airborne receiver. A new formulation of the surface slope distribution function  $f(\alpha, \varphi)$  is used, where

$$\alpha = \lg \theta \quad (1)$$

where  $\theta$  is the inclination of an elementary sea surface area, and  $\varphi$  is the azimuth of an elementary area (Fig. 1). The formula was derived from the

$$f(\alpha, \varphi) = A \exp[-B\alpha^2(1 - C\sin^2\varphi)] \quad (2)$$

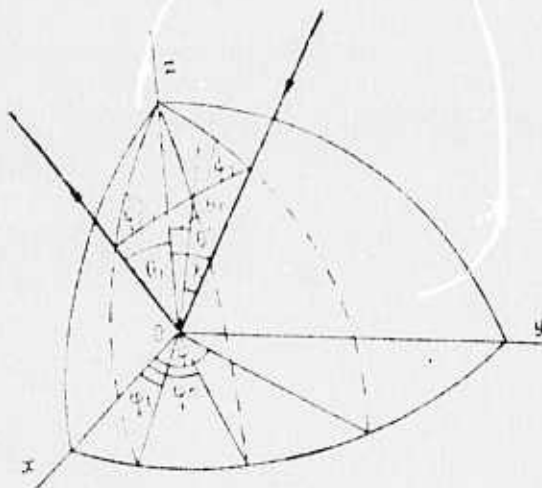


Fig. 1. Reflected beam diagram:  $\lambda$  - true angle of incidence,  $\theta_1$  - view angle,  $\theta'$ ,  $\varphi'$  - incident beam angular coordinates,  $\varphi_1$  - observed azimuth.

experimental surface elevation spectrum. The A and B coefficients in (2) are functions of  $h/\lambda^*$ , the average wave steepness, and  $C = 0.747$ . Solution of the equation for centimeter wave radiation transfer through a real atmosphere is expressed in analytical form with allowance for attenuation by water vapor and atmospheric gases. Radiation transfer is expressed as the integral sum of r-f return from disturbed sea surface and the real atmosphere. This analytical expression can be used to calculate the r-f brightness temperature of a disturbed sea at any surface temperature  $T = 0-40^\circ \text{C}$ , any salinity in the 0-40% range, and sea roughness. The range of variations of the most important parameters,  $h/\lambda^*$ ,  $\alpha$ , and  $\phi$  in the equation of radiation transfer is indicated. The attenuation coefficient, a part of the exponent in the equation of transfer, is strongly dependent on  $\lambda$ . A sample calculation of a 3.2 cm radiation transfer for  $\theta_1 = 0-70$  degrees,  $h/\lambda^* = 0.028$ ,  $T = 25^\circ \text{C}$ , and  $S = 40\%$  shows good agreement with experiments. The selected theoretical model can therefore be considered as a sufficiently accurate description of centimeter-band emission return from a disturbed sea surface.

Shchukin, G. G. R-f return from natural land surfaces. IN: Trudy Glavnoy geofizicheskoy observatorii, no. 291, 1972, 18-23.

In a continuing study of the properties and structure of underlying land surfaces by remote sensing, emission coefficients  $\epsilon_v$  and  $\epsilon_H$  and polarization P % were calculated for various surfaces. Calculations were based on modified Fresnel formulas for the reflection coefficient of smooth surfaces. Dielectric constants, conductivity, and dielectric loss angle data from the literature are tabulated for various surfaces. Plots of  $\epsilon_v$  and  $\epsilon_H$  versus viewangle  $\theta$  for 3.2 cm radiation (Fig. 1) show that dense rocks

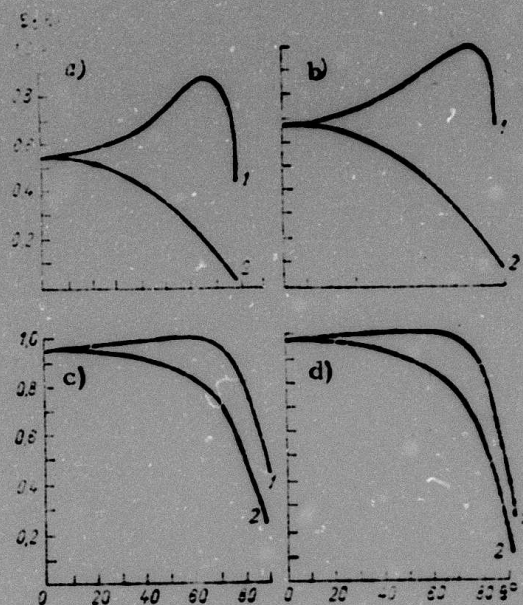


Fig. 1.  $\epsilon_v$  and  $\epsilon_h$  versus viewangle for a- asphalt, b- basalt, c- ash, and d- quartz sand; curves 1- vertical, 2- horizontal polarization.

(e. g. , goethite, limonite, and basalt) exhibit the greatest difference in the  $\theta$  dependence patterns of  $\epsilon_v$  and  $\epsilon_h$ , in contrast to loose and porous rocks, (e. g. , sand, ash, pumice, and lava). Plots of  $P\%$  versus  $\theta$  (Fig. 2) show the strong effect of soil moisture content on  $\epsilon$ . The data support the feasibility of obtaining information on the type, structure, and moisture content of underlying surfaces from measurements of their r-f brightness temperature and  $P$ . This information is of great importance for radio astronomy of planets. In addition, statistical r-f emission data on land surfaces may be used for determining meteorological characteristics of the atmosphere. Some preliminary experimental r-f brightness temperature ( $T_B$ ) data led to the tentative conclusion that probable deviation from the mean  $T_B$  is of the order of  $\pm 10^\circ K$  for a salt solution from the Kara-Bogaz-Gol Bay and from steppe, snow-covered field, desert, and other surfaces.

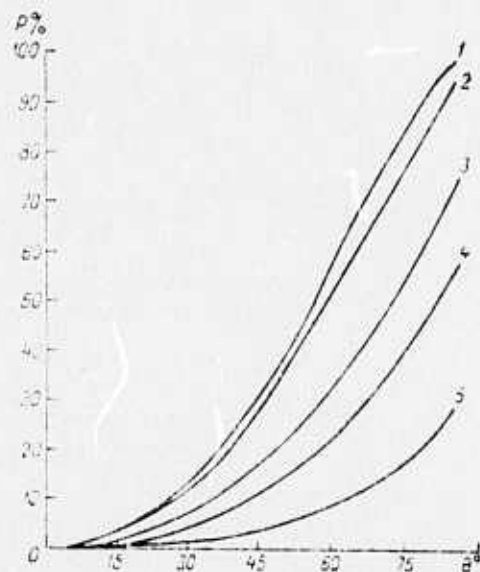


Fig. 2. Polarization versus viewangle.  
 1- sandy soil water saturated, 2- moist  
 turf, 3- dry turf, 4- sandy soil, extremely  
 dry, 5- quartz sand.

Rocket meridian (Launch of Soviet  
 meteorological rockets from Kerguelen  
 Island). Izvestiya, 7 March 1973, p. 4.

The February 27 launch of the first Soviet meteorological rocket M-100 from Kerguelen Island is reported. Temperature, pressure, and wind velocity data in the upper atmosphere to 92 km altitude were transmitted. Twenty more similar launchings were scheduled for March-May in the framework of the Franco-Soviet joint program. According to Yu. A. Izrael', the coordinator of these launchings, the upper atmosphere probing from Kerguelen completes construction of the "rocket meridian"

in the Eastern Hemisphere. Complete data on the upper atmosphere at a single meridian will be available, when the current Soviet launchings from different points of the globe are completed. Launchings from Kerguelen were prepared by a team from the Central Aerological Observatory, headed by S. Perov. The Kerguelen data are considered very valuable for tracking upper atmosphere fluctuations. They will be used in weather forecasting which takes into account the effect of the sun on the Earth's atmosphere.

Kapitsa, P. L. Device for generating high temperature plasma. Author's certificate, USSR, no. 333890, published August 22, 1969. (Otkr izobr, 6/73, p. 62).

Patent 1. This high-temperature plasma generating device, which is intended for the study and realization of thermonuclear reactions, consists of a resonator, filled with the operating medium, e. g. a mixture of deuterium and tritium, and a high-frequency electromagnetic energy supply for the resonator. To improve stability of the plasma and increase its temperature, the resonator and its energy supply is constructed so that the e-m field excited in the resonator provides localization of maximum electric field in the central part of resonator volume. The resonator contains elements which create a rotary circulation of the medium under pressure and which sufficiently secures its (medium) viscous displacement.

Patent 2. This is similar to patent 1 with the difference that the resonator has a circular cross-section for simplicity of construction and tuning.

Patent 3. Similar to patent 2, but with a resonator of toroidal form, which lowers energy losses at the ends.

Patent 4. A combination of patents 1 and 3. For improving heat insulation of the plasma, especially its ion components, this variant includes a means for generating in the resonator a constant magnetic field analogous to a magnetic trap for plasma.

Patent 5. A combination of patents 1 and 4. For additional heating of plasma, especially its ion component, this variant is provided with means for creating a transient magnetic field in the resonator, which provides excitation of magneto-acoustic oscillations in plasma.

Patent 6. A combination of patents 1 and 5. For decreasing energetic losses, especially during thermonuclear synthesis, this variant is equipped with means to secure in the resonator an operating medium pressure, sufficient to absorb the energy carried away from the plasma by neutrons.

B. Recent Selections

Beketov, S. V., A. N. Korolev, and A. V. Potapov. Estimating the location of a pulsed signal source of unknown shape. RiE, no. 8, 1973, 1598-1604.

Bogdanov, S. V., A. M. Boyarskiy, M. D. Levin, and I. B. Yakovkin. Continuous amplification regime of elastic surface waves. FTP, no. 8, 1973, 1604-1606.

Deryugin, L. N., and T. K. Chekhlova. Studying optical micro-wave-guides in gelatinous films. OiS, v. 35, no. 2, 1973, 362-365.

Didenko, A. N., and V. G. Bagrov. The possibility of using stimulated electron emission for amplifying synchrotron radiation. ZhTF, no. 8, 1973, 1773-1776.

Dmitriyev, A. L. Analog technique in non-optical holography. ZhTF, no. 9, 1973, 1938-1941.

Grishchuk, L. P., and M. V. Sazhin. Radiation of gravitational waves by an electromagnetic resonator. ZhETF, v. 65, no. 2, 1973, 441-454.

Izokh, V. V., and A. V. Sergeyev. Optimal quantization of functions presented on a hemisphere. ZhTF, no. 9, 1973, 1942-1949.

Karpman, V. I. Nelineynyye volny v dispergiruyushchikh sredakh. (Nonlinear waves in dispersive media). Moskva, Izd-vo Nauka, 1973, 175 p. (KL, 31/73, no. 24855)

Kaveyeva, Z. M., and V. V. Samartsev. Investigating hyperfine and super-hyperfine interactions by a optical echo method. OiS, v. 35, no. 2, 1973, 379-381.

Likhachev, V. A., M. M. Myshlyayev, S. S. Olevskiy and T. N. Chuchman. Sverkhplastichnost' alyuminiya i yeyo struktura. Preprint. (Superplasticity of aluminum and its structure. Preprint). Chernogolovka, 1973, 7 p. (Dop vyp, 7/73, no. 15246)

Lowering the threshold limit of an ionization vacuum gauge with a heated cathode to  $10^{-13}$  torr. Sdelov. techn., v. 21, no. 3, 1973, 108-109. (RZhElektr, 8/73, no. 8A48)

Novik, D. A. Certain properties of a quasi-holographic scheme of scientific photography OiS, v. 35, no. 3, 1973, 546-551.

Prokh, L. Z. Ball lightning during a winter thunderstorm in Kiyev. Meteorologiya i gidrologiya, no. 19, 1972, 103-107.

Stakhanov, I. P. On the nature of ball lightning. ZhETF P, v. 18, no. 3, 1973, 193-196.

Voronov, G. S., and A. P. Prokhorov. Studying the effectiveness of laser plasma confinement by a magnetic field. ZhTF, no. 8, 1973, 1641-1645.

## 8. SOURCE ABBREVIATIONS

AiT	-	Avtomatika i telemekhanika
APP	-	Acta physica polonica
DAN ArmSSR	-	Akademiya nauk Armyanskoy SSR. Doklady
DAN AzSSR	-	Akademiya nauk Azerbaydzhanskoy SSR. Doklady
DAN BSSR	-	Akademiya nauk Belorusskoy SSR. Doklady
DAN SSSR	-	Akademiya nauk SSSR. Doklady
DAN TadSSR	-	Akademiya nauk Tadzhikskoy SSR. Doklady
DAN UkrSSR	-	Akademiya nauk Ukrainskoy SSR. Dopovidi
DAN UzbSSR	-	Akademiya nauk Uzbekskoy SSR. Doklady
DBAN	-	Bulgarska akademiya na naukite. Doklady
EOM	-	Elektronnaya obrabotka materialov
FAiO	-	Akademiya nauk SSSR. Izvestiya. Fizika atmosfery i okeana
FGIV	-	Fizika gorennya i vzryva
FiKhOM	-	Fizika i khimiya obrabotka materialov
F-KhMM	-	Fiziko-khimicheskaya mekhanika materialov
FMiM	-	Fizika metallov i metallovedeniye
FTP	-	Fizika i tekhnika poluprovodnikov
FTT	-	Fizika tverdogo tela
FZh	-	Fiziologicheskiy zhurnal
GiA	-	Geomagnetizm i aeronomiya
GiK	-	Geodeziya i kartografiya
IAN Arm	-	Akademiya nauk Armyanskoy SSR. Izvestiya. Fizika
IAN Az	-	Akademiya nauk Azerbaydzhanskoy SSR. Izvestiya. Seriya fiziko-tekhnicheskikh i matematicheskikh nauk

IAN B	-	Akademiya nauk Belorusskoy SSR. Izvestiya. Seriya fiziko-matematicheskikh nauk
IAN Biol	-	Akademiya nauk SSSR. Izvestiya. Seriya biologicheskaya
IAN Energ	-	Akademiya nauk SSSR. Izvestiya. Energetika i transport
IAN Est	-	Akademiya nauk Estonskoy SSR. Izvestiya. Fizika matematika
IAN Fiz	-	Akademiya nauk SSSR. Izvestiya. Seriya fizicheskaya
IAN Fizika zemli	-	Akademiya nauk SSSR. Izvestiya. Fizika zemli
IAN Kh	-	Akademiya nauk SSSR. Izvestiya. Seriya khimicheskaya
IAN Lat	-	Akademiya nauk Latviyskoy SSR. Izvestiya
IAN Met	-	Akademiya nauk SSSR. Izvestiya. Metally
IAN Mold	-	Akademiya nauk Moldavskoy SSR. Izvestiya. Seriya fiziko-tehnicheskikh i matematicheskikh nauk
IAN SO SSSR	-	Akademiya nauk SSSR. Sibirskoye otdeleniye. Izvestiya
IAN Tadzh	-	Akademiya nauk Tadzhiksoy SSR. Izvestiya. Otdeleniye fiziko-matematicheskikh i geologo-khimicheskikh nauk
IAN TK	-	Akademiya nauk SSSR. Izvestiya. Tekhnicheskaya kibernetika
IAN Turk	-	Akademiya nauk Turkmenskoy SSR. Izvestiya. Seriya fiziko-tehnicheskikh, khimicheskikh, i geologicheskikh nauk
IAN Uzb	-	Akademiya nauk Uzbekskoy SSR. Izvestiya. Seriya fiziko-matematicheskikh nauk
IBAN	-	Bulgarska akademiya na naukite. Fizicheski institut. Izvestiya na fizicheskaya institut s ANEB
I-FZh	-	Inzhenerno-fizicheskiy zhurnal

IiR	-	Izobretatel' i ratsionalizator
ILEI	-	Leningradskiy elektrotekhnicheskiy institut. Izvestiya
IT	-	Izmeritel'naya tekhnika
IVUZ Avia	-	Izvestiya vysshikh uchebnykh zavedeniy. Aviatsionnaya tekhnika
IVUZ Cher	-	Izvestiya vysshikh uchebnykh zavedeniy. Chernaya metallurgiya
IVUZ Energ	-	Izvestiya vysshikh uchebnykh zavedeniy. Energetika
IVUZ Fiz	-	Izvestiya vysshikh uchebnykh zavedeniy. Fizika
IVUZ Geod	-	Izvestiya vysshikh uchebnykh zavedeniy. Geodeziya i aerofotos'yemka
IVUZ Geol	-	Izvestiya vysshikh uchebnykh zavedeniy. Geologiya i razvedka
IVUZ Gorn	-	Izvestiya vysshikh uchebnykh zavedeniy. Gornyy zhurnal
IVUZ Mash	-	Izvestiya vysshikh uchebnykh zavedeniy. Mashinostroyeniye
IVUZ Priboro	-	Izvestiya vysshikh uchebnykh zavedeniy. Priborostroyeniye
IVUZ Radioelektr	-	Izvestiya vysshikh uchebnykh zavedeniy. Radioelektronika
IVUZ Radiofiz	-	Izvestiya vysshikh uchebnykh zavedeniy. Radiofizika
IVUZ Stroi	-	Izvestiya vysshikh uchebnykh zavedeniy. Stroitel'stvo i arkhitektura
KhVE	-	Khimiya vysokikh energiy
KiK	-	Kinetika i kataliz
KL	-	Knizhnaya letopis'
Kristall	-	Kristallografiya
KSpF	-	Kratkiye soobshcheniya po fizike

LZhS	-	Letopis' zhurnal'nykh statey
MiTOM	-	Metallovedeniye i termicheskaya obrabotka materialov
MP	-	Mekhanika polimerov
MTT	-	Akademiya nauk SSSR. Izvestiya. Mekhanika tverdogo tela
MZhiG	-	Akademiya nauk SSSR. Izvestiya. Mekhanika zhidkosti i gaza
NK	-	Novyye knigi
NM	-	Akademiya nauk SSSR. Izvestiya. Neorganicheskiye materialy
NTO SSSR	-	Nauchno-tekhnicheskiye obshchestva SSSR
OiS	-	Optika i spektroskopiya
OMP	-	Optiko-mekhanicheskaya promyshlennost'
Otkr izobr	-	Otkrytiya, izobreteniya, promyshlennyye obraztsy, tovarnyye znaki
PF	-	Postepy fizyki
Phys abs	-	Physics abstracts
PM	-	Prikladnaya mekhanika
PMM	-	Prikladnaya matematika i mekhanika
PSS	-	Physica status solidi
PSU	-	Pribory i sistemy upravleniya
PTE	-	Pribory i tekhnika eksperimenta
Radiotekh	-	Radiotekhnika
RiE	-	Radiotekhnika i elektronika
RZhAvtom	-	Referativnyy zhurnal. Avtomatika, telemekhanika i vychislitel'naya tekhnika
RZhElektr	-	Referativnyy zhurnal. Elektronika i yeye primeneniye

RZhF	-	Referativnyy zhurnal. Fizika
RZhFoto	-	Referativnyy zhurnal. Fotokinotekhnika
RZhGeod	-	Referativnyy zhurnal. Geodeziya i aeros"- yemka
RZhGeofiz	-	Referativnyy zhurnal. Geofizika
RZhInf	-	Referativnyy zhurnal. Informatics
RZhKh	-	Referativnyy zhurnal. Khimiya
RZhMekh	-	Referativnyy zhurnal. Mekhanika
RZhMetrolog	-	Referativnyy zhurnal. Metrologiya i izmer- itel'naya tekhnika
RZhRadiot	-	Referativnyy zhurnal. Radiotekhnika
SovSciRev	-	Soviet science review
TiEKh	-	Teoreticheskaya i eksperimental'naya khimiya
TKIT	-	Tekhnika kino i televideniya
TMF	-	Teoreticheskaya i matematicheskaya fizika
TVT	-	Teplofizika vysokikh temperatur
UFN	-	Uspekhi fizicheskikh nauk
UFZh	-	Ukrainskiy fizicheskii zhurnal
UMS	-	Ustalost' metallov i splavov
UNF	-	Uspekhi nauchnoy fotografii
VAN	-	Akademiya nauk SSSR. Vestnik
VAN BSSR	-	Akademiya nauk Belorusskoy SSR. Vestnik
VAN KazSSR	-	Akademiya nauk Kazakhskoy SSR. Vestnik
VBU	-	Belorusskiy universitet. Vestnik
VNDKh SSSR	-	VNDKh SSSR. Informatsionnyy byulleten'
VLU	-	Leningradskiy universitet. Vestnik. Fizika, khimiya
VMU	-	Moskovskiy universitet. Vestnik. Seriya fizika, astronomiya

ZhETF	-	Zhurnal eksperimental'noy i teoreticheskoy fiziki
ZhETF P	-	Pis'ma v Zhurnal eksperimental'noy i teoreticheskoy fiziki
ZhFKh	-	Zhurnal fizicheskoy khimii
ZhNPPFK	-	Zhurnal nauchnoy i prikladnoy fotografii i kinematografii
ZhNKh	-	Zhurnal neorganicheskoy khimii
ZhPK	-	Zhurnal prikladnoy khimii
ZhPMTF	-	Zhurnal prikladnoy mekhaniki i tekhnicheskoy fiziki
ZhPS	-	Zhurnal prikladnoy spektroskopii
ZhTF	-	Zhurnal tekhnicheskoy fiziki
ZhVMMF	-	Zhurnal vychislitel'noy matematiki i matematicheskoy fiziki
ZL	-	Zavodskaya laboratoriya

## 9. AUTHOR INDEX

### A

Abrikosova, I. I. 6  
Andreyev, S. D. 135  
Anisimov, S. I. 7  
Armand, S. A. 126  
Askar'yan, G. A. 8

### B

Bakhrakh, S. M. 26  
Barchukov, A. I. 1  
Batanov, V. A. 13  
Beranek, B. 41  
Bergel'son, V. I. 3  
Berger, V. K. 127  
Bochkov, D. S. 133  
Boganov, A. G. 110  
Borovoy, A. G. 131  
Bredikhin, M. Yu. 85  
Brylov, S. A. 106  
Bukatyy, V. I. 131

### C

Cisowski, J. 104

### D

Dolmatov, K. I. 28  
Dugladze, G. M. 94  
Iabrikov, M. Ye. 105

### G

Garkalenko, I. A. 53  
Gavrilin, A. I. 30  
Gernitts, F. 14  
Gershbeyn, E. A. 23  
Getmantsev, G. G. 129  
Golionko, G. B. 80

### K

Kapitsa, P. L. 169  
Kaufman, R. N. 128  
Khinrikus, K. V. 134

Kikvidze, R. R. 87  
Kirshenina, I. I. 92  
Kornilov, I. I. 97  
Kovalchuk, B. M. 83  
Kozlov, V. 24

### L

Lavrenko, V. A. 96  
Lipskis, A. L. 102  
Litvin, Yu. A. 103  
Lursmanashvili, O. V. 80

### M

Markelova, L. P. 4  
Martsinkevich, L. M. 165  
Melent'yev, V. V. 158, 160, 161, 163  
Mints, R. I. 105  
Mituch, E. 60

### N

Novikov, N. P. 3

### O

Ovsyannikov, V. A. 132

### P

Papirova, I. I. 9  
Pashkov, P. O. 27  
Petropavlovskaya, Z. N. 99  
Prosen, D. 49  
Pustovalov, V. K. 5

### R

Regel', V. R. 114

### S

Savarenskiy, Ye. F. 82  
Semenova, V. I. 125  
Semiletenko, B. G. 21  
Shchirzhetskiy, Kh. A. 30  
Shchukin, G. G. 166

Sollogub, V. B. 70  
Subbotin, S. I. 76

T

Turayev, U. 95  
Turchanin, A. G. 103

U

Uglov, A. A. 2  
Umanskiy, E. S. 109  
Uvarov, V. V. 112

V

Vas'kov, V. V. 124  
Vereshchagin, L. F. 89, 90, 92  
Vereshchaka, A. I. 136  
Veyko, V. P. 12  
Volovik, V. D. 84

Y

Yershova, F. P. 93

Z

Zakharov, V. P. 10  
Zavorotnyy, V. U. 130